GEOCAP
Geothermal Capacity Building Program Indonesia - Netherlands

Date: 22nd February 2017

MASTER'S THESIS

Numerical Simulation of Near Wellbore Permeability Reduction Using Colloidal Silica Gel

Author: **Tom Frederic M. Dallemagne**

Faculty supervisor (Utrecht University): ***Prof. Ruud J. Schotting***
Host company supervisor (IF technology): ***Nick Buik***

COOPERATING COMPANIES & UNIVERSITIES

GEOCAP

Geothermal Capacity Building Program Indonesia - Netherlands

INAGA

University of Twente, Faculty ITC

IF technology

University of Indonesia

DNV GL

Gadjah Mada University

Technical University Bandung

Utrecht University, Faculty of Geosciences, Department of Earth Sciences

Delft University of Technology, Department of Geotechnology

Netherlands Organisation for Applied Scientific Research

Universiteit Utrecht

FACULTY OF GEOSCIENCES

MASTER'S THESIS

Study program/ Specialization: **Earth Surface and Water/** **Hydrology**	Fall semester, 2016
Author: **Tom Frederic M. Dallemagne**	..... (Author's signature)

Faculty supervisor: **Prof. Ruud J. Schotting**

Host company supervisor (IF technology): **Nick Buik**

Title of thesis: **Numerical Simulation of Near Wellbore Permeability Reduction Using Colloidal Silica Gel**

Credits (ECTS): 30

Keywords: Colloidal Silica Permeability reduction TOUGHREACT Gel injection pH	Pages: 84 + Appendix: 1 Utrecht, 22nd February 2017

TABLE OF CONTENTS

LIST OF FIGURES

LIST OF TABLES

LIST OF ABREVIATIONS / SYMBOLS

K	Rate constant [T^{-1}]	RRF	Residual resistance factor [-]
T	Absolute temperature [K]	λ_{before}	Mobility of water before DPR fluid flow [mD/cP]
R	Molar gas constant [$J.K^{-1}.mole^{-1}$]	λ_{after}	Mobility of water after DPR fluid flow [mD/cP]
E_a	Activation energy [$J.mole^{-1}$]	Q_l	Discharge in l-direction [$L^3.T^{-1}$]
A_f	Frequency factor [T^{-1}]	K_l	Hydraulic conductivity [$L.T^{-1}$]
r	Reaction rate [$M.T^{-1}.L^{-3}$]	A	Cross-sectional area [L^2]
C_i	Concentration of reactants [$M.L^{-3}$]	$\frac{dh}{dl}$	Hydraulic gradient [-]
e_k	Order of reaction [-]	q_l	Specific discharge in l-direction [$L.T^{-1}$]
q_{inj}	Injection rate [$L.T^{-1}$]	κ	Intrinsic permeability [mD]
ϕ	Porosity [-]	μ	Dynamic viscosity [$M.L^{-1}.T^{-1}$]
ϕ_f	Fluid porosity [-]	ρ_f	Fluid density [$M.L^{-3}$]
ϕ_e	Effective porosity [-]	g	Gravitational acceleration [$L.T^{-2}$]
V	Volume [L^3]	r	Radius [L]
V_B	Bulk volume [L^3]	nm	Number of minerals
V_p	Pore volume [L^3]	fr_m	Volume fraction of mineral m
V_v	Volume of interconnected voids [L^3]	fr_u	Volume fraction of nonreactive rock
V_t	Total volume of the medium [L^3]	k_i	Initial permeability [mD]
V_{res}	Volume reservoir [L^3]	S	Chemical species
t_{res}	Residence time [T]	N_R	Number of reaction
M	Mobility reduction factor [-]	v_{ij}	Stoichiometric coefficient
k_w	Effective water permeability [mD]	M	Number of mechanisms
k_p	Effective DPR fluid permeability [mD]	γ	Activity coefficient
μ_w	Water viscosity [cP]	N_l	Number of reacting species
μ_p	Silicate/Polymer (DPR fluid) viscosity [cP]	N_m	Number of Monod terms
A_n	Specific reactive surface area [$kg\text{-}H_2O^{-1}$]	N_P	Number of inhibition factor
k_r	Relative permeability [mD]	Ω_m	Mineral saturation ratio
k_{rc}	Relative permeability of CO_2 phase [mD]	K_m	Equilibrium constant
k_{rl}	Relative permeability of liquid phase [mD]	SI_m	Mineral saturation index
p_{cap}	Capillary pressure [bar]	S_{gr}	Irreducible gas saturation
P_0	Strength coefficient [kPa]	S_{lr}	Irreducible water saturation
D	Diffusion coefficient [$L^2.T^{-1}$]	S_l	H_2O saturation
F	Mass flux [$M.L^{-2}.T^{-1}$]	M	Mass accumulation [$M.L^{-3}$]
U	Internal energy [$J.M^{-1}$]	X	Mass fraction
P	Pressure [Pa]	μ	Viscosity [$M.L^{-1}.T^{-1}$]
λ	Heat conductivity [$W.L^{-1}.K^{-1}$]		

ABSTRACT

Sometimes, injection wells happen to clog with matter that reduces the permeability around the well and makes it not performing in an optimal way. A possible solution to remove the clogging matter is the chemical treatment of the well by the injection of acids dissolving the clogging particles. The issue is that the acid will preferentially flow in the zones of high permeability not impacted by the clogging matter. To avoid this happening, grouting gel can be injected previously to the acid treatment to reduce the permeability around the well completely and perform then the recovery treatment.

Of the grouting gel reviewed, colloidal silica gels were selected because of the many advantages they have regarding costs, environmental care, and emplacement ease. Colloidal silica gels were used in the past for environmental remediation and permeability reduction. The chemistry and gelation process of colloidal silica gels is complicated. The gelation time is affected by several parameters such as injection rate, pH, temperature, and concentration of the component in the injected solution.

In this research, a numerical model was used to simulate the injection of colloidal silica gel for the reduction of high permeability zones located between clogged layers surrounding a well. Of the many software available, the choice was to use the non-isothermal reactive geochemical code TOOUGHREACT developed by Xu et al. (2004) since it allows to precipitate the hypothetical colloidal silica gel in the form of amorphous silica mineral but also because of its availability at the company where the research was conducted. The formation of gel in TOUGHREACT is related to the chemical reaction implemented into the simulator and the reaction rates of the reactant. The increasing volume ratio of the precipitated gel into the pore throats of the reservoir mainly controls the blocking effect in TOUGHREACT. To input colloidal silica gel in the model, the molar volume of amorphous silica found in the TOUGHREACT database was increased from 60.084 cm^3/mol to 500 cm^3/mol to represent the large volume rise that undergoes upon gelation. With this manipulation, amorphous silica is not considered as mineral but as a colloidal silica gel.

Because this thesis is part of the GEOCAP project, a hypothetical field based on the Wayang Windu geothermal field in Indonesia was created. Sensitivity analysis regarding reservoir porosity-permeability relation, reservoir temperature, injection rate, and colloidal silica concentration are performed. Through simulations, estimation of an optimal injection regime can be reached as the model allows predicting both the time needed to seal the well vicinity completely and the extent from the well of the significant permeability reduction, but also the amount of gel injected regarding injection rate and concentration defined.

It was showed on the following figures that with an injection rate of 13.37 kg-H_2O/s and a 5 wt% colloidal silica solution, a complete grouting of the area next to the well could be realized after approximately 3.6 hours of injection. This operation results in the injection of 8.66 m^3 of gel reducing the permeability to zero over a distance of roughly 5 cm from the well.

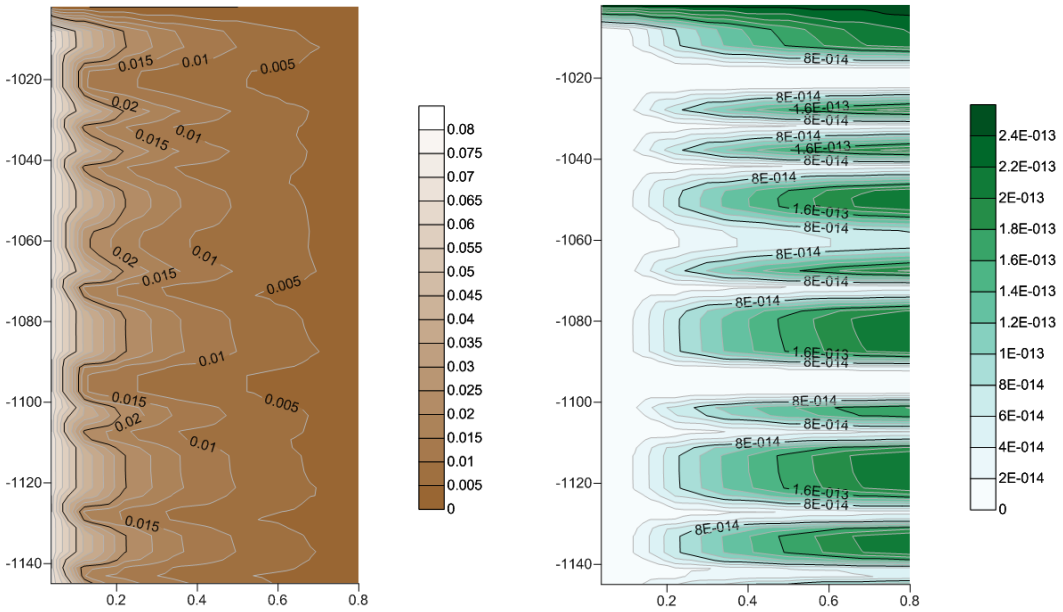

Changing the permeability-porosity relation have a slight effect on the permeability reduction due to the difference between their two functions. Starting at the same initial porosity, the difference between the two relation increases until reaching a maximum at a particular porosity reduction. From the maximum, the difference decreases until the porosity is completely reduced. However, the variation due to the choice of the porosity-permeability relation does not impact the gel emplacement significantly.

Decreasing the reservoir temperature resulted in a faster gel formation because of the temperature impact on the kinetic rates of the gel. Referring to Arrhenius equation, when the temperature is decreased, the dissolution rate decreases faster than the precipitation rate. Therefore, the precipitation becomes more predominant compared to the dissolution rate. At a certain threshold temperature, the precipitation rate is become so dominant compared to the dissolution rate that the gel solution available is entirely precipitated. It results in the maximum gel formation possible and, therefore, the maximum permeability reduction possible regarding the amount of gel solution injected. However, as it can be seen in the following table, the time to reach the complete sealing and the volume of gel injected are almost the same, and the difference regarding permeability reduction is not significant.

Distance from the well [cm]	Time of gel solution injection [hour]	Initial reservoir temperature [°C] = 50		Initial reservoir temperature [°C] = 150		Initial reservoir temperature [°C] = 250	
		Porosity [%]	Permeability [mD]	Porosity [%]	Permeability [mD]	Porosity [%]	Permeability [mD]
Next to the well	1.2	4	24	4	26	4	39
	3.6	1	0	1	0	1	1
	6	0	0	0	0	0	0

It was found through sensitivity analysis a same amount of gel injected, a better grouting is achieved with a low injection rate and a high colloidal silica concentration than with a high injection rate and

a small colloidal silica concentration. Also, as shown in the figure below, using a constant injection rate for each simulation, it is more advantageous to inject a highly concentrated colloidal silica solution than a less concentrated solution. This is because less amount of gel is injected with the first solution to achieve a similar grouting. Similarly, it appeared that for a similar sealing using the same colloidal silica solution, the use of a small injection rate during a long time is more advantageous than a high injection rate during a short period. Finally, it was showed that the main parameters to control are the gel concentration. With the same injection time, a similar grouting is achieved by increasing the gel concentration than by increasing the injection rate. However, the amount of gel injected with the highly concentrated solution is significantly smaller than with the high injection rate.

Injection rate = 13.37 kg-H_2O/s

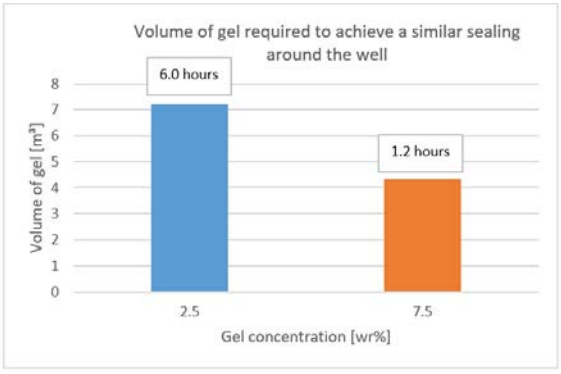

Gel concentration = 5 wt%

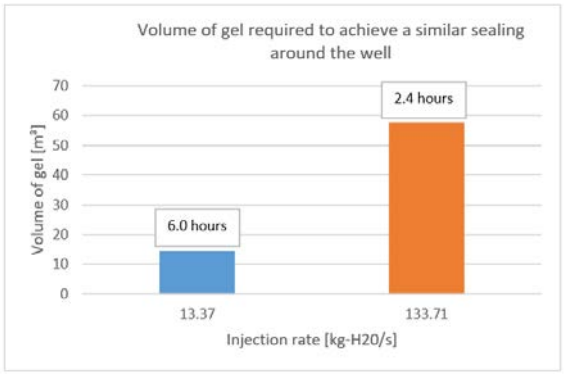

Sensitivity analysis regarding injection rate and colloidal silica concentration presented significant effects on the permeability reduction around the well since it changes considerably the amount of gel injected. Gel concentration is the primary factor to control as it allows to achieve similar grouting as significant injection rate but with a significantly smaller amount of gel injected.

Also, this research investigates the effect of pH on the precipitation and removal of the colloidal silica gel. It was showed that the removal of the gel was possible with the injection of an alkaline solution that rises the pH of the area around the well and dissolves back to liquid phase the gel that was previously formed. The removal of the gel is performed through a different conceptual simulation because it was done before the conception of hypothetical field based on the Wayang Windu field. Through this simulation, the area around the well is grouted with an injection of 12.53 m³ of gel and is removed with the injection of 243.32 m³ of an alkaline solution.

Unfortunately, lack of access to experimental data and information in literature did not allow validating the model by matching the results with field experiment data

CHAPTER 1. INTRODUCTION

1.1. STATEMENT OF THE PROBLEM

When a well is not performing optimal, one of the reason can be that the well is clogged. In this case, the pores of the reservoir close to the well bore are (partly/entirely) filled with matter reducing the permeability. In general, some leading causes for the well to be clogged are (Hund et al. 1936):

- accumulation of gummy, waxy or paraffinic solid matter on the walls of the borehole;
- clogging due to the action of mud fluids used during drilling;
- clogging of the pores, crevices, capillaries and flow channels of the formation due to the precipitation of mineral deposits from water in the well.

A possible solution is the chemical treatment of the well by removing the matter that is blocking the pores. By chemical treatment, an acid is injected into the well, and the acid should dissolve the matter that is causing the clogging. The most commonly used acid is hydrochloric acid (HCl), especially in the development of newly drilled wells. It has been seen that it works the best in limestone field. The acid dissolves the calcium carbonate, resulting in reaction products such as calcium chloride and carbon dioxide. An important fact to note is the recent trend, given environmental considerations, to use food-grade acid as opposed to industrial-grade acid, commonly employed in the past. The use of inhibitors and other additives to the acid is now less common than in the past because of environmental care and because they turn to be considered unnecessary. There is also a realization that careful application of the acid can reduce the typical dosage by at least 50%. Acids are also commonly used in the rehabilitation of wells subject to iron fouling, i.e. where the formation, gravel pack, and well screen become clogged by iron-based deposits. The acid treatment is equally effective for deposits which are chemically or microbially generated (Howsam 1990).

However, the problem with acidizing is that the acid will flow into the most permeable zones and not into the parts that are clogged. During water circulation of a geothermal system, fluid will flow easier, further, and faster in the high permeability zones than in the partly/entirely clogged zones of the reservoir. To avoid this happening a degradable blocking gel can be injected into the well first to block the permeable zones. Isolating the high permeability zones will force the acid to flow in the low permeable areas and contribute to the well repair. The high permeability zones isolation can be realized using disproportionate permeability reduction (DPR) fluids, and it is important to simulate their injections to predict best injection regime for treatment design and optimization.

Therefore, the goal of this study was to develop a model able to simulate the injection and the removal of DPR fluid. A simulator had to be selected, and for this, two primary qualities were sought when deciding which simulator was most suitable. First, it was necessary that the simulator has

the capacity and functionalities for modeling the selected DPR fluid behavior. For instance, the simulator had to be capable of simulating the DPR fluid formation regarding environmental parameters, injection rate, and concentration change and thus simulate permeability reduction. Secondly, it was also important that the simulator was commonly available since the ultimate purpose of conducting this research is to get a better understanding of the selected DPR fluids for field operations.

After careful considerations of the simulators available, the non-isothermal reactive geochemical code TOUGHREACT (Xu et al. 2004; Xu et al. 2011; Xu et al. 2012) was selected because of its availability at the company where the research was conducted. This code was developed by introducing reactive chemistry into the framework of the existing multiphase fluid and heat transport code TOUGH2 (Pruess et al. 1999). Also, the TOUGHREACT code allows simulating the injection of colloidal silica gels which were chosen among the many polymer and gels available for well recovery operations. Simulations are conducted using the EOS2 thermophysical property module for multiphase mixtures of water and CO_2 with temperatures and pressure appropriate for geothermal system simulation and hydrothermal problems (Xu et al. 2004; Xu et al. 2006). The TOUGHREACT code has been used previously to simulate silica gel barrier emplacement for geochemical mitigation of CO2 leaking into a confined aquifer (Druhan et al. 2014) but never to the simulation of colloidal silica gel injection shutting off high permeability zones surrounding clogged wells for remediation strategies.

Besides the fact that the TOUGHREACT code does not have any polymer or gel module but allows the precipitation of colloidal silica gel as minerals, colloidal silica gels were chosen because they proved their ability to operate well recovery treatment. According to Table 1, these gels were the best choice regarding the DPR fluids reviewed. Their main advantages are that they are easy to emplace upon favorable pH conditions, are environmentally friendly and inexpensive.

Finally, the model simulated the colloidal silica gel injection into a hypothetical field based on a field in Indonesia because this thesis is part of the GEOCAP project. The study concern the high permeability reduction of injection wells located in the deep liquid reservoir of the Wayang Windu geothermal field, in Indonesia. The Geothermal Capacity Building Programme - Indonesia-Netherlands (GEOCAP) is an international collaboration between Indonesian and Dutch entities with the goal to develop intimately linked geothermal programs for education and training, research, and subsurface databases. More information can be found at the website (https://www.geocap.nl).

To the author's knowledge, and based on the literature review, there is no published work mainly discussing the experience of colloidal silica gel injection for high permeability zones shut-off regarding clogged wells repair treatments. Considering this fact, the aim of this study is to develop a theoretical model, using TOUGHREACT, which can define the most optimum injection regime of colloidal silica gel to plug high permeability zones.

1.2. SCOPE OF THE RESEARCH

The main objective of this thesis is to set up a well injection model able to simulate the most optimum injection regime of a DPR fluid for field applications. Therefore, a simulator has to be selected to create the model and a DPR fluid to be chosen regarding its advantages for the study. The model will predict the preferential flow paths of the solution injected and the permeability reduction of the zones the solution enters when turning to gel. The outcome of the model is to predict how much gel needs to be injected to block the permeable zones, how far the gel penetrates the areas and how long the gel takes to infiltrate these last. Also, an objective of the model is to predict the gel removal. Finally, the behavior of the gel regarding environmental parameters (i.e. pH, temperature, concentration) will be addressed.

The numerical study should include these objectives:

- The volume of gel needed to plug the high permeability zones should be realistic regarding industry operations;
- Time required by the fluid to infiltrate every high permeability areas and to turn to gel should be in order of hours;
- The model should apply to any situation (i.e. different fields or environmental conditions).

1.3. OUTLINE OF THESIS

This thesis is constructed as a progression of work from a discussion of the theoretical background to model development and, later, a presentation of results. Generalized themes of each section are given in the following paragraphs of this outline.

Review and analysis of previous literature regarding colloidal silica are presented in Chapter 2. This section includes information about the different use of colloidal silica within the environmental field. The properties of the compounds are explored as well as the factors which might influence its gelation.

Chapter 3 is a theoretical background regarding the research problem and describes porous medium properties; fluids flow in a porous medium and geochemical system in relation with the governing equations used in the TOUGHREACT code.

Chapter 4 addresses the model development based on the characteristics of the hypothetical field. The model domain and thermophysical properties are shown, as well as the presentation of the initial geochemical conditions of the reservoir. Also, the way of implementing the colloidal silica gel into the model is explained.

The different simulations and sensitivity analysis with the presentation of their results are expressed in Chapter 5, and the base scenario is described. Sensitivity analysis is presented in

terms porosity-permeability relation, of reservoir temperature change, of various colloidal silica concentration of the injected solution and different injection rates, respectively.

In Chapter 6, a different simulation is proposed to present the ability of the TOUGHREACT code to remove the emplaced gel with the injection of a highly alkaline solution which raises the pH to alkaline conditions.

Chapter 7 includes a discussion of the research.

Chapter 8 gives a summary and conclusion to this research.

Chapter 9 provides suggestions for future work.

CHAPTER 2. LITERATURE SURVEY RELATED TO COLLOIDAL SILICA

2.1. DPR FLUIDS OVERVIEW

At the start, DPR fluids were used for enhanced oil recovery (EOR) operations because a property of DPR fluid is an ability to reduce permeability to water by a greater factor than that to oil or gas (Seright & Liang 1995). A DPR fluid is usually a chemical that forms a gel in the pore space. In addition to gelation, the retention of the DPR fluid also contributes to permeability reduction. Generally, the permeability reduction increases as the initial permeability decreases (Helleren 2011). However, DPR fluids are also used for total blockage of pathways. This application is usually used to shut-off high permeability layers with high water cut, and for casing repairs (Burns et al. 2008).

The types of DPR fluids available today are polymer gels, silica gels and other chemicals (Society of Petroleum Engineers 2015). In Table 1 an overview of the different gels with their advantages and disadvantages is given.

- **Polymer gel**

  Polymer gel consists of a cross-linked polymer macromolecules network inflated with a solvent such as water. They are divided into two groups: synthetic polymers and biopolymers and have the ability to reversibly swell or shrink (up to 1000 times in volume) due to small changes in their environment (pH, temperature, electric field). Micro sized gel fibers contract in milliseconds, while thick polymers layers require minutes to react (up to 2 hours or even days) (MIT Physics Department 2003).

  Synthetic polymers are produced synthetically. Polyacrylamide (PAM) – water-soluble polymers are one of the widely used synthetic polymers for EOR and can be in various forms (i.e. in liquid phase, gels, powder). Their performance depends on the molecular weight and degree of hydrolysis. When partially hydrolyzed, some of the acrylamide is replaced by or converted into acrylic acid. This replacement tends to increase the viscosity of fresh water but reduces the viscosity of hard water.

  Biopolymers are formed by living organisms and have a molecular weight and structure smaller than synthetic polymer. Therefore, it gives hardness due to their excellent molecular stiffness that causes a good viscosifying effect in salinity water and a bad viscosifying force in fresh water (Selle 2005).

- **Inorganic gel and resin/elastomers**

  Inorganic gels consist of inorganic chemicals which need an activator to gel. They serve for plugging lost circulation, zone squeezing and consolidating weak formations and are

easily injected into the reservoir because the chemicals used are as thin as water. However, inorganic gels present some disadvantages such as short gel time and little strength.

Resins such as Phenolic, Epoxy, and Furfuryl alcohol are commonly used due to their physical strength. They are mainly used to seal fractures, vugs, channels and perforations but are relatively expensive (Helleren 2011).

- **Silica gel**

  Silica gels consist of two categories: sodium silicate gel and colloidal silica gels. A colloidal silica based gelling system is used in this study. Therefore, colloidal silica-based gels are discussed in detail in the next sections.

  Sodium silicate is used in field operations because they can form a gel if triggered by an internal or external activator. Internal activators work by decomposing to a species such as an organic acid that can start gelation. These activators are reviewed by Krumrine and Boyce (1985). An external activator such as magnesium chloride or calcium solution initiates the gelation by precipitating silicates when in contact with a sodium silicate solution (Nasr-El-Din & Taylor 2005).

  Colloidal silica gel is a chemical grout that is currently investigated for its potential use in various treatments. Noll et al. (1992) and Moridis et al. (1999) studied colloidal silica in the development of an efficient technology for in situ contaminant containment and placement of subsurface barriers, Gallagher & Finsterle (2004) and Gallagher et al. (2007) investigated the possibility of passive site stabilization and liquefaction mitigation, respectively, and Jurinak & Summers (1991) look into enhanced oil recovery operations through experimental and modeling investigations.

In Table 1, a summary of the DPR fluids reviewed is given and the DPR fluid chosen and used in this study is highlighted.

Table 1: Advantages and disadvantages of DPR fluids

Type	Advantages	Disadvantages
Synthetic polymer	- High yield in normal water - High injectivity - Biological and chemical stability	- No salt resistance - Expensive - Shear sensitivity
Biopolymer	- Environmentally friendly - Shear stable - Insensitive to salinity	- Susceptibility to biological and chemical degradation - Injectability issues due to microorganism fermentation processes

Inorganic gel	- Water thin - Environmentally friendly	- Low strength - Short gel time - Expensive - Short lifetime - Need an activator
Resin	- Good mechanical strength - Good bonding strength - Thermally stable - Excellent chemical inertness	- Limited penetration - Complex operations - Expensive - Limited to shallow reservoir
Sodium silicate	- Controlled penetration - Water thin - Excellent setting characteristics - High strength - Environmentally friendly - Inexpensive	- Need an activator
Colloidal silica gel	- Water thin - Environmentally friendly - Inexpensive - Chemically stable - Thermally stable	- Strong pH dependence

2.2. HISTORY OF COLLOIDAL SILICA INVESTIGATION

In the past, experimental tests used colloidal silica for environmental remediation and permeability reduction. Jurinak & Summers (1991) used colloidal silica to three different applications: water-injection-profile modification, water-production control, and casing repair for environmental regulations. They used Du Pont Ludox® 10 wt% colloidal silica (7-nm particle size) in all laboratory and field testing. Only one of four injection profile treatment was a technical success. The success was the plugging of a sand layer by colloidal silica injection resulting in a 90% reduction in injection rate compared with the initial pretreatment testing. However, even though technically successful, the treatment was not considered an economic success because no increase in oil production occurred to offset the treatment cost. The three failures were attributed to pressure parting. Two of three production-well treatment were technical and economic successes. The colloidal silica solution was used to seal an unproductive sand zone in an oil production well and allowed the production well to return to service. The reason of the unique failure might be a migration of the solution away from the sand zone before gelation. Finally, three of four casing-repair operations lead the wells into temporary compliance with regulatory standards.

Noll et al. (1993) and Persoff et al. (1995) investigated the development of permeability barriers for waste and contaminants isolation. Noll et al. (1993) carried out pilot field application to address the feasibility of using 5 wt% colloidal silica gel to stabilize contamination hot spots and to construct (in situ) containment permeability barrier. The injection was operated through a central injection well and extraction from radial production wells. Results showed desired permeability reduction and good correlation led to confirming the emplacement model. Persoff et al. (1995) reported laboratory work and numerical simulation to support development and demonstration of injectable barriers formed from colloidal silica grout assessing two main parameters, gel time and plume emplacement control.

Field injection through unsaturated heterogeneous unsaturated deposits of sand silt and gravel was conducted by Moridis et al. (1996) to create a subsurface barrier. Excavation of the grout allowed visual evaluation of the successful permeation of the soil and the sufficient strength of the colloidal gel. For this, they injected about 3.8 L of 30 wt% colloidal silica solution into two injection wells at depths of 3.0, 3.6 and 4.2 m.

North-Abbott et al. (2001) deployed the first colloidal silica barrier at a radioactively contaminated site at Brookhaven National Laboratory (BNL) on Long Island, New York. Grout was injected between 6 and 7 meters below ground water level down to approximately 10 meters below ground level. The barrier emplacement took 2 and half weeks and encapsulated the 73 cubic meter [m^3] of activated soil. A test panel was emplaced close to the fence performing in situ hydraulic conductivity measurements. Results showed that the flux through the trial panel met the BNL requirement.

Gallagher & Mitchell (2002), Gallagher et al. (2007) and Gallagher & Lin (2009) assessed the feasibility of colloidal silica gel for mitigation of liquefaction risk. Laboratory and field applications indicated the ability of the gel to reduce liquefaction risk by increasing the deformation resistance of loose sand.

2.3. COLLOIDAL SILICA PROPERTIES

Colloidal silica (Figure 1) refers to stable aqueous dispersions of discrete nonporous particles of amorphous silicon dioxide ($Si0_2$). Commercial solutions contain 15 to 40 wt% $_{Si022}$ as sp_herical particles with specific surface area ranging from 100 to 400 m^2/g. Specific surface area is an important characteristic as it is directly involved in dissolution and precipitation reaction rates. Colloidal silica can be used for water control and near well treatment in the scope of environmental applications. The advantages of colloidal silica well treatment can be summarized as (Lakatos et al. 1999):

- Water-like viscosity allowing deep penetration;
- Environmental friendly;
- Inexpensive;

- Chemically and thermally stable;
- Easily removable in case of treatment failure.

Figure 1: Colloidal silica sol

The disadvantages of Colloidal silica gel are the blocking effect and the gelation mechanisms. The blocking effect of the gel is reduced with time because the gel tends to shrink. Also, the gelation time of colloidal silica gel might be difficult to control as it results from an interaction of pH, temperature, and reacting components concentrations (Helleren 2011).

During manufacture process, colloidal silica solutions are stabilized against gelation by keeping them at moderate pH (9.5 to 10.5) and high silicon dioxide/ alkali ratios (e.g., $Si0_2/Na_20$> 50). Alkaline solutions are used to keep the solutions stable, because of silica particle repulsion resulting from surface ionization in alkaline solution. Gelation can be triggered by decreasing the repulsive forces resulting to particle collision, bonding, and aggregation into long-chain networks which cause the colloidal particles to coagulate. Particle collision is promoted by reducing the pH of a stable alkaline solution and such by different ways (Jurinak & Summers 1991; Gallagher & Mitchell 2002):

- Adding cations to the solution results in charge screening and reduces gel time. Divalent cations (Ca^{2+} and Mg^{2+}) have a greater effect on gelation kinetics than monovalent cations (Na^{+} and K^{+}) because they screen silica more efficiently;
- Increasing the particle concentration in the solution either by increasing total silica concentration at fixed particle size or by decreasing particle size at fixed total silica concentration;
- At fixed pH and salinity, the gel times of colloidal silica solutions follow a simple first order Arrhenius temperature dependence:

$$K = A_f e^{-E_a/(RT)} \quad (2.1)$$

With K being the rate constant, T the absolute temperature [K], A_f the frequency factor [1/min] which is the frequency of collisions between molecules and determined by experimental work, E_a the activation energy for the reaction [J/mol] and R the molar gas constant (8.3145 [J/(°K*mole)]) (Arrhenius 1889).

Minimum gel times tend to occur between pH 5 and 6 and higher gel times can be achieved if the pH is outside this range (Gallagher & Mitchell 2002). Gel time for a 5 wt% sol of LUDOX range from as little as 20 minutes to more than 49 days in the pH range of 5 to 9.5 (Noll et al. 1992). Figure 2 shows the result of a study conducted on silica sol to see the pH effect on gelation time.

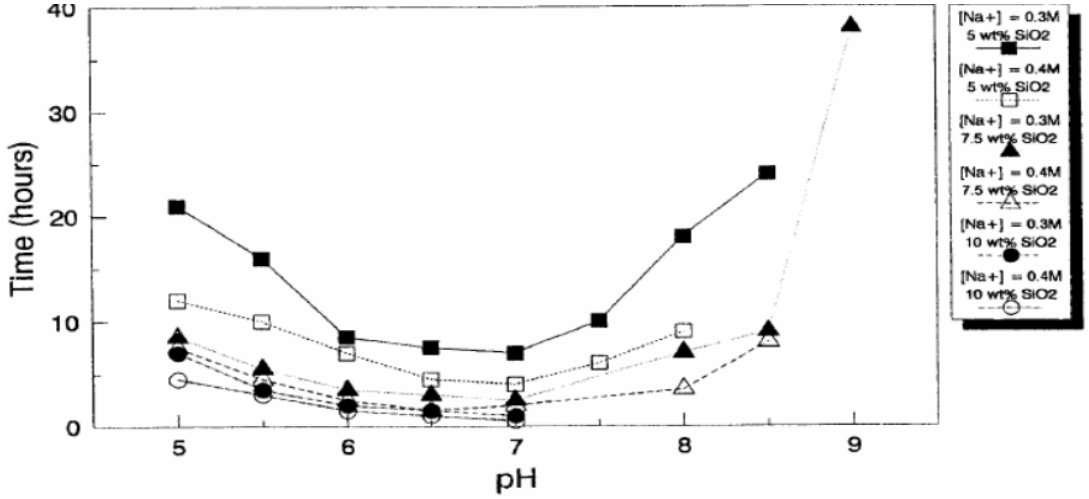

Figure 2: Silica solution gelling time data (Jurinak et al. 1989).

The temperature and pH are essential for the particles solubility. The silica particles are negatively charged above 6-7 pH to 10.5 and repel each other. The particles thereby grow until diameter reaches 5-10 nm, and after that, the growth is slowed. However, at high temperatures growth continues to larger particles. Therefore, gelation can be delayed by reducing the temperature. Figure 3 indicates how the pH of the solution can influence the stability of silicate. When salts are present, gelation occurs because of the reduction in charge repulsion. Gelation can be managed by controlling the pH. When the silicate solution pH is reduced, it can gel by polymerization of the silicate. Therefore, the gelation time can be approximately adjusted by controlling the pH of the solution. Acid is added to the silicate solution to reduce the pH (Helleren 2011).

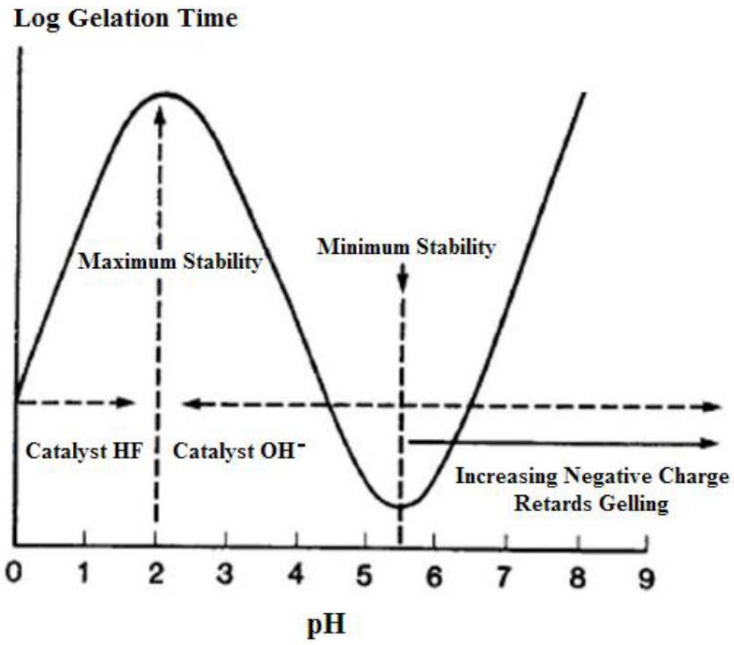

Figure 3: Stability of silicate (Vinot et al. 1989)

Particle bonding probably results from the formation of siloxane (Si-O-Si) bonds at points of interparticle contact. Hydroxide ion catalyzes bonding. Gelation occurs when particle aggregation ultimately forms a uniform 3D network of long, bead-like strings of silica particles (Jurinak & Summers 1991). The polymerization, which is the process where the silicates increase in molecular weight, occurs in three simultaneous stages:

- Condensation of monomer and dimmer silicate species to form particles;
- Growth of particles;
- Linking of individual particles to form chains and subsequent networks, to form microgel.

Figure 4 shows the polymerization of silicate and the effect of pH, salinity and particles size. The “B” way indicates that in a solution of pH between 7 and 10 and with little acid and salinity present, particles grow as the number of particles decreases and remain soluble (liquid phase). The “A” way shows that in a solution of pH inferior to 7 or between 7 and 10 but with the presence of acid and salt, the particles aggregate into 3-D networks and form gels (solid phase) (Helleren 2011).

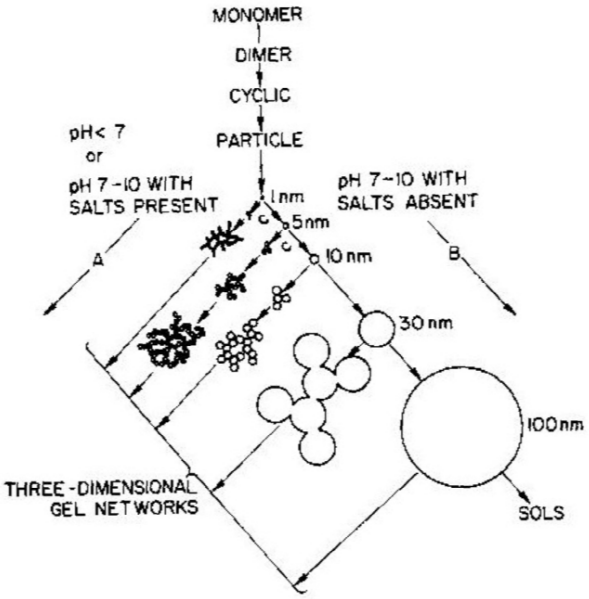

Figure 4: Polymerization of silicate (Iler 1979).

Although the chemistry of silicates is not yet completely understood, Iler (1979) stated the following equilibria:

$$SiO_2 + 2H_2O = Si(OH)_4$$

$$Si(OH)_4 + OH^- = HSiO_3^- + 2H_2O$$

$$2HSiO_3^- = Si_2O_5^- + H_2O$$

$$Si_2O_5^- + H_2O = HSi_2O_6^{3-} + H^+$$

$$HSiO_3^- + OH^- = SiO_3^{2-} + H_2O$$

When the concentration of $Si(OH)_4$ is found to be above 100-200 ppm in an aqueous solution, and in the meantime no solid phase is present, monomer and dimmer silicate condense to particles. However, if the concentration of $Si(OH)_4$ is less than 100 ppm, the solution remains stable and soluble.

2.4. FACTORS AFFECTING GELATION

It is an asset to be aware of the gelling kinetics and the factors that might have an effect on the gelling behavior to perform gel treatment without issues. The factors presented below apply to any gel/polymer, but are in this study, reported to colloidal silica gel. The factors influencing gelation the most are (Helleren 2011):

Reservoir type:

Because the objective of gel treatment is to reduce permeability's zones, these are most successful in stratified reservoirs with layers of different permeability. This setting causes water shut-off in high permeability layers first and is therefore mostly used with injection wells.

Gel system:

The gel system consists of three main components which are the base material, the reactants, and an accelerator. The base material is related to the type of gel used, its structure strength and the ability of injection. It is what will form the matrix. Reactants are the chemical components that make the solution to gel. In this research, the reactants are the SiO_2 particles. The presence of an accelerator is not always needed but can be used to control the gelation time (mostly solution influencing pH in the case of colloidal silica).

Gelation time:

The gelation time starts as soon as the viscosity of the injected solution increases (when the solution starts to gel) and depends on the reaction rate of the gel.

Reaction rate:

The speed at which a chemical reaction proceeds is called reaction rate. It is often expressed regarding either the concentration (amount per unit volume) of a product that is formed in a unit of time or the concentration of a reactant that is consumed in a unit of time (Laidler n.d.). In a rate expression: $C_1 + C_2 \rightarrow$ products, the reaction rate is given by:

$$r_k = \mathrm{K} \prod_{i=1}^{n_c} [C_i]^{e_k} \qquad (2.2.)$$

r_k: Reaction rate [kg/(min*cm³)]
K: Rate constant [1/min]
C_i: Concentration of reactants [kg/cm³]
e_k: Order of reaction [-]

The reaction rate is depending on the reactants concentration because a reaction occurs mainly due to collisions between the molecules of the reactants. When the reactants concentrations increase, the collisions between molecules increase as well resulting in a faster reaction. The reaction rate is also depending on the order of the reaction which is the power of the reactant C_i, expressing the contribution of the component C_i in the reaction. The order of reaction varies from 0, 1, 2, n. An order of reaction equal to zero means that the reaction is not affected by the concentration of the corresponding reactant. The order of reaction is found by experimental work (Masterton & Hurley 2004).

An activation energy (E_a) is required to make the collision between molecules active. As already defined above, the majority of reactions are following the simple first order Arrhenius temperature dependent reaction (Equation 2.1.). Therefore, the reactions are increased as the temperature is increased. The molecules collisions are raised as the molecules obtain higher energy and speed with the higher temperature and therefore more reactions are happening.

Residence time:

Residence time is the average length of time that the fluid remains in a certain location, in most cases, in the reservoir. Too short residence time may result in a gel that is not entirely formed, which affects the strength and blocking effect of the gel. In this research, the gel solution is only injected and is not taken out of the reservoir by a production well. Therefore, the gel is not impacted by a short residence time and has time to form. The residence time can be related to the injection rate as:

$$t_{res} = \frac{V_p}{q_{inj}} = \frac{\phi_f * V_{res}}{q_{inj}} \qquad (2.3.)$$

q_{inj} : Injection rate [l/min]
ϕ_f : Fluid porosity [-]
V_p : Pore volume [l]
t_{res} : Residence time [min]
V_{res} : Volume reservoir [l]

Retention:

The residence time increases as the injection rate decreases leading to an increase in particles size or to a gel network formation. Therefore, more particles accumulate in the pore throats resulting in permeability reduction (Nabzar et al. 1996). The mobility reduction following DPR fluid flooding is given by the mobility reduction factor (Mishra et al. 2014):

$$M = \frac{k_w \mu_p}{k_p \mu_w} \qquad (2.4.)$$

M: Mobility reduction factor [-]
k_w: Effective water permeability [mD]
k_p: Effective DPR fluid permeability [mD]
μ_w: Water viscosity [cP]
μ_p: Silicate/Polymer (DPR fluid) viscosity [cP]

A mobility ratio of approximately 1, or less, indicates that the injected fluid cannot travel faster than the displaced fluid. For instance, when M=10, the water ability to flow is 10 times larger than that of the injected fluid. The permeability reduction is given by the residual resistance factor RRF (Ahmed & Meehan 2012):

$$RRF = \frac{\lambda_{before}}{\lambda_{after}} \qquad (2.5.)$$

RRF: Residual resistance factor [-]
λ_{before}: Mobility of water before DPR fluid flow [mD/cP]
λ_{after}: Mobility of water after DPR fluid flow [mD/cP]

In this research, the water mobility reduction is only considered regarding pore throats reduction and material permeability reduction due to gel emplacement because TOUGHREACT does not allow to calculate the fluid characteristics (mobility, viscosity, liquid permeability).

Dispersion:
When fluid is injected into the reservoir, mixing occurs between the displaced and displacing fluids. In other words, there is dispersion between fluids. During its travel through the formation, the injected fluid gets more and more diluted. Dispersion is crucial regarding the size of the DPR fluid injected to get a complete blockage of the pore throats (Green & Willhite 1998). However, the dispersion is left out of this research to simplify the conceptual model.

Injection rate:
Maybe the most difficult parameter to estimate, the injection rate has to be sufficient enough to get the fluid into the reservoir and the zones targeted, but small enough to prevent pressure parting.

CHAPTER 3. THEORETICAL BACKGROUND OF GEL INJECTION AND TOUGHREACT CODE GOVERNING EQUATIONS

3.1. INTRODUCTION

The following chapter is a theoretical background of concepts regarding the gel injection. The concepts essential for this research are explained regarding the TOUGHREACT code. Further details and more information can be found in the TOUGHREACT versions 2.0 user's guide by Xu et al., (2012).

To investigate fluid, heat and solute transport, as well as chemical reactions in the subsurface, TOUGHREACT was developed. A reactive transport module was implemented in the existing framework of the non-isothermal multi-component fluid and heat transport simulator TOUGH2 (Pruess et al. 1999). Some subsurface thermo-physical-chemical processes are considered under various thermohydrological and geochemical conditions of pressure, temperature, water saturation, and ionic strength. The code applies to one-, two- or three- dimensional porous and fractured media with physical and chemical heterogeneity. The code can deal with any number of chemical species present in liquid, gas and solid phases (Xu et al. 2012)

The major processes for fluid and heat flow consist of (1) fluid flowing in both liquid and gas phases under pressure, viscous, and gravity forces; (2) interactions between flowing phases represented by characteristic curves (relative permeability and capillary pressure); (3) heat flowing by conduction and convection, and (4) diffusion of water vapor and air. Thermophysical and geochemical properties are calculated as a function of temperatures, such as fluid (gas and liquid) density and viscosity, and thermodynamic and kinetic data for mineral-water-gas reactions. Transport of aqueous and gaseous species by advection and molecular diffusion are considered in both liquid and gas phases. Aqueous and surface complexation, acid-base, redox, gas dissolution/exsolution, and multi-site cation exchange are considered under the local equilibrium assumption. Mineral dissolution and precipitation proceed under either equilibrium or kinetic constraints (Xu et al. 1999). Intra-aqueous kinetics and biodegradation (Xu 2008; Xu et al. 2009; Spycher et al. 2009) and surface complexation using non-electrostatic, constant capacity and double layer electrostatic models (Zheng et al. 2009), are incorporated into Version 2 of TOUGHREACT. Mineral dissolution and precipitation can proceed either subject to local equilibrium or kinetic conditions. Linear adsorption and decay can also be included (Xu et al. 2012).

3.2. PRINCIPLES OF FLOW

Grouting gel is injected into the well as a liquid solution to reduce the high permeability layers of the reservoir. Before its gelation, the solution is flowing into the reservoir following the basic concept of Darcy's flow.

3.2.1. Darcy's law

Darcy's law is the equation that defines the ability of a fluid to flow through a porous medium. The principle is that the amount of flow between two points is directly proportional to the difference in pressure between these two points and the medium ability to impede the flow. In other words, Darcy's law is a simple proportional relationship between the instantaneous discharge rate through a porous medium and the pressure drop over a given distance (FracFocus Chemical Disclosure Registry 2016). Darcy's law is usually written as:

$$Q_l = -K_l A \frac{dh}{dl} \qquad (3.1.)$$

where Q_l is the discharge in the l-direction [m³/d], K_l is the hydraulic conductivity [m/d], A is the cross-sectional area [m²], and $\frac{dh}{dl}$ is the hydraulic gradient, that is, the change in head over the length of interest [-]. The minus sign is in Equation 3.1. because head decrease in the flow direction (Fitts 2012). In another form, Darcy's law can be expressed regarding flux as the discharge per cross-sectional area:

$$q_l = \frac{Q_l}{A} = -K_l \frac{dh}{dl} \qquad (3.2.)$$

where q_l is the specific discharge in the l-direction [m/d] also called the Darcy velocity.

3.2.2. Hydraulic conductivity

The hydraulic conductivity K is a measure of the ease with which a medium transmits water. Higher K materials transmit water more efficiently than low K materials. Commonly, the distribution of hydraulic conductivity over a real subsurface material is irregular. Within a heterogeneous material, the value of K varies spatially, whereas in a homogeneous material K is the same over different localities. Anisotropy implies that the value of K depends on direction ($K_x \neq K_y \neq K_z$). Isotropy implies that K is independent of direction at a given location ($K_x = K_y = K_z$). Usually, K_z is often smaller than K_x and K_y due to strong horizontal layering (Fitts 2012).

3.2.3. Porosity

The total porosity is defined as the ratio of the entire pore space in a rock to its bulk volume. In very clean sands, total porosity is equal to effective porosity.

$$\phi = \frac{V_p}{V_B} \qquad (3.3.)$$

where ϕ equal porosity [-]; V_p is pore volume [m³]; V_B is the bulk volume [m³]. Pore volume is the total volume of pore spaces in the rock and bulk volume is physical volume of the rock, including the pore spaces and matrix materials that compose the rock (Ezekwe Nnaemeka 2010).
The effective porosity of a porous medium is defined as:

$$\phi_e = \frac{V_v}{V_t} \tag{3.4.}$$

where ϕ_e is the effective porosity of the medium [-]; V_v is the volume of interconnected voids which is transmitting flow within the porous medium [m³]; V_t is the volume total of the porous medium [m³]. The effective porosity can differ significantly from the total porosity, if the amount of pores that are not interconnected (i.e. isolated pore) is high (Fitts 2012)(Fitts 2012).

3.2.4. Permeability

The hydraulic conductivity is unique to the flow of fresh water through a porous medium. However, the flow of different fluids can be of interest, and another parameter has to be defined, that is the intrinsic permeability. The intrinsic permeability κ [m²], unlike the hydraulic conductivity K, is independent of fluid properties and depends only on the medium. The two parameters are proportional and related as follows (Hubbert 1940):

$$\kappa = \frac{K\mu}{\rho_f g} \tag{3.5.}$$

where μ is the dynamic viscosity [kg/(m*s)] of the fluid, ρ_f is the density of the fluid [kg/m³] and g is gravitational acceleration [m/s²].

3.2.5. Mathematical equation for flow and transport in TOUGHREACT

The flow and transport equations are derived from the principle of mass (or energy) conservation. Aqueous species are subject to carriage in the liquid phase and local chemical interactions with the solid and gaseous phases. Chemical transport equations are written regarding total dissolved concentrations of chemical components comprised of concentrations of their basis species plus their associated aqueous secondary species. Advection and diffusion are considered for chemical transport, and diffusion coefficients are assumed to be the same for all aqueous species. Table 2 summarizes these equations, and Table 3 gives the meaning of symbols used (Xu et al. 2012).

Table 2: Governing equation for fluid and heat flow, and chemical transport.

General governing equation: $$\frac{\partial M_k}{\partial t} = -\nabla F_k + q_k$$

Darcy's Law : $$\boldsymbol{u}_\beta = -k\frac{k_{r\beta}}{\mu_\beta}(\nabla P_\beta - \rho_\beta \boldsymbol{g}) \qquad \beta = l, g$$

	Mass accumulation	Mass flux	Source/Sink
Water :	$M_w = \phi(S_l\rho_l X_{wl} + S_g\rho_g X_{wg})$	$F_w = X_{wl}\rho_l\boldsymbol{u}_l + X_{wg}\rho_g\boldsymbol{u}_g$	$q_w = q_{wl} + q_{wg}$
Air :	$M_c = \phi(S_l\rho_l X_{cl} + S_g\rho_g X_{cg})$	$F_c = X_{cl}\rho_l\boldsymbol{u}_l + X_{cg}\rho_g\boldsymbol{u}_g$	$q_c = q_{cl} + q_{cg} + q_{cr}$
Heat :	$M_h = \phi(S_l\rho_l U_l + S_g\rho_g U_g) + (1-\phi)\rho_s U_s$	$F_h = \sum_{\beta=1,g} h_\beta\rho_\beta\boldsymbol{u}_\beta - \lambda\nabla T$	q_h
Chemical component in the liquid phase $(\boldsymbol{J} = \mathbf{1}, \mathbf{2}, \ldots, \boldsymbol{N_l})$ **:**	$M_j = \phi S_l C_{jl}$	$F_j = \boldsymbol{u}_l C_{jl} - (\tau\phi S_l D_l)\nabla C_{jl}$ $\tau_\beta = \phi^{1/3} S_\beta^{7/3}$	$q_j = q_{jl} + q_{js} + q_{jg}$

Table 3: Symbols used in Table 2.

C	component concentration, mol L^{-1}	ρ	density, kg m^{-3}
D	diffusion coefficient, $m^2 s^{-1}$	μ	viscosity, kg $m^{-1}s^{-1}$
F	mass flux, kg $m^{-2}s^{-1}$ (*)	λ	heat conductivity, W $m^{-1}K^{-1}$
k	permeability, m^2		
k_r	relative permeability	Subscripts:	
g	gravitational acceleration, m s^{-2}	c	air
M	mass accumulation, kg m^{-3}	g	gas phase
N	number of chemical components	h	heat
p	pressure, Pa	j	aqueous chemical component
q	source/sink	l	liquid phase
S	saturation	r	reaction
T	temperature, °C	s	solid phase
U	internal energy, J kg^{-1}	w	water
u	Darcy velocity, m s^{-1}	κ	governing equation index
X	mass fraction	β	phase index
ϕ	porosity	τ	medium tortuosity

(*) For chemical transport and reaction calculations, molar units are used instead of kg.

3.2.6. Radial flow from a well

This study focuses on gel flooding from an injection well followed with direct gel formation around it. Therefore, the model was built considering the well as the center of an axisymmetric domain. According to Haitjema (1995), if flow in the aquifer is due to the well alone, the flow pattern is

radially symmetric as indicated in Figure 5. The origin of a radial (r, θ) coordinate system is chosen at the center of the well and because of radial symmetry, there is only flow parallel to the direction r. Applying continuity of flow across a circle of radius r around the well gives:

$$Q = 2\pi r(+Q_r) \qquad (3.6.)$$

Where Q [L³/T] is the discharge (injection rate) of the well, and where (Q_r) is the discharge vector component across the circle per unit length of the circle. The positive sign in front of Q_r indicates that the flow occurs in the positive r-direction.

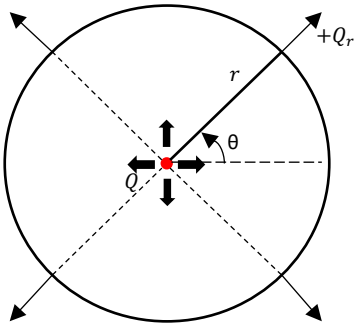

Figure 5: Radial flow toward a well

The discharge vector component Q_r satisfies Darcy's law as defined in Equation 3.1. and 3.2. and is similar in each radial direction. Because of the different permeability layers, the flow from the well at the different elevation is dependent of the layers property.

3.3. MODEL FEATURES

3.3.1. Multi-layer flow

The model can be constructed with layers of different permeability to induce preferential flow into the most permeable layers. This feature is important in the scope of this research since the gel is injected into the high permeability layers of the aquifer (layers without clogging materials). The concept of preferential flow is directly related to Darcy's law define in equations (3.1.) and (3.2.), as well as in Table 2. Increasing the permeability or the related conductivity (see Equation 3.3.), rises the flow velocity as it enhances the ease with which the medium transmits the flowing fluid.

3.3.2. Radial Mesh

A mesh is modeled as a 2D slice through a cylinder centered at (0,0,0) as shown in Figure 6. In this slice, the red line is the portion of the cylinder that is modeled by the RZ mesh. It appears in the model as a 2D regular mesh with the X divisions representing the radial segments and the number of Y division being 1. Although the radial mesh is displayed as a rectangular mesh with only one Y division, all cell data is displayed and written to the TOUGH input file with the correct cell volumes and connection areas to represent the cell revolved around the center of the cylinder (Thunderhead Engineering 2007). This type of mesh is ideal for a simple model of injection/production into the reservoir with axisymmetric homogeneity and wells are typically placed in the "center" of the grid.

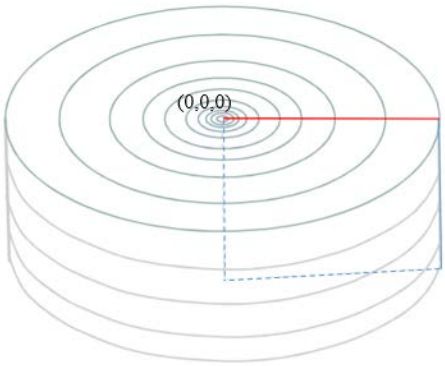

Figure 6: Radial mesh representation

3.3.3. Sink/Source

TOUGHREACT allows injecting only water or predefined "EOS" component using its well function. Therefore, instead of using a well, the solutions of which the composition can be manipulated (gel solution) are injected using cells turned into source/sink condition. To represent the well using these source/sink cells, their width as to be related to the well radius. Sources and sinks are used to define flow into or out of the cell and are typically used to represent production from or injection into a cell as a hypothetical well. The rates can be defined as constant or using a table to give time/rate pairs. In this research, the only injection is considered, and a rate (or flux) and an enthalpy for each component to be injected have to be specified.

3.4. EFFECTS OF MINERAL PRECIPITATION/DISSOLUTION ON THE PHYSICAL PROPERTIES OF THE MEDIUM

Upon its gelation, the gel solution injected is grouting the pore network of the medium. It is, therefore, important to define how the physical properties of the medium are affected by the gel emplacement.

3.4.1. Porosity change

Mineral precipitation and dissolution directly result in changes in matrix and fractures porosity. The molar volumes of minerals created by hydrolysis reactions (i.e., anhydrous phases, such as feldspars, reacting with aqueous fluids to form hydrous minerals such as zeolites or clays) are often larger than those of the primary reactant minerals; therefore, constant molar dissolution-precipitation reactions may result in porosity reductions. Porosity changes are taken into account in TOUGHREACT following this equation:

$$\phi = 1 - \sum_{m=1}^{nm} fr_m - fr_u \qquad (3.7.)$$

ϕ being the porosity of the medium, nm is the number of minerals, fr_m is the volume fraction of mineral m in the rock ($V_{mineral}/V_{medium}$, including porosity), and fr_u is the volume fraction of nonreactive rock. As the fr_m of each mineral changes, the porosity is recalculated at each time step. The porosity is not allowed to go below zero (Xu et al. 2012).

3.4.2. Matrix permeability change

Several different options are available in TOUGHREACT to deal with permeability changes due to mineral precipitation and dissolution. In this research, matrix permeability changes are calculated from changes in porosity using ratios of permeabilities calculated from the simplified Carman-Kozeny relationship (Bear 1972), and ignoring changes in grain size, tortuosity and specific surface area as follows (Xu et al. 2012):

$$k = k_i \frac{(1-\phi_i)^2}{(1-\phi)^2}\left(\frac{\phi}{\phi_i}\right)^3 \qquad (3.8.)$$

where k_i and ϕ_i are the initial permeability and porosity, respectively.

Also, one simulation is performed using the cubic law for porosity-permeability changes considering fracture porosity and permeability, and results are compared to the simulation using the Carman-Kozeny relationship. With the cubic law, fracture permeability changes are estimated from changes in porosity and assuming plane parallel fractures of uniform aperture (Steefel & Lasaga 1994). Therefore, the resulting permeability is calculated as (Xu et al. 2012):

$$k = k_i \left(\frac{\phi}{\phi_i}\right)^3 \qquad (3.9.)$$

3.5. GEOCHEMICAL FORMULATION IN TOUGHREACT

In TOUGHREACT, there is no so-called “gel/polymer module”. The basic component of the gel is injected into a solution as a primary species and the gel forms upon gelation following mineral precipitation. It is thus important to understand how TOUGHREACT deals with the geochemical system and the minerals kinetics.

The geochemical system is a combination of a subset of N_C aqueous species as basis species (or component or primary species) resulting in other species, called secondary species, such as aqueous complexes, precipitated (mineral) and gaseous species (Reed 1982; Yeh & Tripathi 1991; Steefel & Lasaga 1994). The number of independent species must be equal to the number of independent reactions. Any of the secondary species can be presented as a linear combination of the set of basis species such as:

$$S_i = \sum_{j=1}^{N_C} v_{ij} S_j \qquad i = 1, \dots, N_R \qquad (3.10.)$$

where S represents chemical species, j is the basis species index; i is the secondary species index; N_R is the number of reactions (or secondary species); and v_{ij} is the stoichiometric coefficient of j-th basis species in the i-th reaction (Xu et al. 2012).

3.5.1. Kinetic reactions among primary species

This type of reactions involve aqueous and sorption reaction kinetics and biodegradation following a general rate law:

$$r_i = \sum_{s=1}^{M} \left[\begin{array}{ll} k_{i,s} & \text{rate constant} \\ \times \prod_{j=1}^{N_l} \left(\gamma_j^{\nu_{i,j}} C_j^{\nu_{i,j}} \right) & \text{product terms} \\ \times \prod_{k=1}^{N_m} \frac{C_{i,k}}{K_{Mi,k} + C_{i,k}} & \text{Monod terms} \\ \times \prod_{p=1}^{N_p} \frac{I_{i,p}}{I_{i,p} + C_{i,p}} & \text{inhibition terms} \end{array} \right] \qquad (3.11.)$$

where r_i is the reaction rate of the i-th reaction, M is the number of mechanisms or pathways and s is the mechanism counter, k is a rate constant, (often denoted vmax, maximum specific growth constant for biodegradation), γ_j is the activity coefficient of species j, C_j is the concentration of species j (with biodegradation the product term is usually biomass concentration), $v_{i,j}$ is a stoichiometric coefficient, N_l is the number of reacting species in the forward rate term (called product terms), N_m is the number of Monod factors (Monod terms), $C_{i,k}$ is the concentration of the k-th Monod species, $C_{i,p}$ is the concentration of the p-th inhibiting species, $K_{Mi,k}$is the k-th Monod half-saturation constant of the i-th species, N_P is the number of inhibition factors (inhibition terms), and $I_{i,P}$ is the p-th inhibition constant (Xu et al. 2012).

3.5.2. Equilibrium mineral dissolution/precipitation

The mineral saturation ratio can be expressed as:

$$\Omega_m = K_m^{-1} \prod_{j=1}^{N_c} c_j^{\nu_{mj}} \gamma_j^{\nu_{mj}} \qquad m = 1, \dots, N_R \qquad (3.12.)$$

Where m is the equilibrium mineral index, and K_m is the corresponding equilibrium constant. Therefore we have at equilibrium:

$$SI_m = log_{10}\Omega_m = 0 \qquad (3.13.)$$

where SI_m is the mineral saturation index (Xu et al. 2012).

3.5.3. Kinetic mineral dissolution/precipitation

The gel injected follows kinetic dissolution and precipitation as its kinetics rates are not equal and are a function of pH and temperature. Kinetic rates can be functions of basis and non-basis species. Usually, the species appearing in rate laws happen to be basis species. In TOUGHREACT, the rate expression used is given by (Lasaga et al. 1994):

$$\mathrm{r}_n = f\left(c_1, c_2, \dots, c_{N_C}\right) = \pm k_n A_n |1 - \Omega_n^{\theta}|^{\eta} \qquad n = 1, \dots, N_q \qquad (3.14.)$$

positive values of r_n indicate dissolution, and negative values precipitation, k_n is the rate constant [moles per unit mineral surface area and unit time] which is temperature dependent, A_n is the specific reactive surface area per kg H_2O, Ω_n^θ is the kinetic mineral saturation ratio defined in (5.4.). The parameters θ and η must be determined from experiments; usually, but not always, they are taken equal to one. The temperature dependence of the reaction rate constant can be expressed reasonably well via an Arrhenius equation (Arrhenius 1889). Due to the fact that many rate constants are reported at 25°C, it is convenient to approximate rate constant dependency as a function of temperature as:

$$k = k_{25} \exp\left[\frac{-E_a}{R}\left(\frac{1}{T} - \frac{1}{298.15}\right)\right] \qquad (3.15.)$$

k_{25} is the rate constant at 25°C, E_a is the activation energy, R is gas constant, T is absolute temperature.

3.6. FLOW CHART OF THE TOUGHREACT PROGRAM

Figure 7 shows the flow chart for solving coupled non-isothermal fluid flow, solute transport, and reactive geochemistry in TOUGHREACT.

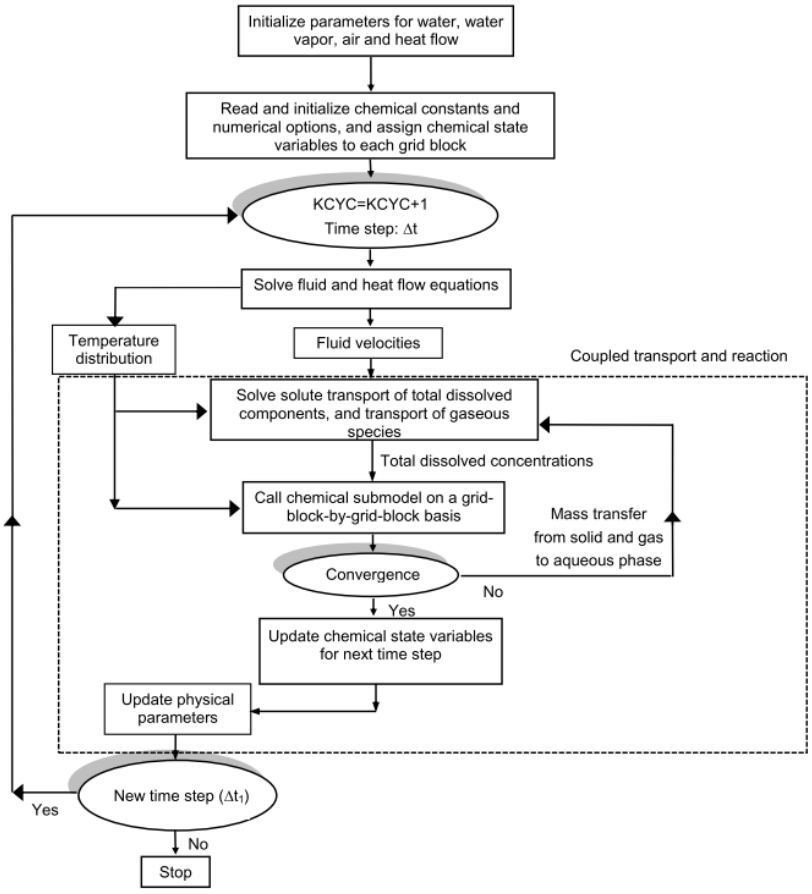

Figure 7: Flow chart of the TOUGHREACT program (Xu et al. 2012).

CHAPTER 4. MODEL DEVELOPMENT

4.1. MODEL DOMAIN AND THERMOPHYSICAL CONDITIONS

The lack of relevant information and access to data regarding the Wayang Windu field did not allow to represent the field accurately. Therefore, the hypothetical model is built only to show the feasibility of colloidal silica gel simulation with TOUGHREACT regardless the exact field characteristics. However, it was tried to match as much as possible the sparse field information found in the literature. This information is given in a literature review about the Wayang Windu field in Appendix 1.

4.1.1. Domain setup

The conceptual domain is composed of a 2D radial axisymmetry with an extent of 5 km in the lateral direction (x-direction) and 1.5 km in the vertical direction (z-direction). The model is divided in the x-direction into 50 parts increased exponentially in width by a factor of 1.21 from the left to yield a quasi-infinite boundary condition on the right side of the domain. The value of the increase factor was chosen in order to have a highly refined grid directly next to the well on the left boundary of the domain since the gel penetrates the reservoir to the extent of approximately 1 meter from the well. The conceptual model is divided into 300 cell of 5.0 m long in the z-direction. In the y-direction, the model has a width of 0.1 m.

To represent the deep liquid reservoir, the top layer of the domain corresponds to an elevation of -1.0 km above sea level and the bottom layer to an elevation of -2.5 km above sea level. As a result of the division of the cell, the domain is composed of 15000 grid blocks (50*300). The injection well of interest is located in the upper left corner of the domain (Figure 8) and has a vertical extent of 140 m starting at an elevation of -1.0 km. The well radius, corresponding to the first column of the domain, has a width of 0.076 m.

It was decided to represent the whole extent of the reservoir to avoid boundary effects from the boundaries of the domain. The well was set in the top part of the domain, close to the top boundary, to respect the situation in practice at the Wayang Windu field (See Figure 33 in Appendix). This setup might cause boundary effect on the gel injection from the top boundary. However, due to the close emplacement of the gel next to the well, the top boundary effect is negligible.

The domain parameters are given in Table 4.

Table 4: Domain setup and space discretization of the conceptual model

Parameters	Value
Horizontal extent (x-direction)	5000 m
Horizontal extent (y-direction)	0.1 m
Vertical extent (z-direction)	1500 m
X-direction division	50 cells

X-direction first column cell size (well radius)	0.076 m
X-direction increasing factor	1.21
Z-direction division	300 cells
Z-direction increasing factor	1
Total mesh	15000 grid blocks
Top layer elevation	-1000 m
Bottom layer elevation	-2500 m
Well length	140 m
Elevation of the top of the well	-1000 m
Elevation of the bottom of the well	-1140 m

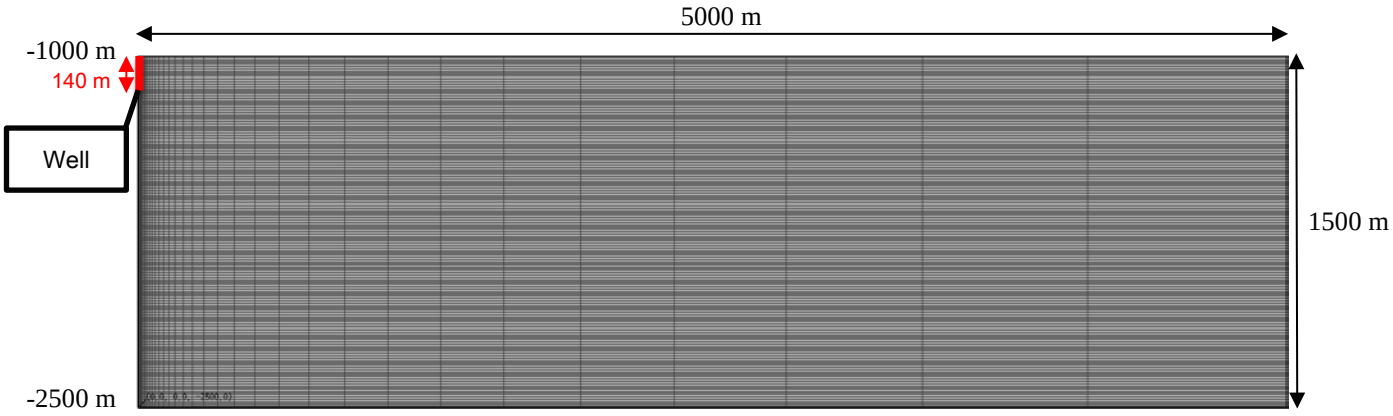

Figure 8: Domain of the conceptual model

4.1.2. Model materials

According to literature, average porosity of the reservoir is 8%, average permeability is 250 mD, rock density is 2550 kg/m³, and wet heat conductivity is 2.5 W/(m*K) (Bogie et al. 2008; Ashat 2011). These values were assigned to the entire domain, however, to represent the clogging materials reducing the optimal functioning of the injection well, several layers next to the injection well were assigned with materials of small porosity and low permeability (Figure 9). Only porosity and permeability of these clogging materials (Table 5) differ from the reservoir material.

Table 5: Materials of the model

Material	Porosity [%]	Permeability [mD]	Density [kg/m³]	Conductivity [W/(m*K)]	Specific heat [J/(kg*K)]
Reservoir material	8	250	2550	2.5	1000
Clogging materials:					
Low por/perm (Lperm)	2	5	2550	2.5	1000
Medium-Low por/perm (MLper)	3	25	2550	2.5	1000
Medium por/perm (Mperm)	4	100	2550	2.5	1000

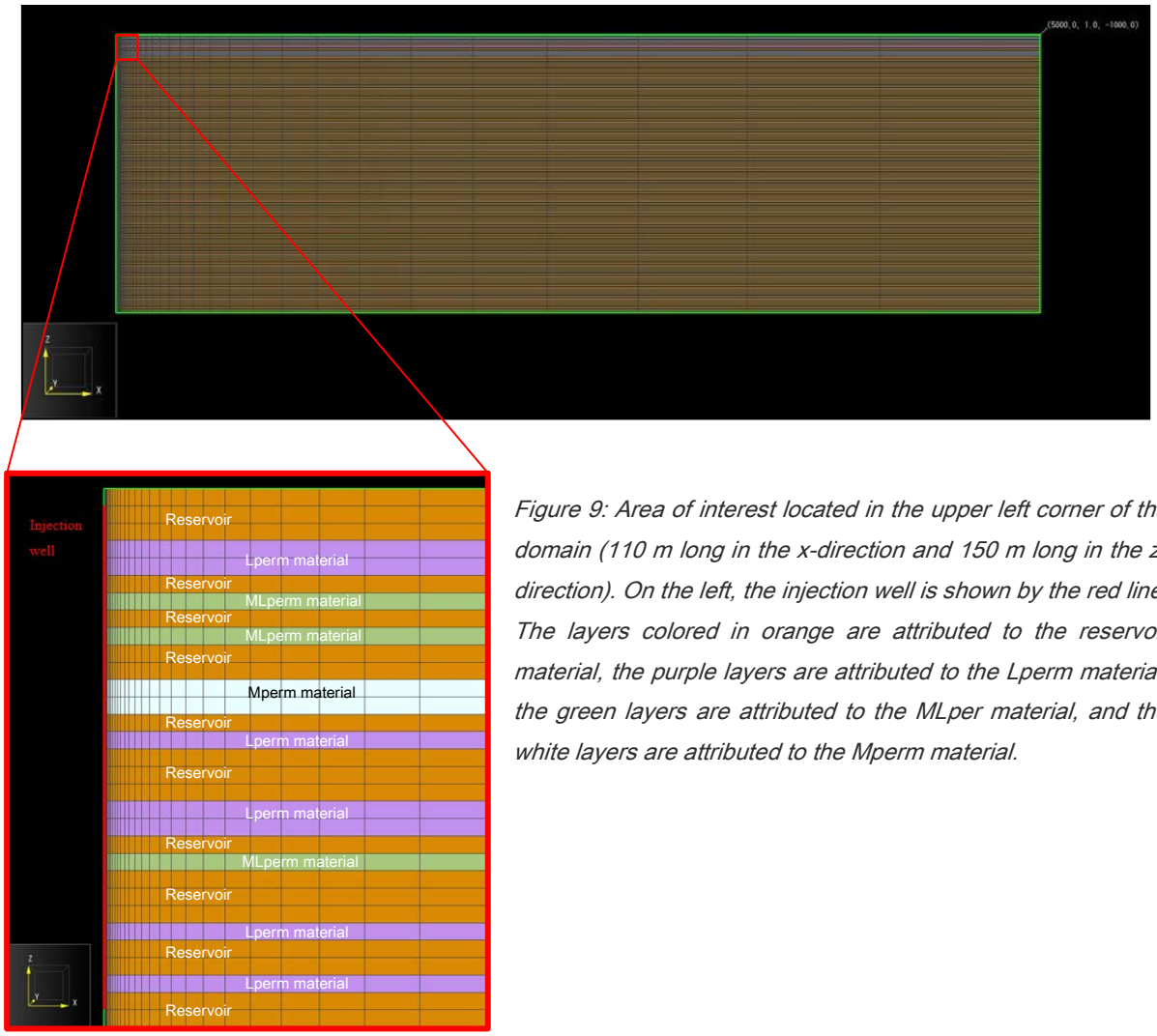

Figure 9: Area of interest located in the upper left corner of the domain (110 m long in the x-direction and 150 m long in the z-direction). On the left, the injection well is shown by the red line. The layers colored in orange are attributed to the reservoir material, the purple layers are attributed to the Lperm material, the green layers are attributed to the MLper material, and the white layers are attributed to the Mperm material.

4.1.3. Static and dynamic pressure and temperature conditions

First, a static condition was created with an initial temperature of 250 °C and an initial pressure of 160 bars that were specified across the domain. At the temperature and pressure set in this model, one liquid phase is present as saline H_2O. The relative permeability of the brine liquid phase (k_{rl}) is calculated regarding H_2O saturation (S_l) using van Genuchten (van Genuchten 1980) relation for a specified irreducible water saturation as (see parameters in Table 6):

$$k_{rl} = \sqrt{S^*}\left\{1 - \left(1 - [S^*]^{1/m}\right)^m\right\}^2 \qquad (6.1.)$$

with

$$S^* = \frac{S_l - S_{lr}}{1 - S_{lr}} \qquad (6.2.)$$

Even though, gas transport is not taken into account in these simulations, relative permeability of CO_2 phase (k_{rc}) is calculated following Corey relation (Corey 1954) based on H_2O saturation, irreducible water and CO_2 saturation as (see parameters in Table 6):

$$k_{rc} = (1 - S')^2(1 - (S')^2) \quad (6.3.)$$

with

$$S' = \frac{S_l - S_{lr}}{S_l - S_{lr} - S_{gr}} \quad (6.4.)$$

Although CO_2 is not present in this study, the capillary pressure (p_{cap}) is needed to come through interfacial tension between H_2O and CO_2 phases in the porous media and has to be specified. The capillary pressure is also calculated based on a van Genuchten relationship (van Genuchten 1980) as (see parameters in Table 6):

$$p_{cap} = -P_0\left([S^*]^{-1/m} - 1\right)^{1-m} \quad (6.5.)$$

Table 6: Initial condition parameters of the hypothetical model. Default values are based on Bogie et al. (2008), Ashat (2011), Xu et al. (2011).

Model parameters		Value
T	temperature [°C]	250
P	pressure [bar]	160
Relative permeability – van Genuchten (default values)		
m	exponent	0.457
S_{lr}	irreducible water saturation	0.3
S_{gr}	irreducible gas saturation	0.05
Capillary pressure – van Genuchten (default value)		
m	exponent	0.457
S_{lr}	irreducible water saturation	0
P_0	Strength coefficient [kPa]	19.61

With these conditions, the model run for 10 000 years to reach a steady state that was used as initial conditions for the dynamic calculations. The top layer of the domain was set to fixed state to keep its pressure and temperature constant inducing a pressure and temperature gradient (Table 7 and Figure 10). The created pressure gradient is of 80 bars/km with a pressure of 160 bars at the top of the model and 280 bars at the bottom of the model. A similar temperature gradient should be created to represent realistic conditions. However, to facilitate the simulations calculations and since only the top of the domain is of interest in this study, a constant temperature of 250°C was set to the domain. With this input, the model created a thermal gradient of 0.33 °C/km while reaching a steady state. The top of the domain has a temperature of 250°C, and the bottom of the domain has a temperature of 250.5°C. The pressure and temperature values fall within the range

bounded by the hydrostatic and lithostatic gradients and correspond to the pressure conditions of the deep liquid reservoir of the Wayang Windu field lying between -1.0 and -2.5 km above sea level.

Table 7: Pressure and temperature conditions after 10 000 years of static simulation.

Parameter	Value
Pressure at the top of the domain	160 bars
Pressure at the bottom of the domain	280 bars
Pressure gradient	80 bars/km
Temperature at the top of the domain	250°C
Temperature at the bottom of the domain	250.5°C
Temperature gradient	0.33 °C/km

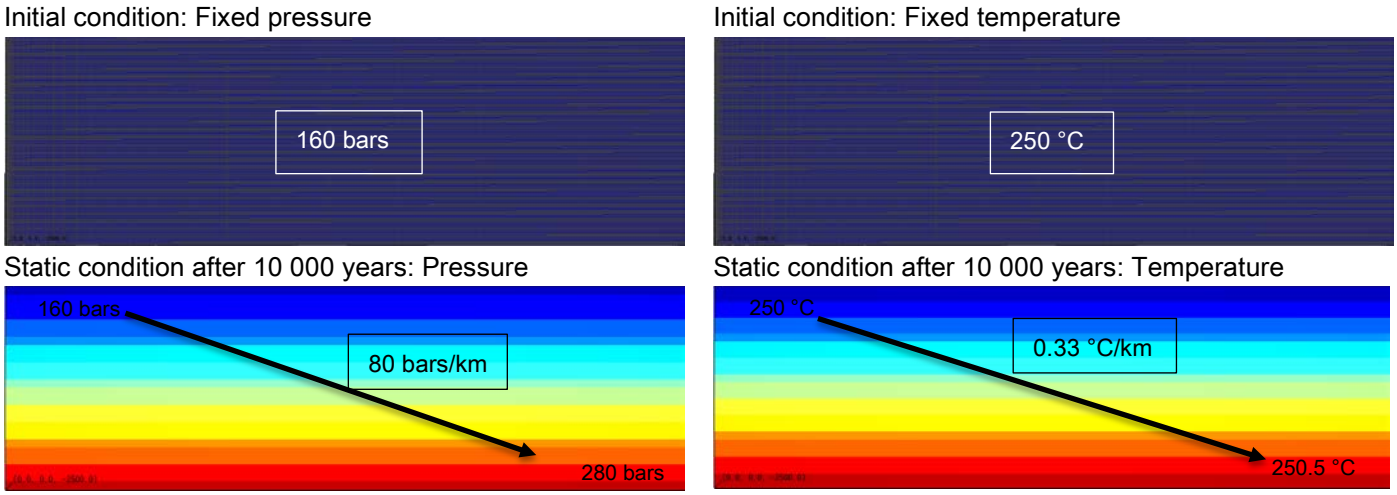

Figure 10: Initial pressure and temperature conditions (top). Static pressure and temperature conditions after 10 000 years and the resulting gradients.

The lower and upper boundary of the domain were set to fixed state to hold a no-flow condition, representing a lower and an upper confining units surrounding the reservoir. The left border of the domain corresponds to the injection well located at the center of the domain. The right boundary was set to fixed state may be considered as a flow boundary (Figure 11).

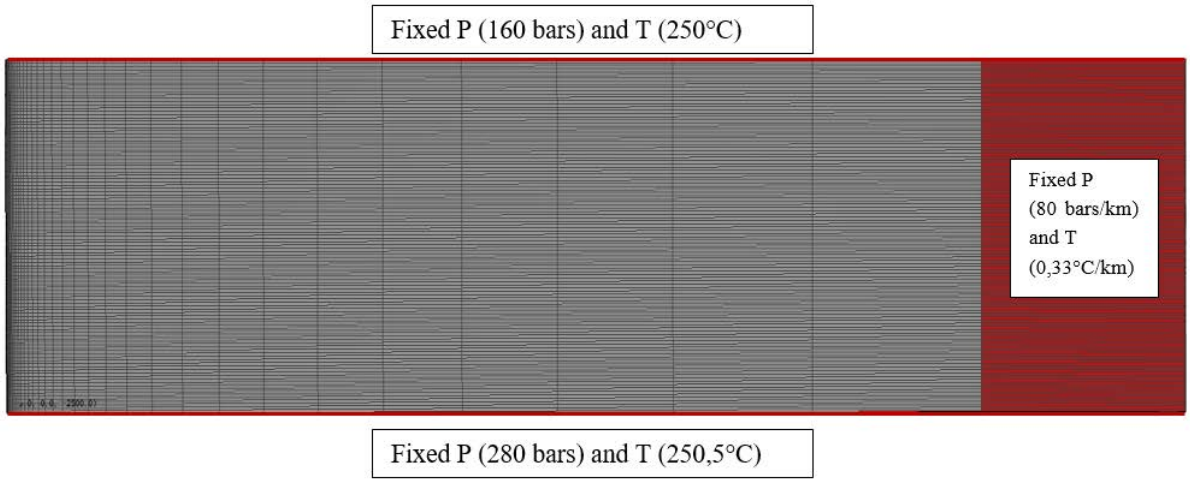

Figure 11: Fixed state cells (red cells) to hold no flow conditions and fixed pressure and temperature during dynamic simulations

4.2. GEOCHEMICAL CONDITIONS

The short time interval of the simulation justifies the use of simplified geochemical conditions. As a cause, the extent of primary species dissolution and secondary species accumulation expected to occur in this interim is extremely limited and will not significantly change the initial geochemical conditions. According to literature regarding the Wayang Windu geothermal field, the original reservoir composition is simplified to 95% of illite as main sheet silicate $((K, H_3O)\ (Al, Mg, Fe)_2(Si, Al)_4O_{10}[(OH)_2, (H_2O)])$ and 5% of prehnite as common alteration and vein minerals $(Ca_2Al(AlSi_3O_{10})(OH)_2)$. All the thermodynamic data such as dissolution and precipitation rates are taken from Palandri & Kharaka (2004) who compiled and fitted experimental data reported by many investigators. Parameters for illite were set to those of smectite. Initial mineral volume fractions, kinetic rate parameters, mineral grain radius and reactive surface area are provided in Table 8.

Table 8: List of parameters for minerals considered in the present research (Xu et al. 2004; Palandri & Kharaka 2004). *The first line indicates dissolution parameters and the second line precipitation parameters. For illite and prehnite, the third and fourth lines are acidic and basic additional mechanisms. The reactive surface area of illite and prehnite are default values from* Tianfu Xu et al., (2004) *and the one of the hypothetical colloidal silica gel is based on the average value from the LUDOX colloidal silica solution* (Anon n.d.).

Mineral	Volume fraction [cm³ mineral/cm³ solid]	Rate constant k_{25} [mol/m²/s]	Activation energy E_a [kJ/mol]	Reaction order n regarding H^+	Mineral grain radius [cm]	Reactive surface area [cm²/ g mineral]
Illite	0.95	1.66e-13	35.0	0.0	0.001	151.6
		1.66e-13	35.0	0.0		
		1.047e-11 (H^+)	23.6	0.34		
		3.02e-17 (H^+)	58.8	-0.4		
Prehnite	0.05	6.91e-14	93.4	0.0	0.001	9.8
		6.91e-14	93.4	0.0		

		2.18e-11 (H^+)	80.5	0.256		
		1.38e-15 (H^+)	93.4	-0.2		
Hypothetical colloidal silica gel	0.0	7.32e-13	60.9	0.0	5.0e-8	1000000.0
		3.80e-10	49.8	0.0		

The initial fluid composition of the deep liquid reservoir set in these simulations could not be compared with the liquid composition in practice as no sample data were found in the literature. Therefore, the initial composition (Table 9) was set to approach the weakly acidic/neutral pH of the brine found in the Wayang Windu reservoir on the simplified mineral composition and because it is a major factor in the gel emplacement.

Table 9: Initial fluid composition of the reservoir (T=250 °C).

Primary species	Concentration [mol/kg H_2O]
pH	± 6.5
AlO_2^-	7.03e-10
Ca^{2+}	0.002
Fe^{2+}	3.11e-10
H^+	1.5e-7
H_2O	1
HCO_3^-	1.0e-4
K^+	0.05
Mg^{2+}	0.01
Na^+	0.01
$SiO_2(aq)$	0.001164
Cl^-	0.01

4.3. MODEL STABILITY

Parameters regarding output controls and simulation convergence have to be defined to run a simulation with TOUGHREACT. Tables 10 gives a summary of the parameters that were manually modified for simulation stability. The other parameters in TOUGHREACT were left to their default values. For more information regarding the TOUGHREACT simulation parameters see the TOUGHREACT user's guide (Xu et al. 2012).

Table 10: TOUGHREACT parameters modified for simulation convergence and stability:

Parameters	Definition	Value
DELTEN	Time step	100.0 sec
MCYC	Max Num Time Steps	300
NOITE	Max Iterations Per Step	8
DELTMX	Max Time Step	Infinite
SL1MIN	Geochemical calculations are skipped at grid blocks where the liquid saturation is less than SL1MIN	1.0e-6

STIMAX	Geochemical calculation are skipped at grid blocks where the stoichiometric ionic strength is more than STIMAX	10 mol/kg-H_2O
MAXITPTR	Maximum number of sequential iterations between transport and chemistry.	1
TOLTR	Convergence criterion (as relative change of aqueous concentrations) for the sequential iterative (transport/chemistry) scheme.	1.0e-4
MAXITPCH	Maximum number of iterations allowed for solving chemical speciation.	400
TOLCH	Convergence criterion (as relative change of aqueous concentrations) for chemical speciation computations.	1.0e-5

4.4. TIME DISCRETISATION

The simulations were run for a total of 35 days and injection was performed during 6 hours starting on the twelfth day. It was decided to launch the injection on the twelfth day to be able to see the grouting emplacement accurately. The printed outputs were chosen to focus on the injection process as it can be seen in Table 11.

Table 11: Printed outputs times of the simulations

Printed outputs times
1 days
10 days
12 days
12.05 days *(12 days and 1.2 hours)*
12.1 days *(12 days and 2.4 hours)*
12.15 days *(12 days and 3.6 hours)*
12.2 days *(12 days and 4.8 hours)*
12.25 days *(12 days and 6 hours)*
12.3 days *(12 days and 7.2 hours)*
15 days
25 days
35 days

4.5. HYPOTHETICAL COLLOIDAL SILICA GEL EMPLACEMENT

The TOUGHREACT module has no option available concerning gel or polymer injection. However, it allows the dissolution and precipitation of various minerals included in its thermodynamic database. Therefore, a hypothetical colloidal silica gel was placed in the model based on the thermodynamic and kinetic properties and pH dependence of amorphous silica (SiO_2(am)).

Due to lack of literature regarding colloidal silica gel, the formation of amorphous silica from dissolved SiO_2(aq) was modeled in such a way that the molar volume of SiO_2(am) is increased,

representing a hypothetical gel that undergoes a large volume rise during gelation. The molar volume of SiO_2(am) was changed manually in the TOUGHREACT thermodynamic database to represent this gel. The molar volume was increased from 60.084 cm³/mol to 500 cm³/mol based on a silica gel under development at the Lawrence Berkeley National Laboratory (Druhan et al. 2014). This hypothetical gel is hereafter referred to as the “colloidal silica gel” and was injected in the model as a dissolved solute which subsequently precipitates upon contact with the neutral/acidic fluid of the reservoir.

When the colloidal silica gel undergoes gelation and accumulates at the interface between the injected solution and the neutral/acidic reservoir fluid, it is expected to reduce the porosity (Φ) and therefore the permeability (k) of the reservoir in the location where the reaction occurs. Different porosity-permeability relationships are available in the TOUGHREACT module.

However, these relations are difficult to define and are often dependent on the porous media specific geometry and reactivity. For lack of published information on the porosity-permeability relationship of the Wayang Windu field, the simplified Carman-Kozeny relationship was chosen for this paper as already mentioned in Chapter 3 (see equation 3.8.). However, one simulation using the cubic law was performed as a comparison (see equation 3.9.) (Xu et al. 2012).

CHAPTER 5. SIMULATION OF THE COLLOIDAL SILICA GEL INJECTION

5.1. INTRODUCTION

For all simulations, the domain is equivalent to the one described in the model development (Chapter 4 (Figure 9)). The following simulations and analysis differ regarding parameters only. TOUGHREACT displays permeability results using the square meter [m²] unit and does not allow to change it to millidarcy [mD]. Therefore, to give a better understanding, some value conversion from m² to mD are presented in Table 12.

Table 12: Permeability values conversion from square meter [m²] to millidarcy [mD].

Square meter [m²]	Millidarcy [mD]
9.869233E-16	1
9.869233E-15	10
4.934616E-14	50
9.869233E-14	100
1.480385E-13	150
1.973847E-13	200
2.467308E-13	250

It has to be noted that in the following sections, each diagrams plotting porosity or permeability against distance from the well have their curves starting at the first location impacted by the gel emplacement. This location is the center of the second column of the domain from the left and is at a distance of 4 cm from the well center. This first recorded location explains why the curves do not start at the origin of the x-axis (x-axis represents the distance from the well). Naturally, the direct contact between the well and the reservoir would present the average value of the reservoir material (250 mD; 0.08). However, it is left out of the diagrams to get a better vision of the curves.

Each diagrams representing permeability reduction are meant to show the permeability reduction into a high permeability zone since the interest of this research is to emplace the grouting gel in these distinct layers (see orange layers in Figure 9). Therefore, permeability reduction of the already low-permeability clogged layers was left out of the results even though a small amount of gel also penetrates the few remaining pore throats of these parts.

In the following sections, several diagrams show permeability against time. For these particular charts, it was chosen to plot the permeability reduction with time at a distance of 12 cm from the well. This location was selected to show the gel emplacement at a distance which neither too close nor too far from the well.

5.2. BASE SCENARIO: SIMULATION OF THE pH-DEPENDENT HYPOTHETICAL COLLOIDAL SILICA GEL UNDER SIMPLIFIED CONDITIONS

5.2.1. Initialization

As a first simulation, a test of the viability of the pH-dependent hypothetical colloidal silica gel to reduce the permeability of high permeability zones significantly was set up. A multiple hours injection of the gel solution was performed in the upper left corner of the domain (see Figure 8). As described in Chapter 2, colloidal silica particles remain in a stable dissolved phase at high pH (+ 9). However, solutions of high alkalinity present a gelation time of multiple hours to days and could result in failure of permeable zones shut off around the well. Therefore, the injected fluid was set to a slightly alkaline (almost neutral) solution to reduce the gelation time of the gel and to trigger the gelation process upon direct contact with the weakly acidic fluid of the reservoir. The colloidal silica gel (represented as $SiO_2(aq)$) concentration was increased to 0.822M resulting in a 5 wt% colloidal silica solution. The first porosity-permeability relationship described in Chapter 3 was used. Primary species concentrations are shown in Table 13.

Table 13: Injected 5 wt % colloidal silica solution composition (T_{sol}= 50°C)

Primary species	Concentration [mol/kg H_2O]
pH	+ 7.0
AlO_2^-	0.0303
Ca^{2+}	0.002
Fe^{2+}	3.11e-18
H^+	1.885e-7
H_2O	1
HCO_3^-	0.05
K^+	0.001
Mg^{2+}	0.005
Na^+	0.8
$SiO_2(aq)$	0.822
Cl^-	0.1

The colloidal silica solution was introduced into the system by the injection well at a uniform flow rate of 13.37 Kg-H_2O/s. The gel solution was injected for a total of 6 hours starting on the twelfth day of simulation. Figure 12 presents the situation of the colloidal silica gel (referred as $SiO_2(am)$) and permeability before the start of the gel injection and Table 14 gives the injection regime of the simulation. The case highlighted in green shows the time and volume of gel needed to achieve a complete sealing of the area next to the well.

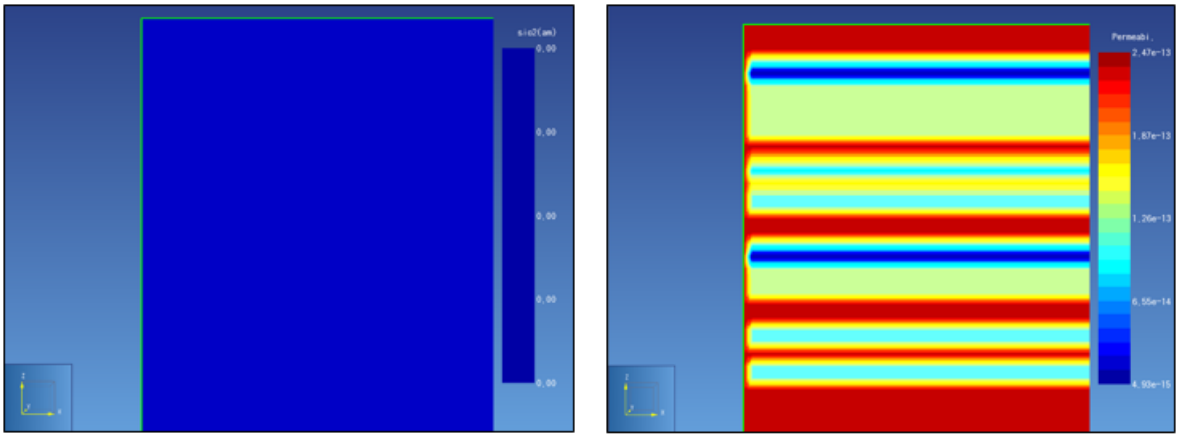

Figure 12: Initial colloidal silica gel referred as SiO_2(am) [volume fraction] (left) and permeability [m²] (right) (day one of simulation). The part of the model displayed is 165 m long in the vertical direction and 6.5 m long in the horizontal direction.

Table 14: Injection regime of the base scenario simulation.

Simulation time [days]	SiO_2 concentration [wt%]	Injection rate [kg-H_2O/s]	Total volume of solution injected [m³]	Total volume of gel injected [m³]
0	0	0	0	0
Start of injection	5	13.37	0	0
1.2 hours of injection	5	13.37	57.75	2.89
3.6 hours of injection	5	13.37	173.28	8.66
6 hours and end of the injection	5	13.37	288.79	14.44
12 days after the end of injection	0	0	288.79	14.44

While this model is a clear simplification of the conditions encountered in a high-temperature geothermal reservoir, it shows the ability to use the TOUGHREACT code to precipitate a hypothetical colloidal silica gel in the vicinity of an injection well and this to a sufficient extent to reduce the permeability of permeable zones and to shut off fluid flow.

5.2.2. Base scenario results

Due to the almost neutral pH of the injected solution, colloidal silica gel starts to precipitate directly upon contact with the acidic/neutral reservoir fluid and reduces the permeability of the area surrounding the well. Figure 13 allows seeing the preferential flow paths of the colloidal silica gel into the high permeability zones and the resulting permeability reduction. As the time of injection continues, the front of the gel penetrates further into the reservoir. The many curvatures of the gel front show that the gel enters the high permeability layers preferentially.

Figure 13D shows that the gel remains stable around the well for many days after the well is closed in and the grouted zones remain sealed. As explained in Chapter 2, colloidal silica gel stays in a stable gel phase if pH conditions do not change, permitting, therefore, the well recovery treatment.

Furthermore, the model allows seeing the preferential flow paths of the colloidal silica gel into the high permeability zones as it can be seen by the many curvatures of the gel front and their corresponding larger extents of permeability reductions.

The results regarding colloidal silica gel propagation and permeability reduction are shown in Figure 13.

A) 1.2 hours of injection

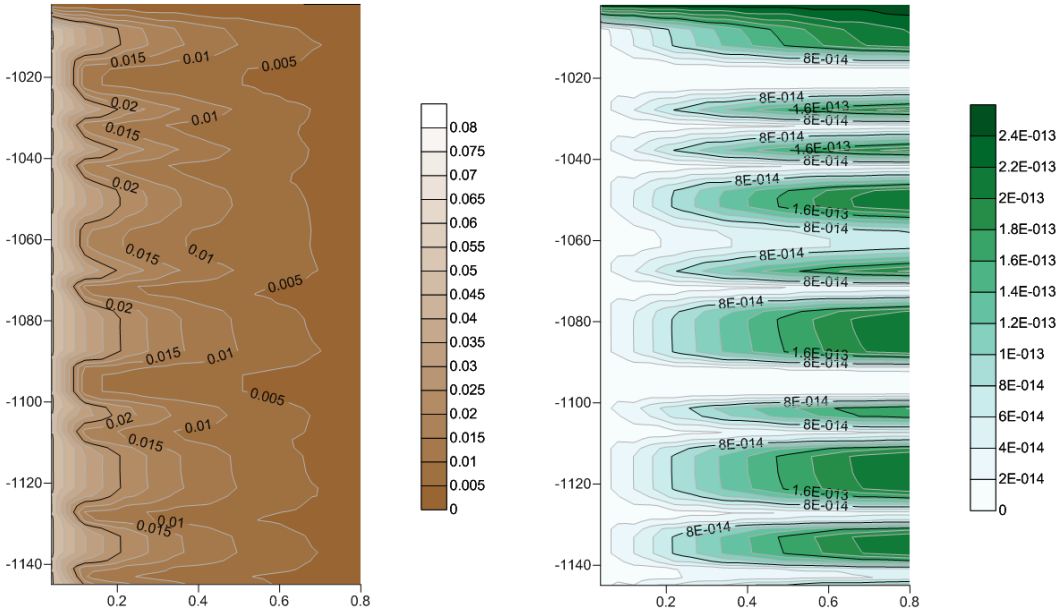

B) 3.6 hours of injection

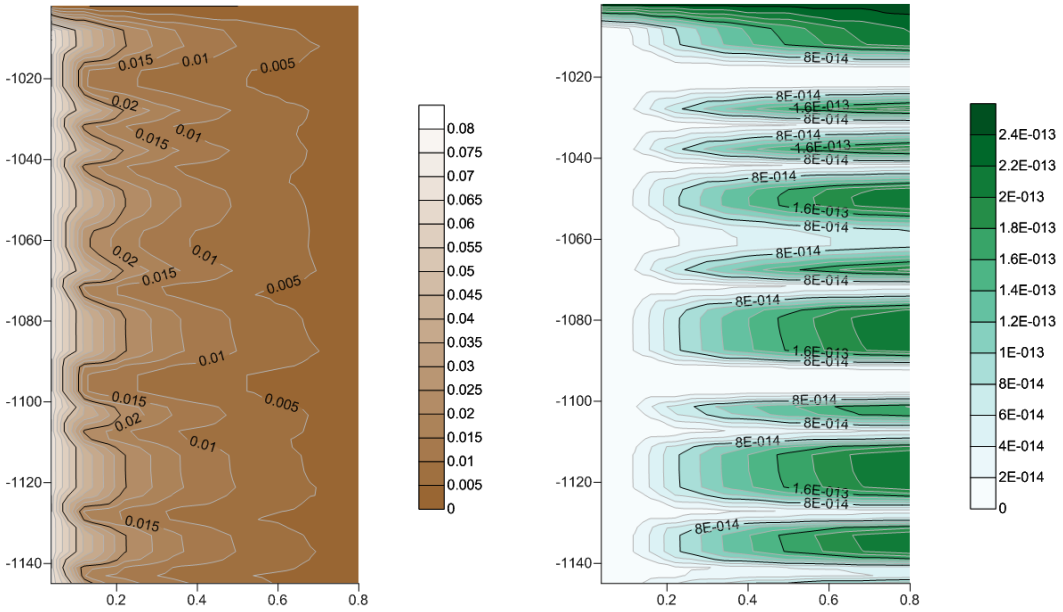

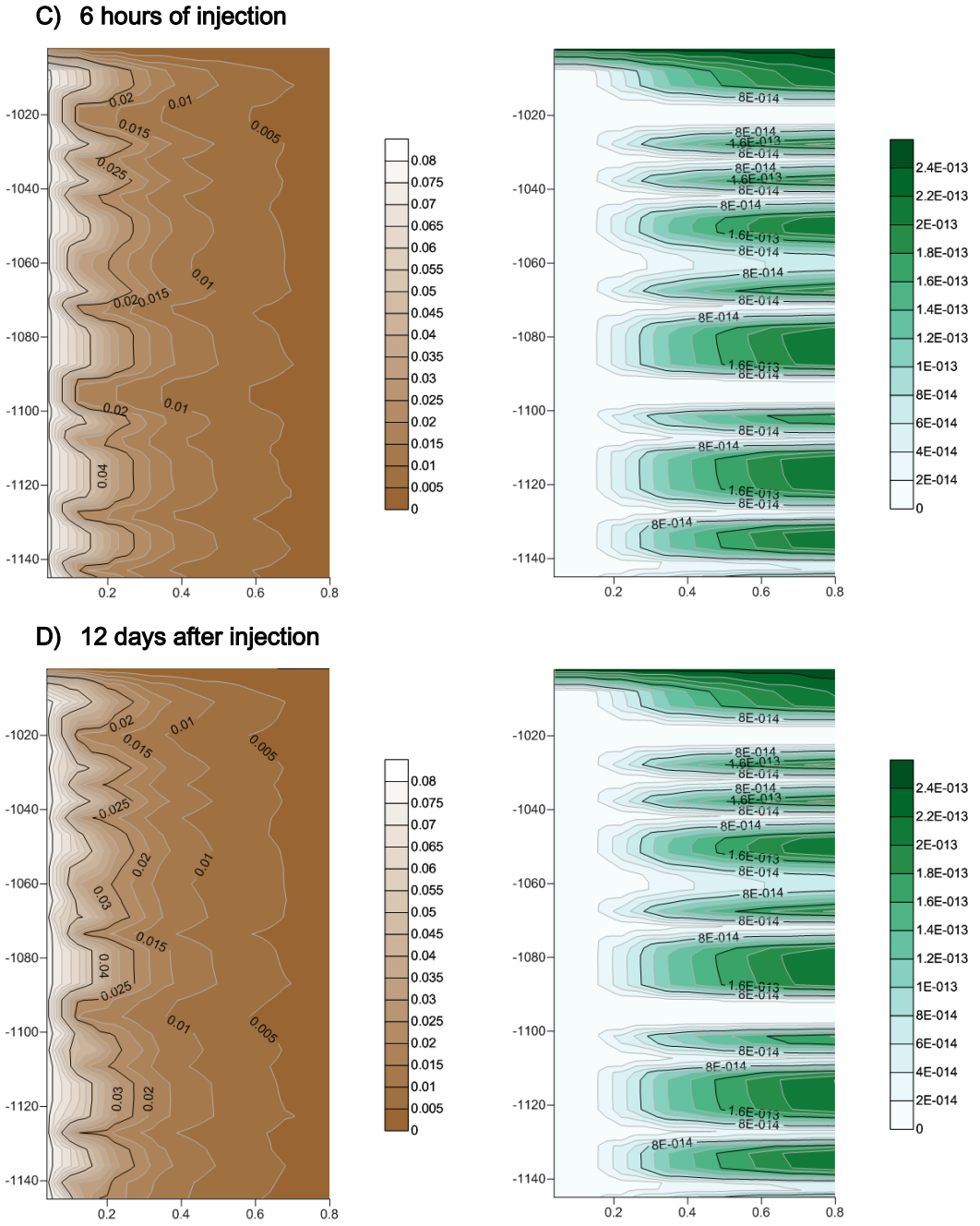

Figure 13: Time series of colloidal silica gel propagation in volume fraction (left) and permeability reduction for injection process of colloidal silica gel in m³ (right). A) 1.2 hours after the start of gel injection; B) 3.6 hours of continuous gel injection; C) end of gel injection after 6 hours of constant flooding and D) 12 days after the injection well is closed in.

Figure 14 presents the permeability reduction regarding the time at different locations from the well in a high permeability layer. The permeability is significantly reduced in the first minutes of injection due to direct triggering of the gelation process upon contact between the gel solution and the reservoir fluid and this to the extent of approximately 35 cm.

After a few minutes, the permeability decreases slower than at the beginning of the injection. The reduction is slower at distances further from the injection well. As a cause, the massive reduction

occurring close to the well results in a harder penetration of the injected solution, and this, more and more as the time of injection is running.

After 1 hour of injection, a small rise in permeability is observed, an explanation could be that part of the gel already formed is displaced with the fluid flow. Such displacement is not possible after a certain time as the flow becomes too small due to emplacement of the gel into the reservoir pores.

After 4 hours of injection, the permeability next to the well is equal to approximately 0. However, the porosity at the same location is still around 1 and goes to zero after 6 hours of injection. An explanation could be that gel partly formed in the pore throats and reduced the permeability to zero. However, some pore throats, which are not connected to each other, remained empty of gel. As a result, a little remaining porosity due to the isolated voids. As injection continues, the already formed gel moved forward because of injection pressure and filled the isolated voids. Finally, the porosity went to zero when the pore throats are completely filled with gel.

Also, it has to be noted that the main material of the reservoir was set to illite. As many clay mineral, illite can presents high porosity with very low permeability because of their structural configuration. It could also be a reason for the faster reduction of the permeability compared to the decrease of porosity.

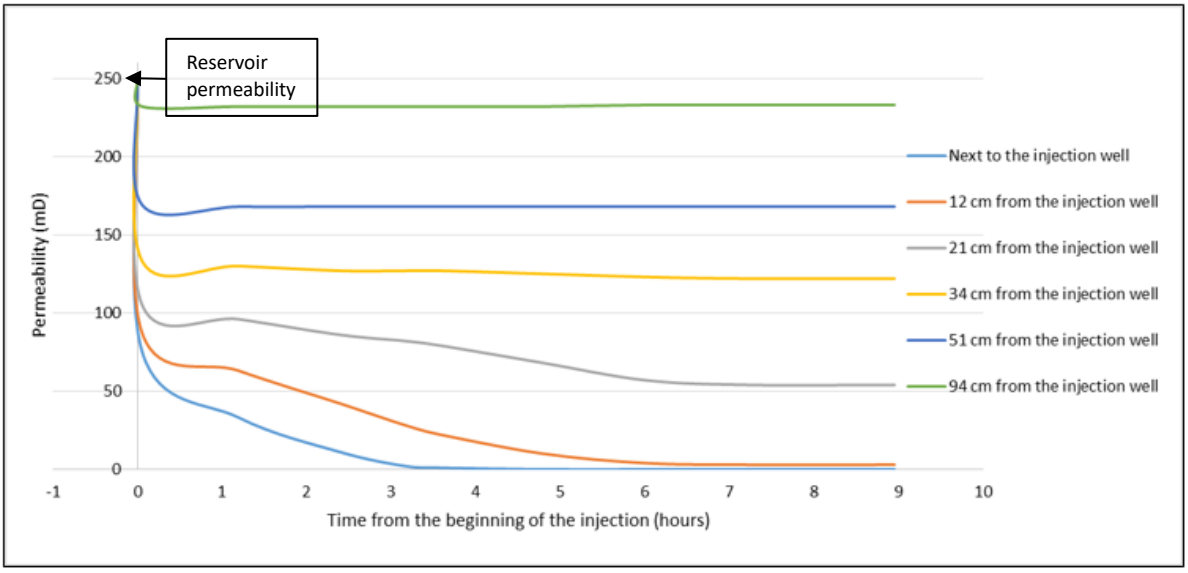

Figure 14: Permeability reduction regarding time at different locations from the injection well. (Injection rate = 13.37 kg- H_2O/s ; Gel concentration = 5 wt%)

As it can be seen in Figure 14, the permeability is not further reduced as soon as the injection well is shut off (6 hours). However, the permeability reduction could not continue for long even if the injection would last longer. No more solution can be injected because the porosity next to the well almost goes to zero (Figure 15).

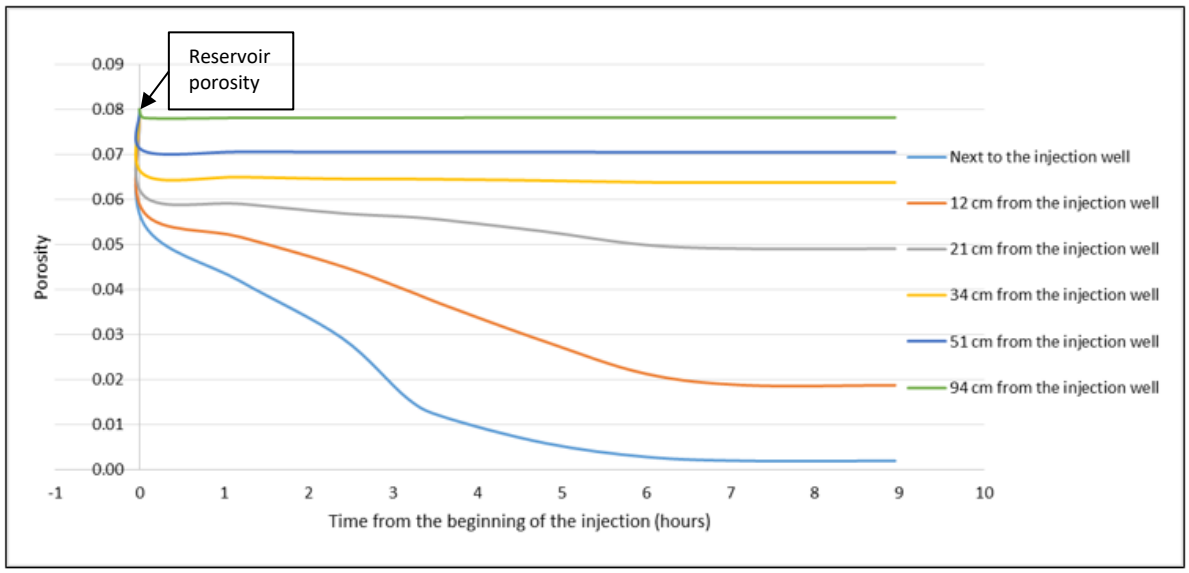

Figure 15: Porosity reduction regarding time at different locations from the injection well. (Injection rate = 13.37 kg- H_2O/s ; Gel concentration = 5 wt%)

Plotting permeability against distance from the well during the injection process gives information regarding the grouting of the well area. The output time's curves come together at a certain distance from the well where the permeability is no longer reduced with further injection (Figure 16). Meaning that no matter the time of injection, there is a location at a certain distance from the well where the gel cannot penetrate deeper while the area before that point can be completely sealed. This graph can be related to Figure 14 where it can be seen that the green and blue curves (94 cm and 51 cm) have steep decreases at the start of the injection but do not change as the injection continues.

Running several simulations showed that this particular location is further from the well either when increasing the injection rate or decreasing the gel concentration and vice versa. A higher injection rate allows a deeper penetration due to higher pressure. A lower gel concentration results in a deeper penetration because, for the same injection time, fewer gel forms in the direct vicinity of the well allowing more solution to flow further from it.

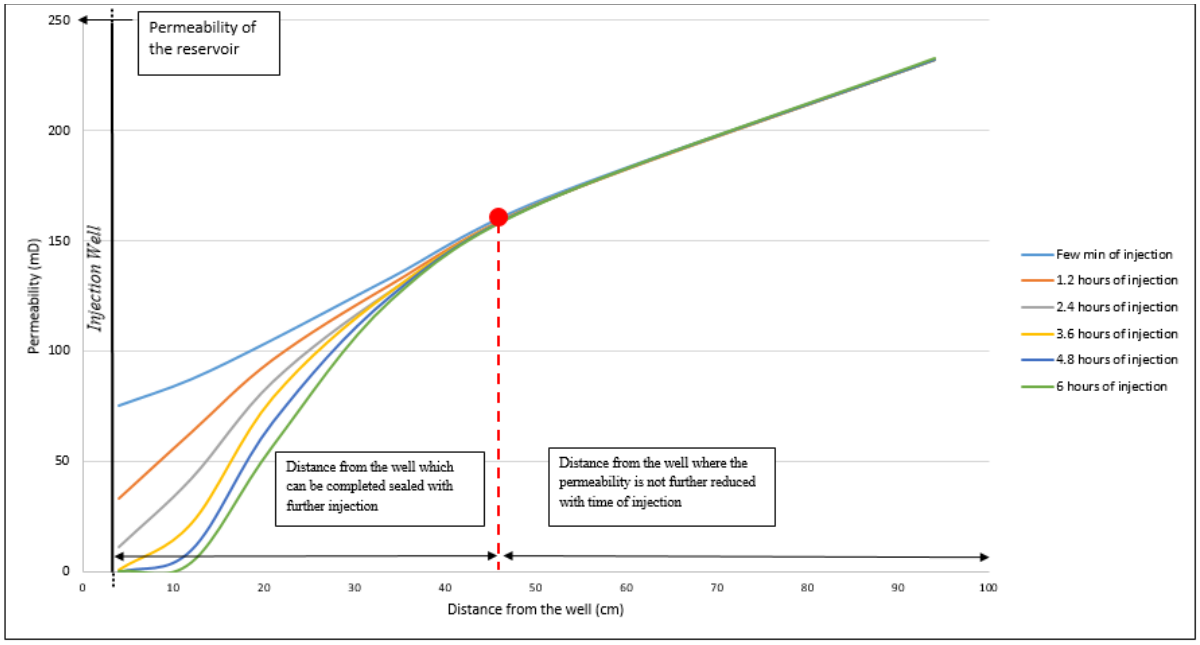

Figure 16: Permeability reduction regarding distance from the well during the injection process. (Injection rate = 13.37 kg- H_2O/s ; Gel concentration = 5 wt%)

Table 15 gives the simulation results. The cases highlighted in green show when the grouting is achieved. It can be seen that the location next to the well is sealed after 4 hours of injection corresponding to a gel volume of 8.66 m³. If an extent of 12 cm has to be grouted, 6 hours of injection and a gel volume of 14,44 m³ are required (Table 14).

Table 15: Simulation results regarding porosity and permeability

Distance from the well [cm]	Time of gel solution injection [hour]	Porosity [%]	Permeability [mD]
Next to the well	1.2	4	33
	3.6	1	1
	6	0	0
12	1.2	5	63
	3.6	4	22
	6	2	4
21	1.2	6	96
	3.6	6	79
	6	5	57
34	1.2	7	130
	3.6	7	127
	6	6	123

5.3. SENSITIVITY ANALYSIS OF THE PERMEABILITY REDUCTION REGARDING THE BASE SCENARIO

Several simulations were performed with changing of certain parameters values to get a better understanding of the model sensitivity. The analysis allows understanding how the model reacts to different conditions such as opposed porosity-permeability relation, different reservoir

temperature, changing colloidal silica concentration in the injected solution and modified injection rate. The injection regime is the same as the base scenario using the Carman-Kozeny relation and can be found in Table 14.

5.3.1. Changing factor: Porosity-permeability relation

After using the Carman-Kozeny relationship, a similar simulation was performed using the cubic law for porosity-permeability changes (Equation 3.9.). Figure 17 shows the results regarding porosity and permeability change using the cubic law equation.

Results of the sensitivity analysis (Porosity-permeability relation)

The simulation results are in good agreement with those obtained for the Carman-Kozeny relationship. In Figure 17, the difference between the two relationships is the most noticeable at an average distance ranging between 25 and 35 cm from the well. Also, the difference between the relations in every point is larger in the first hours of injection and decreases as simulation time increases.

At approximately 40 cm from the well, the porosity and permeability remain the same as it is in the first minutes of injection and this during the entire injection. As explain previously, this feature is important since it gives an idea of the distance where the permeability will not change with further injection. But also, it provides an idea about the maximum interval from the well that can be completely sealed by the gel. Although the porosity and permeability are different for the two relations, the distance from the well where the permeability is not reduced with time of injection is similar. It means that this particular location is not depending on the relation used but on the injection regime (injection rate and gel concentration) only.

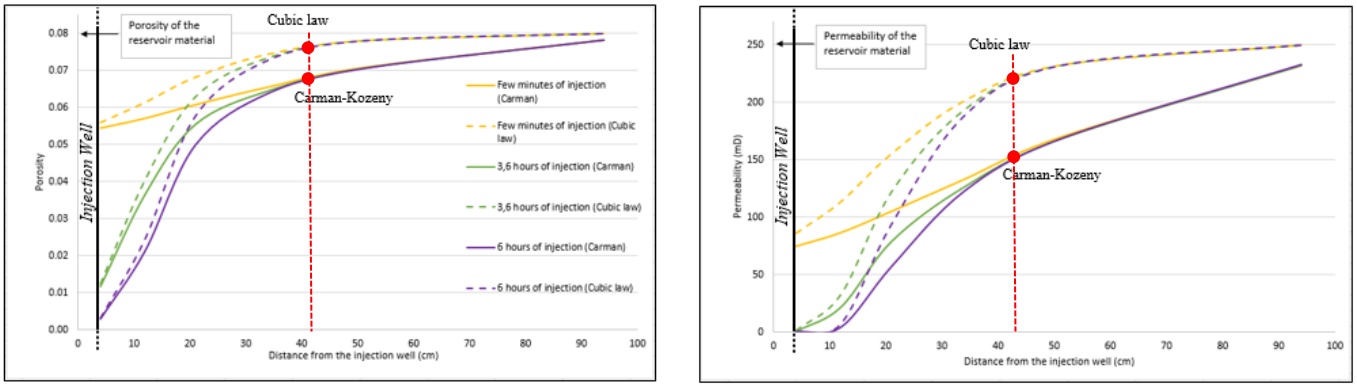

Figure 17: Comparison of Carman-Kozeny porosity-permeability relationship and Cubic law porosity-permeability relationship regarding permeability and porosity on distance from the injection well. (Injection rate = 13.37 kg-H_2O/s ; Gel concentration = 5 wt%)

The two porosity-permeability relationships can be computed analytically to verify the different outcomes. The resulting permeability can be calculated knowing the initial porosity and permeability of the reservoir and the resulting porosity after injection. For instance, taking the approximate values of resulting porosity at the 12 cm from the well recorded and this after the 6 hours of injection, it is straightforward to compute the corresponding permeability following

equations (3.8.) and (3.9.) (Table 16). Figure 18 represents the difference between the two relations regarding resulting porosity and gives a better understanding regarding the shape of the relations curves in Figure 17. As it can be seen, the equation parts responsible for the difference between the two relations have their functions starting and ending at the same value. The absolute difference between the relations increases as porosity decreases until reaching a maximum of absolute variation at 25% of porosity reduction. Then the absolute difference between the two relations decreases slowly and becomes null at 100% of porosity reduction. Regarding relative difference, however, the variations between the two relations increases continuously until reaching a maximum of 25% of relative difference at 95% of porosity reduction. At 100% of porosity reduction, the relative difference is null since the porosity is completely reduced for both relations. The relative difference is harder to see on the graph because the resulting porosity values become minuscule as porosity is reduced.

Table 16: Analytical estimation of the resulting permeabilities for different initial permeabilities and porosities at 12 cm from the well and after 6 hours of gel injection using Carman-Kozeny relation and Cubic law.

Initial permeability k_i [mD]	Initial porosity ϕ_i	Resulting porosity ϕ	Carman-Kozeny resulting permeability k [mD] $k = k_i \frac{(1-\phi_i)^2}{(1-\phi)^2}\left(\frac{\phi}{\phi_i}\right)^3$	Cubic law resulting permeability k [mD] $k = k_i\left(\frac{\phi}{\phi_i}\right)^3$
250	8	2.157	4.3325	4.9003
100	4	0.589	0.2977	0.3193
25	3	0.35	0.0376	0.0397
5	2	0.176	0.0033	0.0034

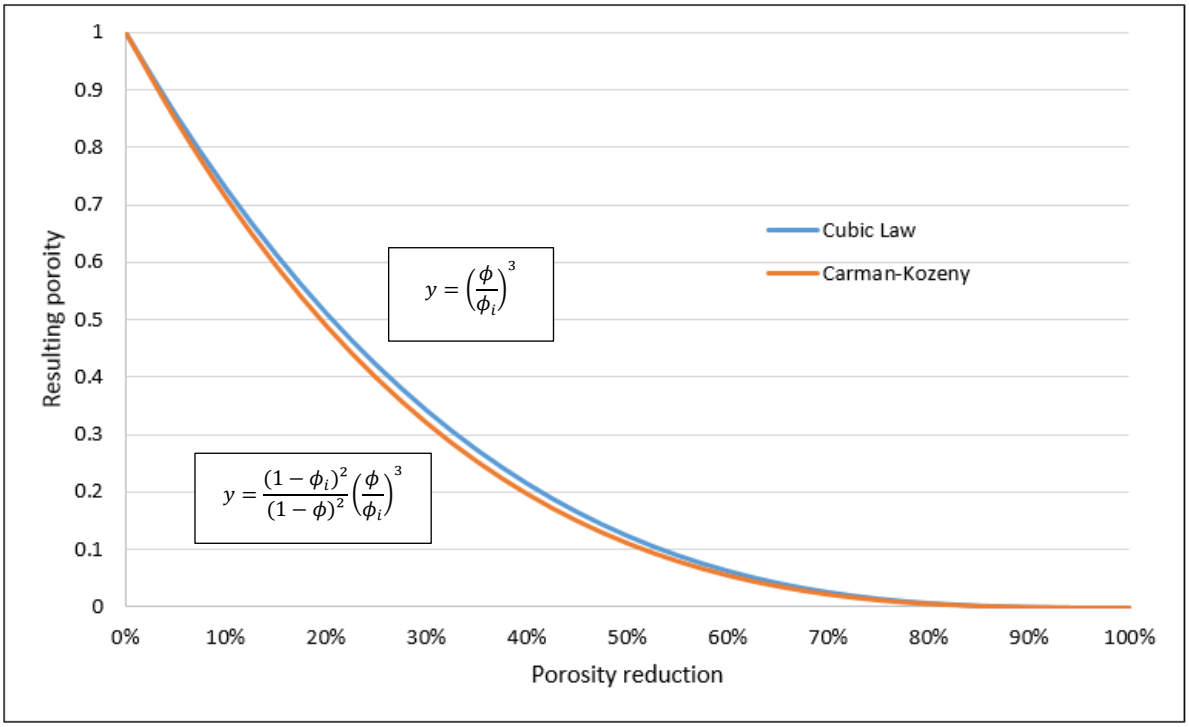

Figure 18: Resulting porosity regarding percentage of porosity reduction from initial porosity (ϕ=0.10) for both Carman-Kozeny relation and Cubic law.

Table 17 summarizes the simulation results. The green cases indicate when the grouting is realized. As for the first simulation using the Carman-Kozeny relation, the time require to achieve a complete sealing of the close area around the well is 3.6 hours. However, the difference between the two relationships increases with distance from the well.

Table 17: Simulation results regarding porosity and permeability using Carman-Kozeny relation and Cubic law

Distance from the well [cm]	Time of gel solution injection [hour]	Carman-Kozeny Porosity [%]	Carman-Kozeny Permeability [mD]	Cubic law Porosity [%]	Cubic law Permeability [mD]
Next to the well	1.2	4	33	4	39
	3.6	1	1	1	1
	6	0	0	0	0
12	1.2	5	63	6	85
	3.6	4	22	4	33
	6	2	4	2	7
21	1.2	6	96	7	143
	3.6	6	79	6	122
	6	5	57	6	94
34	1.2	7	130	7	198
	3.6	7	127	7	194
	6	6	123	7	189

Conclusion of the sensitivity analysis (Porosity-permeability relation)

The Cubic law tends to reduce the porosity and the permeability less than the Carman-Kozeny relation. This because the two relations exhibit the same equation excepted that the Carman-Kozeny is composed of an additional term ($\frac{(1-\phi_i)^2}{(1-\phi)^2}$) which multiplies the rest of the equation. If the porosity is reduced, this term is always between 0 and 1 and causes a deeper reduction of the resulting permeability. This term has a falling linear trend when going from low initial porosity to high initial porosity. Therefore, the resulting permeability difference between the Carman-Kozeny relation and the Cubic law increases with higher initial permeability and porosity. Looking at Figure 18, the difference between the two relations increases with porosity reduction until reaching a maximum of difference. From that point, the difference decreases until the porosity is completely reduced.

The difference between the two relationships is the most noticeable during the first hours of injection since the initial permeability and porosity are the largest at that time. After a few hours, the difference is reduced, and the effect of the relationship becomes less significant. Especially in the direct vicinity of the well where most of the permeability is reduced. While the Carman-Kozeny relation should be used if the user would consider more optimistic predictions regarding permeability reduction, the Cubic law should be employed if the user would consider more pessimistic predictions

The difference between the two porosity-permeability relations is that the Carman-Kozeny relation considers the material to be composed of a matrix permeability while the Cubic law considers it to consist of a fracture permeability. In the absence of information regarding the porosity-permeability

of the field, the choice of the relationship is the user, but the suggestion is to consider a matrix permeability and to use the Carman-Kozeny relation since the fracture network of the field is unknown. Also, after the entire injection process, the choice of the relation does not impact the results to a large extent since in both cases a quasi-complete sealing of the first centimeters surrounding the well is achieved. However, if one would like to approach the reality, site-specific investigation of the materials porosity-permeability relationship should be realized by the mean of core sample and laboratory experiment.

5.3.2. Changing factor: Reservoir temperature

Four simulations were run using reservoir temperature of 250°C, 150°C, 100°C, and 50°C, respectively. The injection regime can be found in Table 14.

Results of the sensitivity analysis (Reservoir temperature)

Although the two first simulation using 250°C and 150°C run correctly until the end of the simulation time (20 days), the simulation using 100°C and 50°C crashed at the end of the injection period (6 hours of injection). As a cause, the steep increase of pressure (Total P = 380 bars) just next to the injection well due to a quasi-complete sealing of the area surrounding it (Figure 19).

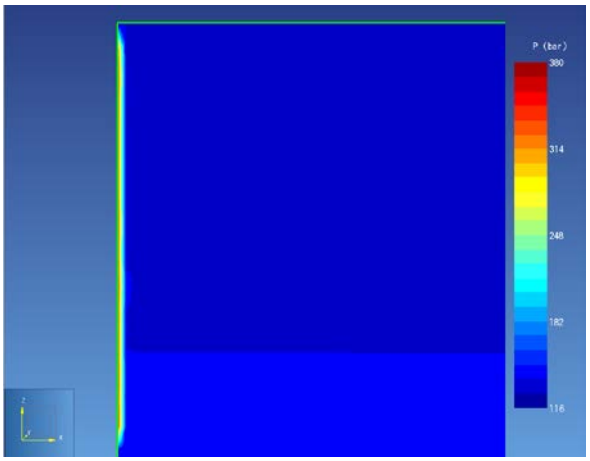

Figure 19: Steep pressure increase at the injection well location due to quasi complete sealing of the area

Referring to the Arrhenius equation which is responsible for the temperature dependence of the gel dissolution and precipitation rates, the reduction of the dissolution rate with decreasing temperature is larger than the decline in the precipitation rates (Table 18). In other words, with decreasing temperature, dissolution is more reduced than precipitation is. As a result, a higher amount of gel is formed when lowering temperature than an amount of gel is dissolved and therefore a better sealing is realized. Table 18 shows the rates decrease with temperature drop regarding the percentage of decrease compare to the rates at 300°C. Figure 20 gives a better visualization of the faster reduction of the dissolution rate with reduced temperature compare to the precipitation rate reduction.

Table 18: Dissolution and precipitation rates of colloidal silica gel for several reservoir temperatures using Arrhenius equation. Rates decrease with temperature drop using a percentage of decrease compare to the kinetic rates at 300°C. Dissolution rate constant at 25°C ($k_{(d)25}$)=7.32e-13 mol/m²/s; Dissolution activation energy ($E_{(d)}a$)=60.9 kJ/mol; Precipitation rate constant at 25°C ($k_{(p)25}$)=3.80e-10 mol/m²/s; Precipitation activation energy ($E_{(p)}a$)=49.8 kJ/mol.

Arrhenius equation	T Reservoir temperature [°C]	k rate constant [mol/m²/s]	Dissolution rate decrease compare to dissolution rate at 300°C [%]	Precipitation rate decrease compare to precipitation rate at 300°C [%]
$k = k_{25} \exp\left[\frac{-E_a}{R}\left(\frac{1}{T} - \frac{1}{298.15}\right)\right]$	300	7.407e-13 3.837e-10	0	0
	250	7.398e-13 3.834e-10	0.122	0.100
	200	7.387e-13 3.828e-10	0.270	0.221
	150	7.373e-13 3.823e-10	0.452	0.370
	100	7.356e-13 3.815e-10	0.683	0.559
	50	7.334e-13 3.806e-10	0.984	0.805
	0	7.304e-13 3.793e-10	1.394	1.141

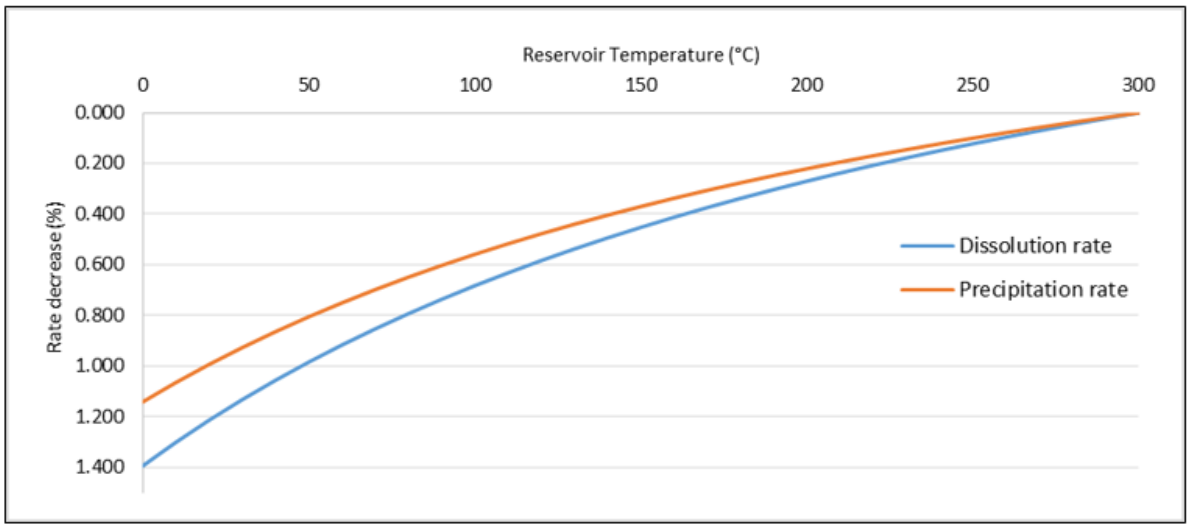

Figure 20: Dissolution and precipitation rates reduction with reduced temperature regarding the percentage of decrease compare to the rates at 300°C.

Figure 21 shows the permeability reduction relating to the distance from the well at the end of the injection process (6hours). The model is the most sensitive to reservoir temperature change in the well vicinity and becomes insensitive at distances where the gel is less emplaced.

Also, it seems that the 100 °C temperature drop from 250°C to 150°C has a bigger effect than the drop from 150°C to 50°C since the 150 °C curve and 50 °C have almost the same curve. However,

referring to Figure 20 the drop between 150°C and 50°C should have a larger effect than the drop from 250°C to 150°C since the difference between the precipitation rate and the dissolution rate keep increasing with temperature decrease. Moreover, it appears that the 100°C curve and the 50°C curve are similar.

An explanation is that for every simulation with different reservoir temperature, the same injection rate is input and the same amount of gel is injected. Therefore, there is a certain threshold temperature where the precipitation rate is become so predominant compared to the dissolution rate that the gel solution available is entirely precipitated. It results in the maximum gel formation possible and, therefore, the maximum permeability reduction possible regarding the amount of gel solution injected. In this case, it seems that the threshold is located between 150°C and 100°C since the permeability is not further reduced while the temperature is decreased. Looking at the simulations values, it appears that the amount of SiO_2(aq) (gel solution) is of the order of E-03 at the temperature of 150°C and below while it is of the order of E-02 at the temperature of 250°C.

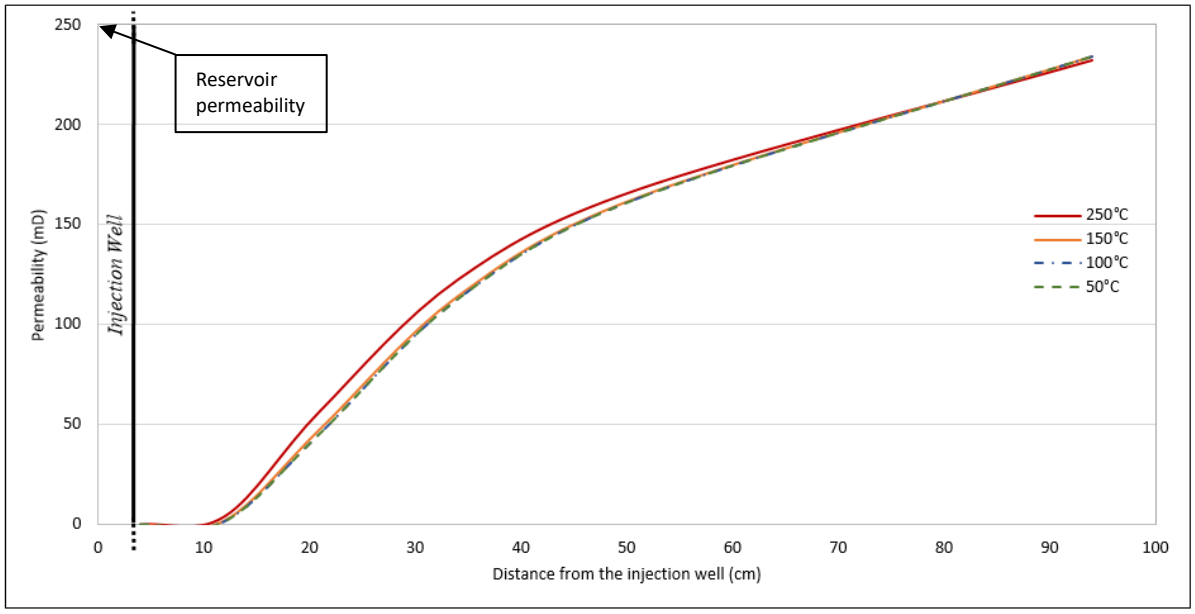

Figure 21: Permeability regarding distance from the well at the end of the injection (6 hours of injection) comparing reservoir temperatures, 250°C, 150°C and 50°C, respectively. (Injection rate = 13.37 kg- H_2O/s ; Gel concentration = 5 wt%)

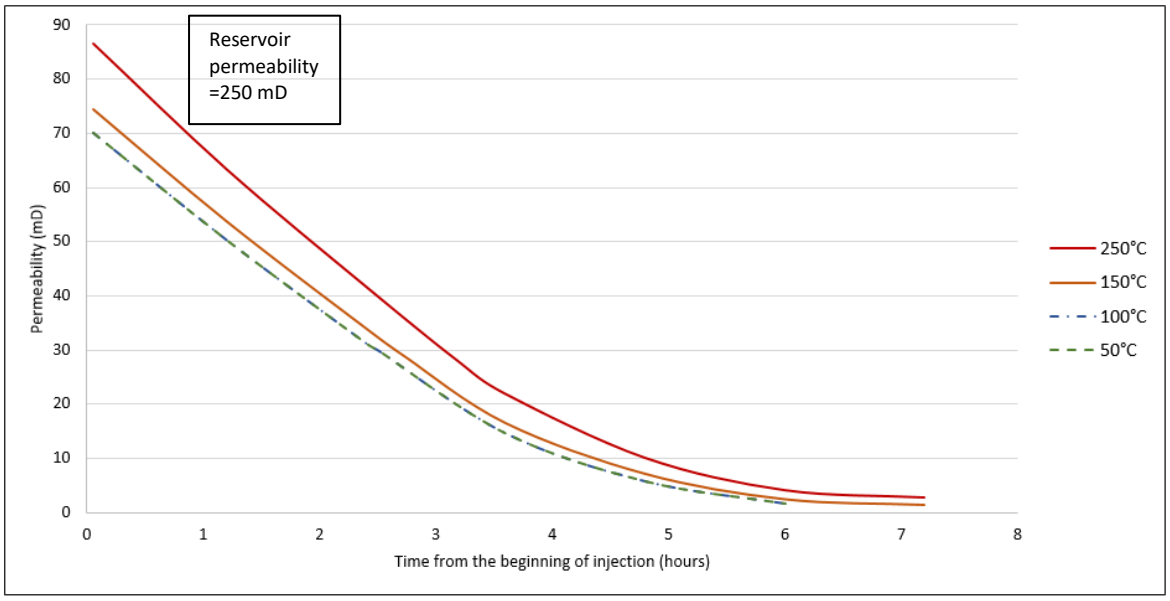

Figure 22: Permeability reduction for the three reservoir temperature 250 °C, 150 °C and 50 °C, respectively, at 12 cm from the well regarding time from the beginning of injection. (Injection rate = 13.37 kg- H_2O/s ; Gel concentration = 5 wt%)

The permeability functions show similar trend regardless initial reservoir temperature (Figure 21). During the first 3 hours, the curves follow a falling linear function and are then gradually decreasing more gently. As explained above, the simulation with initial reservoir temperature of 100°C and 50°C crashed at the end of the injection due to complete sealing of the well vicinity. It explains why the green dotted curve stops at 6 hours of injection.

Table 19 shows simulation results regarding each different initial temperature. The cases highlighted in green show when the grouting is done. For each reservoir temperature, the time needed to achieve the complete grouting of the area next to the well is 3.6 hours corresponding to a gel volume of 8.66 m³ as seen in Table 14.

Table 19: Simulation results regarding porosity and permeability regarding the different initial reservoir temperatures

Distance from the well [cm]	Time of gel solution injection [hour]	Initial reservoir temperature [°C] = 50		Initial reservoir temperature [°C] = 100		Initial reservoir temperature [°C] = 150		Initial reservoir temperature [°C] = 250	
		Porosity [%]	Permeability [mD]	Porosity [%]	Permeability [mD]	Porosity [%]	Permeability [mD]	Porosity [%]	Permeability [mD]
Next to the well	1.2	4	24	4	24	4	26	4	39
	3.6	1	0	1	0	1	0	1	1
	6	0	0	0	0	0	0	0	0
12	1.2	5	50	5	50	5	54	6	85
	3.6	3	15	3	15	3	16	4	33
	6	2	2	2	2	2	2	2	7
21	1.2	6	82	6	82	6	85	7	143
	3.6	5	67	5	67	5	69	6	122
	6	5	46	5	46	4	48	6	94

34	1.2	6	120	6	120	6	122	7	198
	3.6	6	116	6	116	6	118	7	194
	6	6	113	6	113	6	114	7	189

Conclusion of the sensitivity analysis (Reservoir temperature)

Changing the temperature has an impact on the gel emplacement since it influences its formation speed by modifying the kinetics rate of the gel. Referring to the Arrhenius equation, with decreasing temperature, the dissolution rate decreases faster than the precipitation rates. Leading to the precipitation rate being more predominant than the dissolution rate. Although varying the kinetic rates, the temperature change does not induce substantial difference regarding permeability reduction. As explain above, when reducing temperature the permeability reduction curves become closer and closer until they match. An explanation is that there is a certain threshold temperature where the precipitation rate is become so predominant compared to the dissolution rate that the gel solution available is entirely precipitated. It results in the maximum gel formation possible and, therefore, the maximum permeability reduction possible regarding the amount of gel solution injected. Regarding distance, the temperature change presents most of its impact within the 10 cm from the well, while regarding time, the effect on the model increases with it and is the most significant at the end of the injection process.

5.3.3. Changing factor: Colloidal silica concentration of the injected solution

Sensitivity analysis was performed by changing the colloidal silica concentration of the injected solution. Four different simulations including colloidal silica concentration of 1 wt% (SiO_2(aq) = 0.1644 moles), 2.5 wt% (SiO_2(aq) = 0.411 moles), 5 wt% (SiO_2(aq) = 0.822 moles) and 7.5 wt% (SiO_2(aq) = 1.233 moles), respectively, were realized. Apart from colloidal silica concentration, all parameters were kept constant and similar to the first simulation (Section 7.1.).

Table 20 gives the injection regime regarding the different colloidal silica concentrations. The cases highlighted in green indicate the time and the volume of gel needed to achieve a complete sealing of the area next to the well according to the gel concentration in the injected solution.

Table 20: Injection regime of the simulations regarding the different colloidal silica concentrations

Simulation time [days]	Injection rate [kg-H_2O/s]	Total volume of solution injected [m³]	Total volume of gel injected [m³] with 1 wt% silica solution	Total volume of gel injected [m³] with 2.5 wt% silica solution	Total volume of gel injected [m³] with 5 wt% silica solution	Total volume of gel injected [m³] with 7.5 wt% silica solution
0	0	0	0	0	0	0
Start of injection	13.37	0	0	0	0	0
1.2 hours of injection	13.37	57.75	0.58	1.44	2.89	4.33
3.6 hours of injection	13.37	173.28	1.73	4.33	8.66	13
6 hours and end of the injection	13.37	288.79	2.89	7.22	14.44	21.66

12 days after the end of injection	0	288.79	2.89	8.22	14.44	21.66

Results of the sensitivity analysis (Colloidal silica concentration)

Similarly to the simulation using 50°C as reservoir temperature in the previous sensitivity analysis, the simulation using 7.5 wt% as colloidal silica concentration crashed due to complete sealing of the area surrounding the well and tremendous pressure increase at the well location. However, in this case, the simulation crashed after only 4.8 hours of injection. Therefore, Figure 23 exhibits the permeability after 4.8 hours of injection considering the distance from the well for the different colloidal silica concentrations.

Changing the SiO_2(aq) content makes the solution pH varied as more moles of SiO_2(aq) induces a more alkaline solution and fewer moles a more acidic solution. However, these variations are slight and do not impact the simulations.

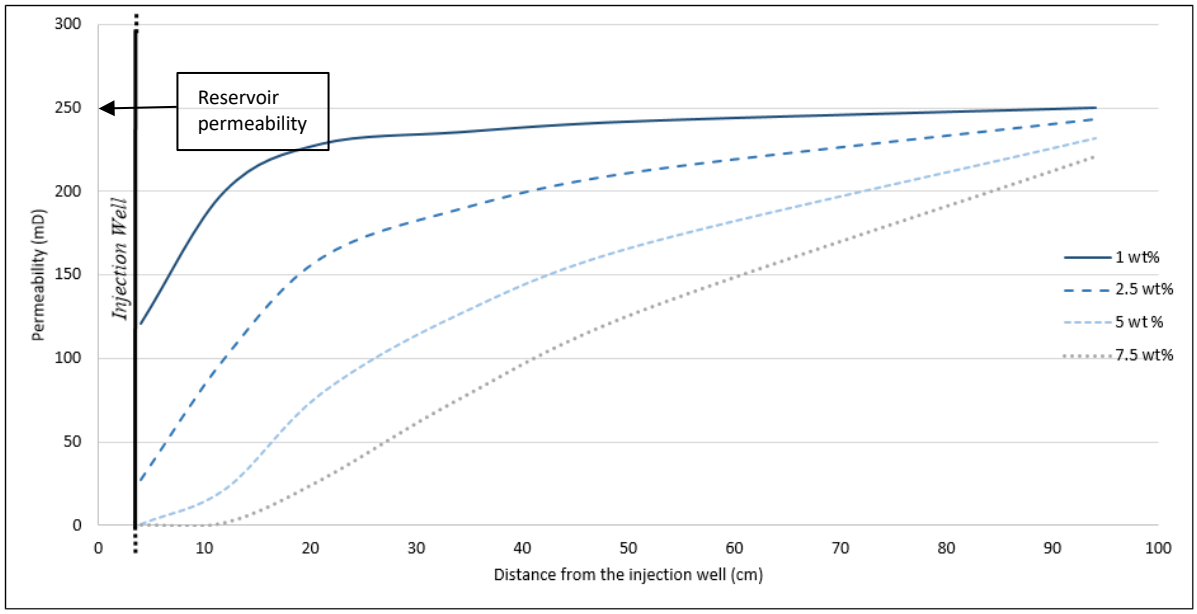

Figure 23: Permeability regarding distance from the well after the 4.8 hours of injection comparing colloidal silica concentration of 1 wt%, 2.5 wt%, 5 wt% and 7.5 wt%, respectively. (Injection rate = 13.37 kg- H_2O/s)

The colloidal silica content of the injected solution influences greatly the permeability and results indicate significant differences over the 95 cm from the well in these simulations. Results at a further distance are available, but because the scope of this research is to seal the area around the well, the choice is made to consider only the first meter from it.

The differences regarding permeability are the biggest in the direct vicinity of the well with more than 100 mD of variation between 1 wt% colloidal silica solution and 5 wt% colloidal silica concentration and this over approximately 35 cm from the well. Also, although decreasing with distance, differences remained remarkable at distant locations. Moreover, it can be noticed that

the range of permeability between the site directly next to the well and the place at 95 cm from the well is larger when increasing the colloidal silica content.

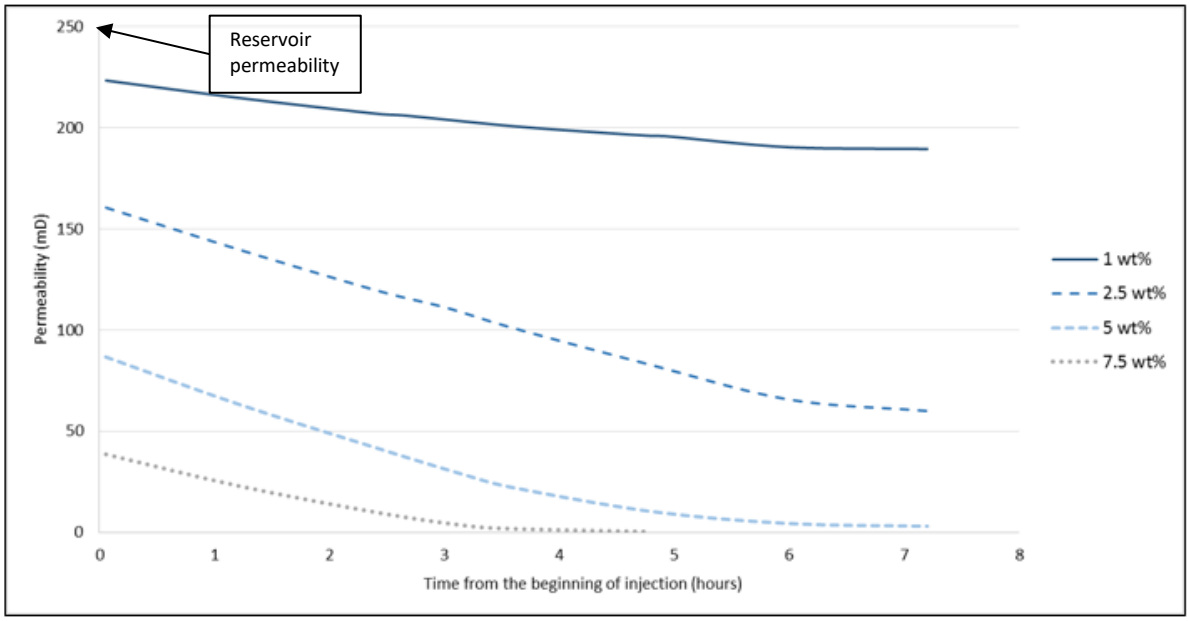

Figure 24: Permeability reduction for the four colloidal silica concentration 1 wt%, 2.5 wt%, 5 wt% and 7.5 wt%, respectively, at 12 cm from the well regarding time from the beginning of injection. (Injection rate = 13.37 kg-H_2O/s)

Similar falling linear trends regardless colloidal silica concentration are observed looking at permeability reduction regarding time at a distance of 12 cm from the well. Also, each curve presents a curvature at a particular time resulting in a smoother decrease of the permeability (Figure 24). These curves happen sooner with a higher colloidal silica content and are the result of less gel reaching the 12 cm location. As a cause, a larger reduction in the permeability in the area before the 12 cm caused by the injection of a solution of higher colloidal silica content. As explained above, the simulation using 7.5 wt% of colloidal silica concentration crashed at 4.8 hours of injection due to complete sealing of the well vicinity. It explains why the grey curves stop at 4.8 hours of injection.

The difference due to concentration change is very significant at any times of injection. It goes from 225 mD to approximately 45 mD after few minutes of injection between for the solutions of 1 wt% and 7.5 wt%, respectively, and from 200 mD to less than 1 mD after 4 hours of injection. As a result, a consistent difference of more or less 200 mD between the two solutions over the 4.8 hours of injection.

Table 21 shows the simulation results. The green cases indicate when the grouting is realized. The complete sealing is achieved after 3.6 hours of injection for the solution with the two highest gel concentration. The sealing with the 5 wt% silica solution corresponds to a volume of 8.66 m³ while the sealing with the 7.5 wt% silica solution corresponds to a volume of 13 m³.

However, an almost complete grouting is reached after 1.2 hours using the 7.5 wt% silica solution corresponding to a gel volume of 4.33 m³. A similar grouting is achieved after 6 hours with the 2.5 wt% silica solution involving 7.22 m³ of gel. The solution with the smallest gel concentration does not achieve a complete sealing within the 6 hours of the injection process.

Table 21: Simulations results of porosity and permeability regarding the different colloidal silica concentrations

Distance from the well [cm]	Time of gel solution injection [hour]	SiO_2 concentration of the injected solution [wt%] = 1		SiO_2 concentration of the injected solution [wt%] = 2.5		SiO_2 concentration of the injected solution [wt%] = 5		SiO_2 concentration of the injected solution [wt%] = 7.5	
		Porosity [%]	Permeability [mD]	Porosity [%]	Permeability [mD]	Porosity [%]	Permeability [mD]	Porosity [%]	Permeability [mD]
Next to the well	1.2	7	195	6	105	4	33	3	7
	3.6	6	121	4	28	1	1	0	1
	6	5	60	2	7	0	0	/	/
12	1.2	8	215	7	140	5	63	4	23
	3.6	7	201	6	101	4	22	2	2
	6	7	190	5	66	2	4	/	/
21	1.2	8	228	7	169	6	96	5	47
	3.6	8	228	7	160	6	79	4	27
	6	8	228	7	149	5	57	/	/
34	1.2	8	235	7	190	7	130	6	82
	3.6	8	236	7	189	6	127	5	76
	6	8	236	7	189	6	123	/	/

Conclusion of the sensitivity analysis (Colloidal silica concentration)

Changing the colloidal silica concentration of the injected solution has a significant impact on the gel emplacement. Because the injection process lasts for a total of 6 hours, changing the colloidal silica content leads to a big difference regarding the amount of gel injected. Regarding distance, the concentration change presents most of its impact within the first 50 cm from the well, although differences regarding permeability are seen over the 95 cm from the well. Regarding time, the effect on the model increases with it and is the most significant at the end of the injection process. The slope of the permeability decrease is reduced and observed at a time unique to each colloidal silica concentration.

Changing the colloidal silica concentration allows estimating the most optimal solution to inject. For instance, a similar grouting (Porosity = $\pm$ 2 %; Permeability = 7 mD) is achieved next to the well after 6 hours of injection with the 2.5 wt% solution as after 1.2 hours of injection with the 7.5 wt% solution (Table 21). However, the amount of gel injected is different with 7.22 m³ for the first solution and 4.33 m³ for the second solution (Table 20). Therefore, regarding cost savings, it appears that injecting a highly concentrated colloidal silica injection is more advantageous than a less concentrated solution both regarding gel injected and time of injection.

5.3.4. Changing factor: Injection rate

The last sensitivity analysis includes four different injection rates, 0.13 kg- H_2O/s, 1.34 kg- H_2O/s, 13.37 kg- H_2O/s and 133.71 kg- H_2O/s, respectively. All other parameters were kept similar to the

first simulation (Section 5.1.). Again, one of the four simulations (133.71 kg- H_2O/s) crashed due to complete sealing and massive pressure increase of the area around the well. This time, however, the simulation crashed after only 2.4 hours of injection, and therefore, Figure 25 displays the permeability curves after 2.4 hours to compare the effects on the model of the four simulated injection rates but also after 6 hours to compare the three simulations that do not fail.

Table 22 shows the injection regime regarding the different injection rates. The cases highlighted in green shows the time, the volume of solution injected, and the volume of gel needed to achieve a complete sealing of the area next to the well.

Table 22: Injection regime of the simulations regarding the different injection rates

Simulation time [days]	Injection rate [kg-H_2O/s] = 0.13		Injection rate [kg-H_2O/s] = 1.34		Injection rate [kg-H_2O/s] = 13.37		Injection rate [kg-H_2O/s] = 133.71	
	Total volume of solution injected [m³]	Total volume of gel injected [m³]	Total volume of solution injected [m³]	Total volume of gel injected [m³]	Total volume of solution injected [m³]	Total volume of gel injected [m³]	Total volume of solution injected [m³]	Total volume of gel injected [m³]
0	0	0	0	0	0	0	0	0
Start of injection	0	0	0	0	0	0	0	0
1.2 hours of injection	0.56	0.028	5.78	0.29	57.75	2.89	577.63	28.88
2.4 hours of injection	1.12	0.056	11.56	0.58	115.5	5.78	1155.26	57.76
3.6 hours of injection	1.68	0.084	17.37	0.87	173.28	8.66	-	-
6 hours and end of the injection	2.8	0.14	28.94	1.45	288.79	14.44	-	-
12 days after the end of injection	2.8	0.14	28.94	1.45	288.79	14.44	1155.26	57.76

Results of the sensitivity analysis (Injection rate)

Similarly to the different colloidal concentrations, changing the injection rate has a huge effect on the permeability reduction regarding distance (Figure 25).The two smallest injection rates (0.13 kg- H_2O/s and 1.34 kg- H_2O/s) are not able to reduce permeability far from the well.

The injection of solution at a rate of 0.13 kg- H_2O/s reduced permeability only within the 15 first centimeters but without being significant, and therefore, it does not result in a complete sealing of the well vicinity.

The injection rate of 1.34 kg- H_2O/s has a greater effect than the smallest injection rates with a reduction of the permeability over approximately 40 cm from the well. However, although the reduction is high at the direct contact with the well leading to a permeability of almost 10 mD, the

curve follows a logarithmic function, and the permeability reduction becomes rapidly less important with distance (200 mD at 15 cm from the well).

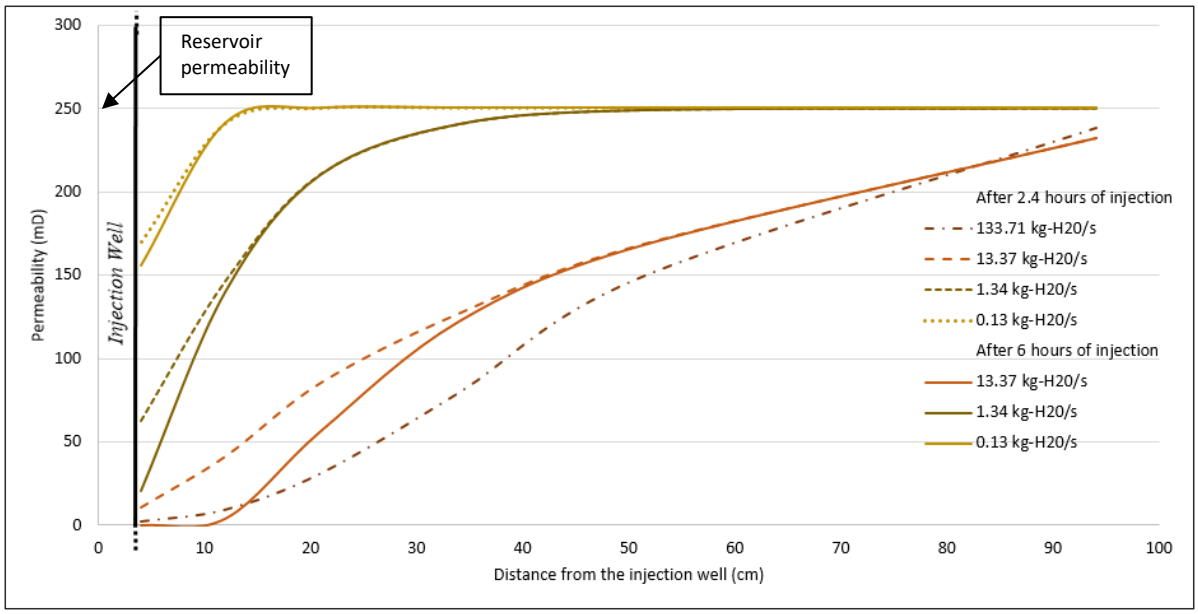

Figure 25: Permeability regarding distance from the well after 2.4 hours of injection and at the end of the injection (6 hours) comparing injection rate 0.13 kg- H_2O/s, 1.34 kg- H_2O/s, 13.37 kg- H_2O/s and 133.71 kg- H_2O/s, respectively. (Gel concentration = 5 wt%)

The two highest injection rates (13.37 kg- H_2O/s and 133.71 kg- H_2O/s) reduced the permeability over the entire cross section with complete high permeability zones shut off in the vicinity of the well. The complete sealing is achieved after 6 hours for the 13.37 kg- H_2O/s injection rate and after only 2.4 hours for the 133.71 kg- H_2O/s injection rate, respectively.

As in the previous analysis, the time's curves of each injection rate come together at a certain distance from the well which appears to be further with higher injection rates. Beyond this location, the time of injection does not have any effect on the permeability reduction but a complete sealing of the area before it can be reached.

Similar linear decreasing trends regardless colloidal silica concentration are observed considering permeability functions regarding time at a distance of 12 cm from the well (Figure 26). However, similarly to the previous analysis described, each curve presents a curvature resulting in a smoother decrease of the permeability with time. These curves are observed earlier with higher injection rates and are the result of less gel reaching the 12 cm location due to a larger reduction in the permeability in the area before the 12 cm. As a cause, the higher amount of gel injected. As explained previously, the simulation using a rate of 133.71 kg- H_2O/s crashed after 2.4 hours of injection due to complete sealing of the well vicinity. This explains why the brown curve stops at 2.4 hours of injection.

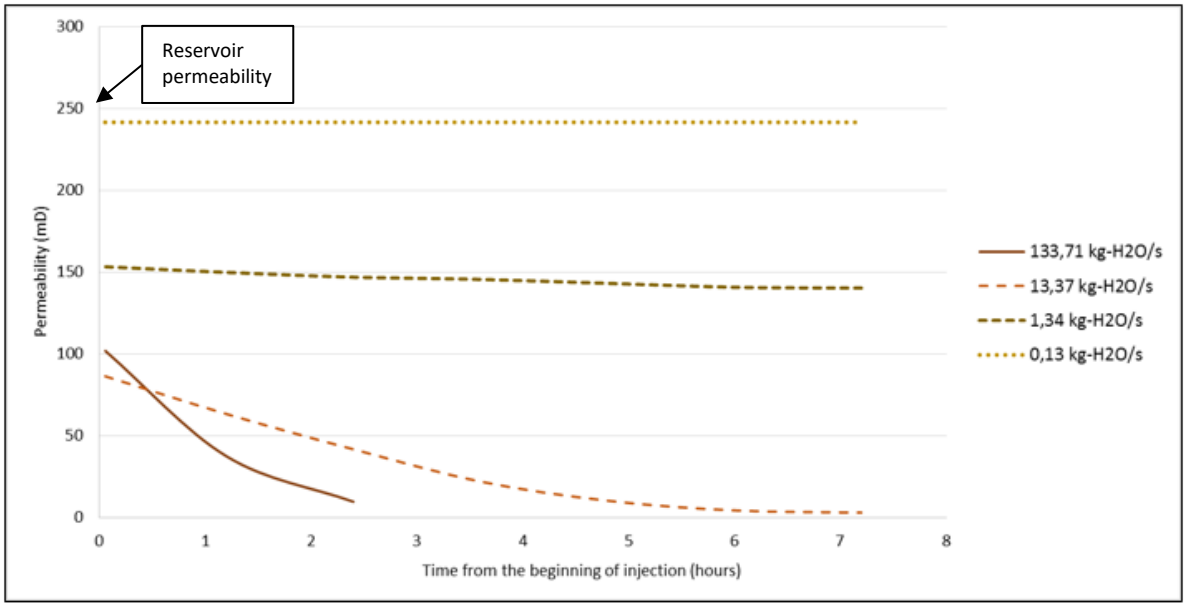

Figure 26: Permeability reduction for the four injection rates 0.13 kg- H_2O/s, 1.34 kg- H_2O/s, 13.37 kg- H_2O/s and 133.71 kg- H_2O/s, respectively, at 12 cm from the well regarding time from the beginning of injection. (Gel concentration = 5 wt%)

The curves of the two smallest injection rates simulations do not present significant evolution with time and can be linked to the fact that most of the reduction happens within the 10 first cm from the well for the both simulation and that this diagram displays results at a distance of 12 cm from the well. However, these two simulations present a constant permeability difference of almost 100 mD over the entire injection process.

The simulations using the two highest rates experienced remarkable permeability reduction with time, and both achieved an almost complete sealing of the well vicinity. It can be noticed that the curve of the simulation using the injection rate of 133.71 kg- H_2O/s crosses the one using 13.37 kg-H_2O/s. It implies that in the first minutes of injection, the permeability is more reduced at 12 cm by the second highest rate than by the highest one. It can be because the maximum rate of injection results in a bigger flow pressure that carries the injected solution at a further distance from the well in the first minutes of injection. Therefore a smaller amount of solution is present at the 12 cm location to reduce the permeability.

Table 23 shows the simulation results. The cases highlighted in green show when the grouting is done. A complete sealing of the well is achieved after 2.4 hours with the highest injection rate equals to 133.71 kg-H_2O/s involving a gel volume of 57.71 m³. With the injection rate of 13.37 kg-H_2O/s, the complete sealing is reached after 3.6 hours and 8.66 m³ of gel.

The two smallest injection rates do not achieve a complete sealing within the 6 hours of the injection process.

Table 23: Simulations results of porosity and permeability regarding the different injection rates

Distance from the well [cm]	Time of gel solution injection [hour]	Injection rate [kg-H_2O/s] = 0.13		Injection rate [kg-H_2O/s] = 1.34		Injection rate [kg-H_2O/s] = 13.37		Injection rate [kg-H_2O/s] = 133.71	
		Porosity [%]	Permeability [mD]	Porosity [%]	Permeability [mD]	Porosity [%]	Permeability [mD]	Porosity [%]	Permeability [mD]
Next to the well	1.2	7	179	6	82	4	33	4	21
	2.4	7	170	5	63	3	11	0	0
	3.6	7	165	5	55	1	1	-	-
	6	7	156	4	21	0	0	-	-
12	1.2	8	242	7	150	5	63	4	37
	3.6	8	242	7	146	4	22	-	-
	6	8	242	7	141	2	4	-	-
21	1.2	8	250	8	211	6	96	5	73
	3.6	8	250	8	211	6	79	-	-
	6	8	250	8	211	5	57	-	-
34	1.2	8	250	8	241	7	130	6	127
	3.6	8	250	8	241	6	127	-	-
	6	8	250	8	241	6	123	-	-

Conclusion of the sensitivity analysis (Injection rate)

Changing the injection rate of the process has a significant impact on the permeability reduction. Because the injection process lasts for a total of 6 hours, changing the injection rate leads to a big difference regarding the amount of gel injected, as it was the case when changing the colloidal silica concentration. Regarding distance, the injection rate change presents most of its impact within the first centimeter from the well or at a further distance depending on the injection rate. Regarding time, the effect on the model increases with it and is the most significant at the end of the injection process. The slope of the permeability decrease is reduced and observed at a time unique to each injection rate.

As for changing the colloidal silica concentration, changing the speed of injection allows estimating the most optimal amount of solution to inject. At some locations, similar grouting is achieved for different injection regime with different time of injection. For instance, at the site next to the well, the injection rate of 1.34 kg-H_2O/s achieved after 6 hours the same porosity and permeability reduction (Porosity = 4; Permeability = 21 mD) as the injection rate of 133.71 kg-H_2O/s after 1.2 hours. However, for this particular grouting, the first injection rate only injected 8.66 m^3 of gel while the second injection rate injected 28.88 m^3. A similar comparison is possible for the location at 34 cm from the well where after 3.6 hours the injection rate of 13.37 kg-H_2O/s (8.66 m^3 of gel) achieved an equal grouting as the injection rate of 133.71 kg-H_2O/s (28.88 m^3 of gel) after 1.2 hours. Therefore, regarding cost savings regarding water and gel volume injected, it appears that using a smaller injection rate during a longer time is more advantageous than higher injection rate during a shorter time.

5.4. CONCLUSION OF THE SENSITIVITY ANALYSIS

The sensitivity analysis of porosity-permeability relation showed that the Carman-Kozeny relation tends to reduce more the porosity and the permeability than the Cubic law. As a cause, the additional multiplying term ($\frac{(1-\phi_i)^2}{(1-\phi)^2}$) in the Carman-Kozeny equation being less than 1 if porosity is reduced. Due to the decreasing linear trend of this term when going from low initial porosity to high porosity, the difference between the two relations increases with increasing initial porosity. However, the difference in term of permeability reduction is not really large. The choice of the relation is the user and can be accurately define only if site-specific investigations are realized. In absence of accurate information, suggestion is made to choose the Carman-Kozeny relation as it consider matrix permeability only.

The sensitivity analysis regarding reservoir temperature showed that temperature has an impact on the gel grouting because it modified the gel formation. As a cause, the fact that the kinetic rates of the gel are temperature dependent following the Arrhenius equation. When reducing temperature, the Arrhenius equation causes a larger reduction in the dissolution rate of the gel than of its precipitation rate. As a result, more gel forms than is dissolved and permeability is further reduced. However, reducing temperature showed that there is a certain temperature threshold where the precipitation rate is become so predominant compared to the dissolution rate that the entire gel solution is formed. Therefore, from this threshold, the maximum gel formation and permeability reduction possible are reached regarding the amount of gel solution injected.

The sensitivity analysis regarding colloidal silica concentration and injection rate gave relevant information to define the most optimum injection regime. It was seen that similar grouting could be experienced with different colloidal silica concentration and different injection rate respectively. It appeared that with the same injection regime, it is more advantageous to inject a highly concentrated colloidal silica solution than a less concentrated solution since less amount of gel is injected with the first solution to achieve a similar grouting. Similarly, it appeared that for a similar sealing with the same colloidal silica solution, using a small injection rate for a long time is more advantageous than high injection rate during a short time.

Also, the analysis showed that for a same amount of gel injected, a better grouting was achieved with a lower injection rate and a higher colloidal silica concentration than with a higher injection rate and a lower colloidal silica concentration. For instance, after 6 hours of injection, the injection of 1.45 m³ of the gel using a solution of 5wt% and an injection rate of 1.34 kg-H_2O/s resulted in a porosity of 4% and a permeability of 21 mD. As a comparison, after 1.2 hours of injection, the injection of 1.44 m³ using a solution of 2.5 wt% and an injection rate of 13.37 kg-H_2O/s resulted in a porosity of 6% and a permeability of 105 mD.

The tornado plots in Figure 27 below are built to show the results of the sensitivity analysis considering the parameters of concentration, of injection rate and reservoir temperature. The setting of porosity-permeability relation is not incorporated into the plot since this parameter is related to equations and not to values. Each parameter is increased, or decreased compare to a

base case mentioned on the left of the plots. The plots show the resulting permeability after 2.4 hours of injection and this at 12 cm from the well, but also the volume of gel that was injected to realize the grouting. Also, the last tornado plot indicates the relative influence on permeability reduction of each parameter.

The gel concentration of the solution is the parameter which has the biggest influence on the permeability reduction, followed by the injection rate and then the reservoir temperature. For both the concentration parameter and the injection parameter, the negative effect of reducing their value is significantly larger than the positive effect of increasing them. However, the difference between increasing the gel concentration and increasing the injection rate is quite significant since increasing the gel concentration has an important effect on the permeability reduction while enhancing the injection rate has not.

Also, the plot allows appreciating the advantage of changing the gel concentration compared to changing the injection rate. The high and low value of both parameters achieved an almost similar permeability reduction after 2.4 hours of injection. However, for a quasi-similar grouting, the amount of gel injected by changing the gel concentration is remarkably smaller than for the injection rate parameter which allows saving much money. Therefore, to conduct an effective grouting with the lowest costs, the gel concentration of the solution is the main factor to control.

Regarding reservoir temperature, the adverse effect on permeability reduction of increasing it is slightly larger than the positive effect of reducing it. However, the influence of reservoir temperature on permeability reduction has almost no effect and is subtle compared to the other parameters since the resulting permeabilities after 2.4 hours of injection are almost similar.

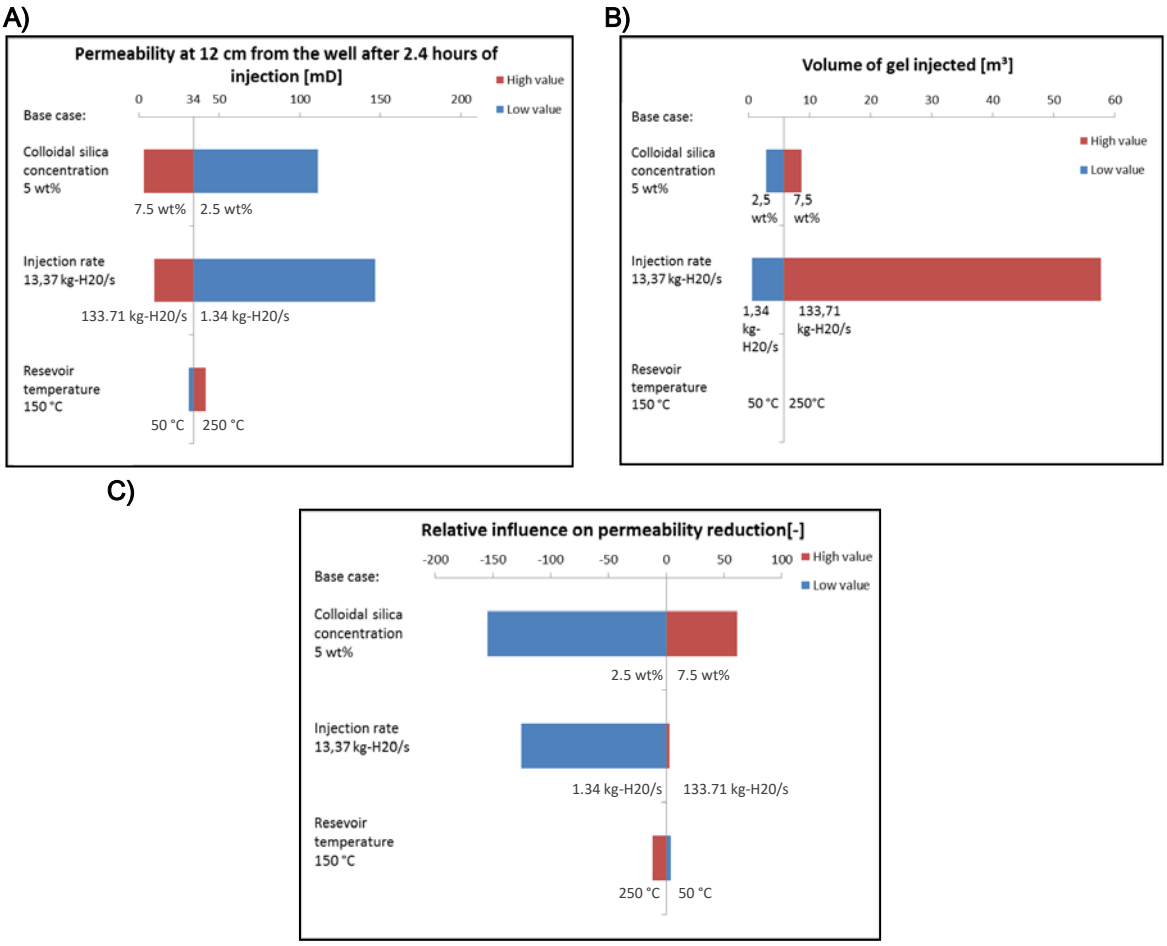

Figure 27: Tornado plots of the gel concentration parameter, injection rate parameter and reservoir temperature parameter. A) Resulting permeability at 12 cm from the well after 2.4 hours of injection; B) Volume of gel injected; C) Relative influence on permeability reduction.

CHAPTER 6. SIMULATION OF THE COLLOIDAL SILICA GEL REMOVAL BY A HIGHLY ALKALINE SOLUTION

6.1. INTRODUCTION

In addition to the previous simulation experiencing the injection of colloidal silica gel through the hypothetical field, another simulation was built to show the TOUGHREACT code ability to remove the emplaced gel by controlling the pH condition of the medium with the injection of a highly alkaline solution. However, this simulation was realized before the creation of the hypothetical conceptual field. Therefore, due to a lake of time and an expiring TOUGHREACT module license, the removal of the colloidal silica gel is not applied to the hypothetical field, but this stochastic simulation allows appreciating the TOUGHREACT ability to remove the gel.

It has to note that even though the possible gel implementation in the TOUGHREACT code follows the same manipulations as the previous simulations, many parameters were set randomly. Worthing for the domain setup, materials parameters, initial temperature and pressure condition and solution composition. However, it was tried to approach realistic values.

Because this simulation was built before the creation of the conceptual field, it has to be noted that the results cannot be compared with the results and sensitivity analysis of the previous chapter. The only goal of this simulation is to proof the TOUGHREACT ability to remove the gel by controlling the pH regardless accurate predictions.

6.2. MODEL DEVELOPMENT

6.2.1. Domain setup

The domain of the model is built by a 2D rectangle of 20 meters long in the vertical direction starting at -1000 m. In the horizontal direction, the domain has an extent of 10 m. The grid of the model is composed of 50 cells in the x-direction and 50 cells in the z-direction resulting in a total of 2500 cells over the entire domain. In the y-direction, the model is 0.1 m width. The injection well was attributed to the two columns of highlight cells (Figure 28). These cells were turned to source/sink condition and were injecting the two different solutions with the left column injecting the colloidal silica gel solution and the right column the alkaline solution. The reason of the different injection sources is that the TOUGHREACT code does not allow assigning different solutions to inject into a same sink/source cell. The well has a vertical extent of 16 m and a radius of 0.1 m.

The domain parameters are given in Table 24.

Table 24: Domain setup of the alkaline injection conceptual model

Parameters	Value
Horizontal extent (x-direction)	10 m
Horizontal extent (y-direction)	0.1 m
Vertical extent (z-direction)	20 m
X-direction division	50 cells
X-direction cell size	0.2 m
Y- direction cell size	0.1 m
Z-direction division	50 cells
Z-direction cell size	0.5 m
Total mesh	2500 grid blocks
Top layer elevation	-1000 m asl
Bottom layer elevation	-1020 m asl
Well length	16 m
Elevation of the top of the well	-1002 m asl
Elevation of the bottom of the well	-1018 m asl
Well radius	10 cm

6.2.2. Model materials

The average porosity of the reservoir is 25% and the average permeability to 10118 mD, rock density is 2600 kg/m³, and wet heat conductivity is 2.0 W/(m*K). These values were assigned to the entire domain. However, several cells next to the injection well were assigned with materials of lower porosity and permeability to represent the clogging materials reducing the optimal functioning of the injection well (Figure 28). Only porosity and permeability of these clogging materials (Table 25) were different the reservoir material. Excepted porosity and permeability, the parameters values of the input materials were left to the default values in TOUGHREACT.

Table 25: Materials of the model

Material	Porosity [%]	Permeability [mD]	Density [kg/m³]	Conductivity [W/(m*K)]	Specific heat [J/(kg*K)]
Reservoir material	25	10118	2600	2.0	1000
Clogging materials:					
Low por/perm (Lperm)	10	1.0e-3	2600	2.0	1000
Medium-Low por/perm (MLper)	15	1	2600	2.0	1000
Medium por/perm (Mperm)	18	10	2600	2.0	1000

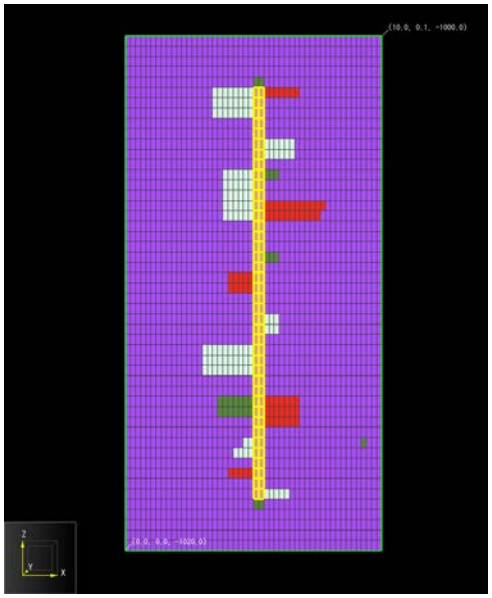

Figure 28: Materials distribution within the domain. The injection well corresponds to the highlight cells. The cells colored in purple are attributed to the reservoir material, the blue cells are attributed to the Lperm material, the red cells are attributed to the MLper material, and the green cells are attributed to the Mperm material.

6.2.3. Initial, static and dynamic pressure and temperature conditions

Before initialization, an initial temperature of 75°C and an initial pressure of 170 bars were specified across the domain. The initial thermophysical conditions of the system are shown in Table 26. Relative permeability and capillary pressure were set to the same relationships and values as in Chapter 4.

Table 26: Initial parameters of the conceptual model for the alkaline injection. Default values are based on Xu et al. (2011)

Model parameter		Value
T	temperature [°C]	75
P	pressure [bar]	170
Relative permeability – van Genuchten		
m	exponent	0.457
S_{lr}	irreducible water saturation	0.3
S_{gr}	irreducible gas saturation	0.05
Capillary pressure – van Genuchten		
m	exponent	0.457
S_{lr}	irreducible water saturation	0
P_0	Strength coefficient [kPa]	19.61

With these initial conditions, the model run for 100 000 years to reach a steady state across the domain. Again, the first layer of the domain was set to fixed state to keep its pressure and temperature constant to induce a pressure and temperature gradient (Table 27). The created pressure gradient is of 100 bars/km with a pressure of 170 bars at the top of the model and 172 bars at the bottom of the model. A similar temperature gradient was created to represent realistic conditions. However, due to the short extent of the domain in the vertical direction, a temperature of 75°C was induced over the entire domain.

Table 27: Pressure and temperature conditions after 100 000 years of static simulation.

Parameter	Value
Pressure at the top of the domain	170 bars
Pressure at the bottom of the domain	172 bars
Pressure gradient	100 bars/km
Temperature	75°C

During the dynamic simulations, the static condition after 100 000 years was used as initial conditions. Also, the lower and upper boundaries of the domain were set to fixed state to hold a no-flow condition, representing a lower and an upper confining units surrounding the reservoir. The left and right boundaries of the domain were specified as no flow as well and may be considered as surrounding faults.

6.2.4. Geochemical conditions

As for the first simulation, the short time interval of the current simulation regarding colloidal silica gel injection encourages the use of simplified geochemical conditions, as the extent of primary species dissolution and secondary species accumulation expected to occur in this interim is extremely limited and will not significantly change the initial geochemical conditions. Therefore, based on the model of Druhan et al. (2014), the original reservoir composition is simplified to 80% of quartz (SiO_2), 16% of albite ($NaAlSi_3O_8$) and 4% of anorthite ($CaAl_2Si_2O_8$). In addition to the initially present minerals, kaolinite and calcite are allowed to form even though the small time of interval of the simulation neglects appreciable accumulation of these secondary minerals. All the thermodynamic data such as dissolution and precipitation rates are taken from Palandri & Kharaka (2004) who compiled and fitted experimental data reported by many investigators. Initial mineral volume fractions, kinetic rate parameters, mineral grain radius and reactive surface area are provided in Table 28.

Table 28: List of parameters for minerals considered in the present simulation (Xu et al. 2004; Palandri & Kharaka 2004). *The first line indicates dissolution parameters and the second line precipitation parameters. For albite, anorthite, and kaolinite, the third and fourth lines are acidic and basic additional mechanisms.*

Mineral	Volume fraction [cm³ mineral/cm³ solid]	Rate constant k_{25} [mol/m²/s]	Activation energy E_a [kJ/mol]	Reaction order n regarding H^+	Mineral grain radius [cm]	Reactive surface area [cm²/ g mineral]
Quartz	0.80	3.98-14	87.7	0.0	0.001	9.8
		3.98-14	87.7	0.0		
Albite	0.16	1.479e-12	69.8	0.0	0.001	9.8
		1.479e-12	69.8	0.0		
		6.9e-10 (H^+)	65.0	0.457		
		2.51e-16 (H^+)	71.0	-0.572		
Anorthite	0.4	7.58e-10	17.8		0.001	9.8
		7.58e-10	17.8			
		3.16e-4 (H^+)	16.6	1.411		

Kaolinite	0.0	6.09e-14	22.2	0.0	0.001	151.6
		6.09e-14	22.2	0.0		
		4.9e-12 (H^+)	65.9	0.777		
		8.912e-18 (H^+)	17.9	-0.472		
Calcite	0.0	Equilibrium				
Hypothetical colloidal silica gel	0.0	7.32e-13	60.9	0.0	5.0e-8	1000000.0
		3.80e-10	49.8	0.0		

As the initial mineral composition, the initial fluid composition of the reservoir was based on Druhan et al. (2014). However, the fluid compositions of the injected solutions were set by trial and error. The fluid composition of the reservoir, of the gel solution and the alkaline solution, are presented in Table 29.

Table 29: Fluids composition of the simulation (T=75 °C).

Primary species	**Concentration [mol/kg H_2O]** *Fluid reservoir*	**Concentration [mol/kg H_2O]** *Colloidal silica gel solution*	**Concentration [mol/kg H_2O]** *Akaline solution*
pH	± 7.0	± 7.5	± 10.0
AlO_2^-	7.03e-8	7.03e-8	3.0
Br^-	1.0e-13	0.01	0.0
Ca^{2+}	6.49e-5	6.49e-5	6.49e-5
Cl^-	1.0	1.0	1.0
H^+	1.0e-7	1.0e-7	1.0e-7
H_2O	1	1	1.0
HCO_3^-	0.0455	0.0455	0.0455
Na^+	0.0992	1.0	1.0
$SiO_2(aq)$	8.45e-4	0.1	8.45e-4

Similarly to the first simulation performed in this paper, the porosity-permeability relationship used for this simulation is the Carman-Kozeny relationship. All the parameters regarding the hypothetical colloidal silica gel are those described in section 6.3.

6.2.5. Model stability

Parameters regarding output controls and simulation convergence have to be defined to run a simulation with TOUGHREACT, The parameters that were manually modified are the same as those described for the gel injection scenario in Section 4.3. Moreover, their values are equal. These parameters can be found in Tables 10. The other parameters in TOUGHREACT were left to their default values. For more information regarding the TOUGHREACT simulation parameters see the TOUGHREACT user's guide (Xu et al. 2012).

6.2.6. Time discretization

The simulation was run for a total of 150 days. Injection of the gel was performed during 10 days starting on the fortieth day, and alkaline solution injection lasts for 30 days starting on the hundredth day. It was decided to initiate the injection on the fortieth day to be able to see the grouting emplacement accurately. The printed outputs were chosen to focus on the injection processes (Table 30).

Table 30: Printed outputs times of the alkaline injection simulation

Printed outputs times
1 days
10 days
20 days
30 days
40 days *(Start of the gel injection)*
43 days *(3 days of gel injection)*
45 days *(5 days of gel injection)*
48 days *(8 days of gel injection)*
50 days *(10 days and end of gel injection)*
75 days
100 days *(Start of alkaline solution injection)*
101 days *(1 day of alkaline solution injection)*
105 days *(5 days of alkaline solution injection)*
110 days *(10 days of alkaline solution injection)*
115 days *(15 days of alkaline solution injection)*
120 days *(20 days of alkaline solution injection)*
130 days *(30 days and end of alkaline solution injection)*
150 days

6.3. SIMULATION RESULTS

The purpose of this simulation is to present the TOUGHREACT ability to precipitate colloidal silica gel under neutral pH condition and to dissolve the emplaced gel by raising the pH to alkaline condition with the injection of a highly alkaline solution. More information about factors affecting colloidal silica gel stability is described in Chapter 2.

For this simulation, multiple days of injection of the gel and the alkaline solution are performed from the injection well. As for the simulation in Section 7.1., the injected gel solution is set to a slightly alkaline (almost neutral) solution to reduce the gelation time of the gel and to trigger the gelation process upon direct contact with the reservoir fluid. The colloidal silica solution is injected for a total of 10 days starting on the 40th day of simulation and at a rate of 0.03 kg/m²/s, or a total of 0.29 kg/s over the entire well extent.

The alkaline solution is injected 50 days after the end of the colloidal silica gel injection for 30 days. The injection was set at a rate of 0.001 kg/m²/s or a total of 9.6e-3 kg/s throughout the entire well. Figure 29 presents the situation of the colloidal silica gel (referred as SiO_2(am)) during the entire simulation, including its emplacement, and its removal.

The injection rates of both the gel solution and the alkaline solution are very small resulting in large injection time. Such injections time are not realistic regarding industrial operations. However, the injection time can be reduced either by increasing the injection rate or the solution concentration. As seen in the previous chapter, the emplacement of the gel can be achieved within a few hours. With a suitable alkaline solution injection rate, the removal of the gel can speed up and realized within a few hours as well.

While this model is a clear simplification of the conditions encountered in a high-temperature geothermal reservoir, it serves as a mean of demonstrating the ability of using the TOUGHREACT code to precipitate hypothetical colloidal silica gel in the vicinity of an injection well and this to a sufficient extent to reduce permeability of permeable zones but also to show the possibility of removing the gel emplaced with the injection of a highly alkaline solution.

Table 31 presents the injection regime of both the gel solution and the alkaline solution. The green cases show the time and the volume of gel required to achieve the grouting of the well vicinity. The orange cases indicate the time and the amount of alkaline solution needed to remove the gel.

Table 31: Injection regime of the simulation of the gel removal by alkaline solution.

Simulation time [days]	Injection rate of gel solution [kg-H_2O/s]	Total volume of H_2O injected [m³]	Total volume of gel injected [m³]	Injection rate of alkaline solution [kg-H_2O/s]	Total volume of alkaline solution injected [m³]
0	0	0	0	0	0
40 *(start of gel injection)*	0.29	0	0	0	0
43 *(3 days of gel injection)*	0.29	75.16	3.76	0	0
48 *(8 days of gel injection)*	0.29	200.44	10.02	0	0
50 *(10 days and end of gel injection)*	0.29	250.56	12.53	0	0
100 *(start of alkaline solution injection)*	0	250.56	12.53	9.6e-3	0
101 *(1 days of alkaline solution injection)*	0	250.56	12.53	9.6e-3	8.29

105 *(5 days of alkaline solution injection)*	0	250.56	12.53	9.6e-3	41.47
110 *(10 days of alkaline solution injection)*	0	250.56	12.53	9.6e-3	82.94
115 *(15 days of alkaline solution injection)*	0	250.56	12.53	9.6e-3	124.41
130 *(30 days and end of alkaline solution injection)*	0	250.56	12.53	9.6e-3	248.82

A) Few minutes of colloidal silica gel injection

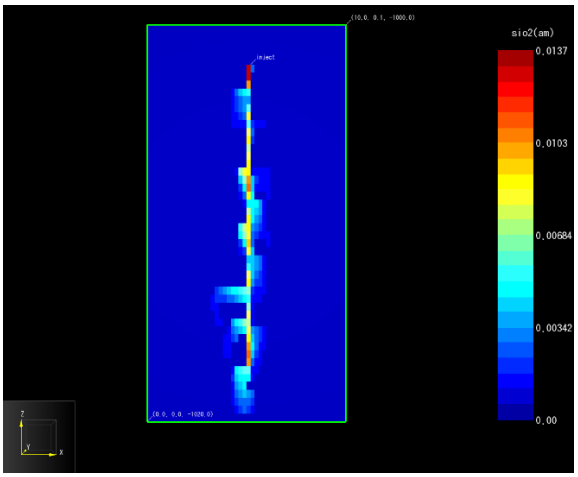

B) 3 days of colloidal silica gel injection

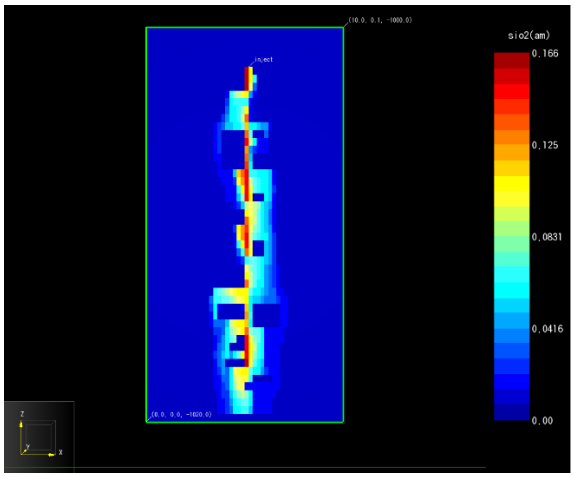

C) 8 days of colloidal silica gel injection

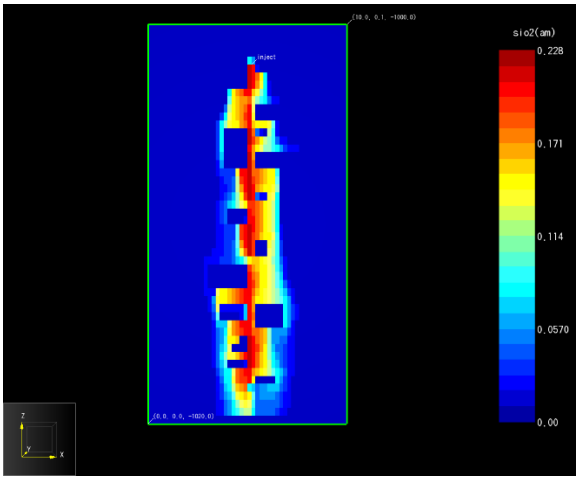

D) 10 days of colloidal silica gel injection

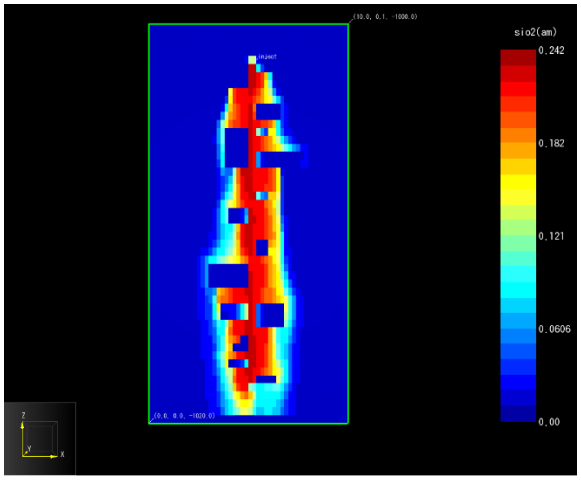

E) 30 days after the end of the colloidal silica gel injection

F) 1 day of alkaline solution injection

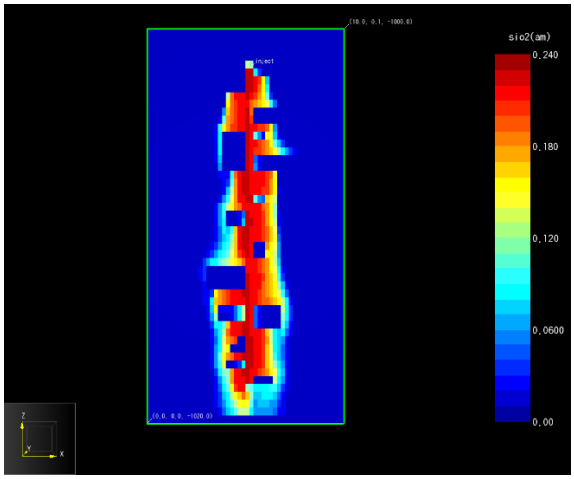

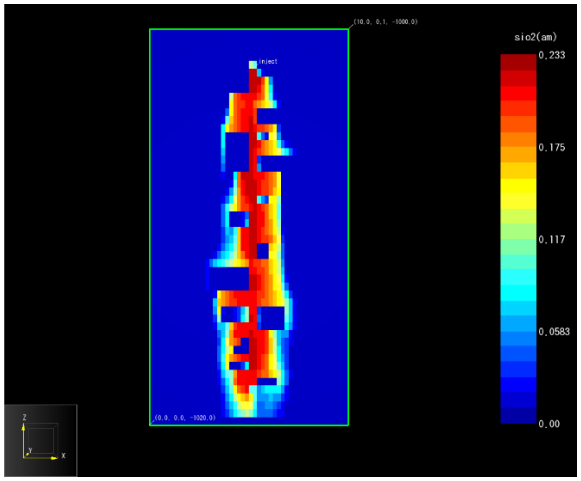

G) 5 days of alkaline solution injection

H) 10 days of alkaline solution injection

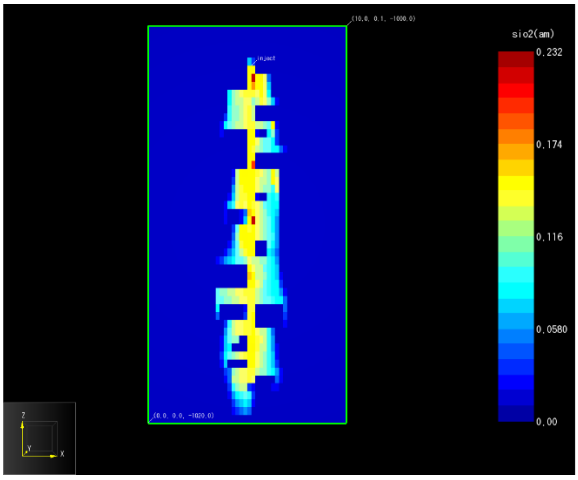

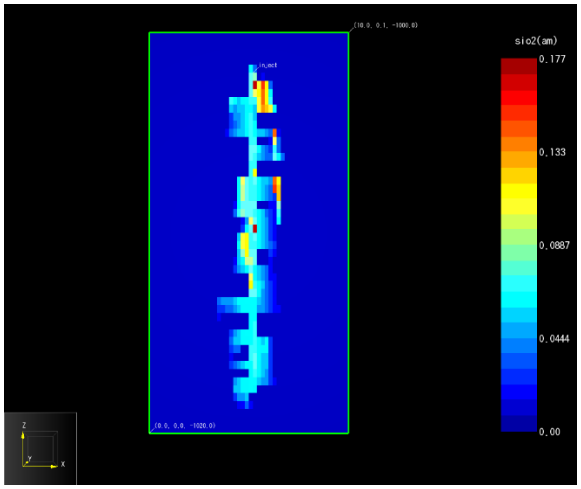

I) 15 days of alkaline solution injection

J) 30 days of alkaline solution injection

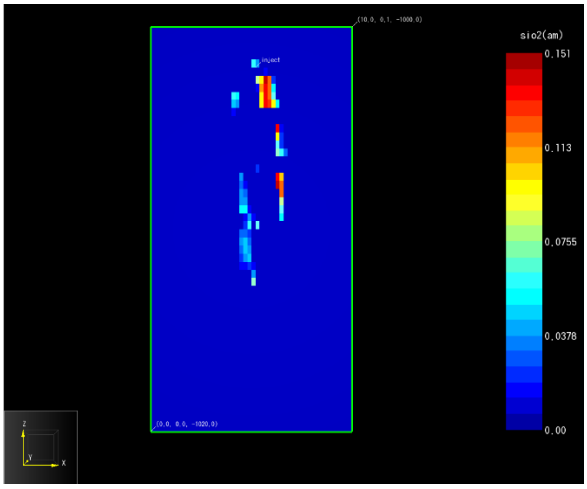

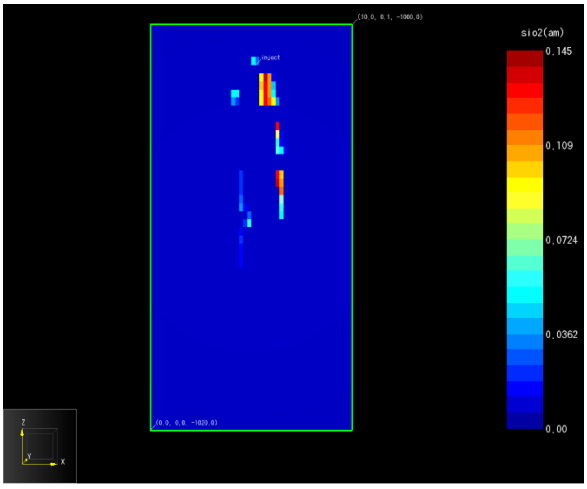

Figure 29: Time series of colloidal silica gel (SiO_2(am)) propagation for 10 hours of continuous injection of colloidal silica solution from a 16 meters long injection well and removal of the gel by the 30 days continuous injection of a highly alkaline solution, starting 50 days after the end of the colloidal silica gel injection. A) Few minutes of colloidal silica gel injection; B) 3 days of colloidal silica gel injection; C) 8 days of colloidal silica gel injection; D) 10 days of colloidal silica gel injection; E) 30 days after the end of the colloidal silica gel injection; F) 1 day of alkaline solution

injection; G) 5 days of alkaline solution injection; H) 10 days of alkaline solution injection; I) 15 days of alkaline solution injection; J)30 days of alkaline solution injection. The domain extent is 20 m long in the vertical direction and 10 m long in the horizontal direction.

Due to the almost neutral pH of the injected solution, colloidal silica gel starts to precipitate directly when reaching the reservoir fluid and reduce the permeability of the area surrounding the well. The gel is emplaced and remains stable in this pH conditions even after the end of the colloidal silica gel injection. After a while, the highly alkaline solution is injected for several days raising the pH to alkaline conditions.

In this range of pH, the colloidal silica gel is not stable as a solid phase (gel) anymore and is dissolved back into a liquid solution. As explained in Chapter 2, colloidal silica gel stays in a stable gel phase if pH conditions do not change permitting, therefore, the well recovery treatment. As soon as the chemical treatment of the well is completely performed, the TOUGHREACT code allows estimating the optimal injection of alkaline solution used to raise the pH of the area and dissolve the gel. Furthermore, the model shows clearly the preferential flow paths of the colloidal silica gel into the high permeability zones as it can be seen by the extent of the gel front.

Figure 30 presents on the left y-axis the permeability reduction (blue curve) regarding time within high permeability zones. Also, the figure exhibit on the right y-axis the porosity reduction and the corresponding gel emplacement using volume fraction and this, regarding time. Both permeability and porosity are reduced to almost zero due to the colloidal silica gel injection starting at the 40th day. At the same time, the colloidal silica gel is emplaced, and its volume fraction increases to almost 25% which is equal to the reservoir porosity. After remaining stable for 50 days from the injection shut off, the gel started to be dissolved back to the liquid phase on the 100th days of simulation as the injection of the highly alkaline solution began. At the same moment, permeability and porosity rise back to almost their initial values with the gel withdrawal.

Table 32 gives the simulation results regarding porosity and permeability. The cases highlighted in green show when the grouting is achieved and the cases highlighted in orange indicates when the removal of the gel is done.

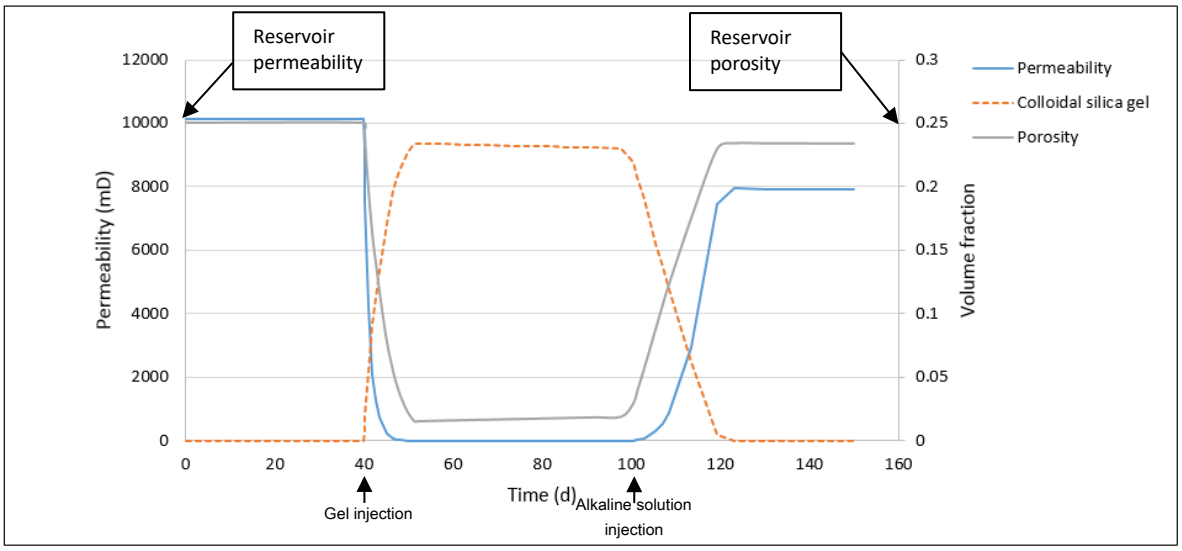

Figure 30: Both permeability reduction (left y-axis) and porosity reduction and gel emplacement (right y-axis, regarding time, concerning the simulation involving colloidal silica gel injection and gel removal with highly alkaline solution injection.

Table 32: Simulation results regarding porosity and permeability

Simulation time [days]	Porosity [%]	Permeability [mD]
40 (start of gel injection)	25	10118
43 (3 days of gel injection)	13	873
48 (8 days of gel injection)	4	10
50 (10 days and end of gel injection)	2	2
100 (start of alkaline solution injection)	2	2
101 (1 days of alkaline solution injection)	4	15
105 (5 days of alkaline solution injection)	7	226
110 (10 days of alkaline solution injection)	13	1365
115 (15 days of alkaline solution injection)	19	3854
130 (30 days of alkaline solution injection)	23	7902

CHAPTER 7. DISCUSSION

7.1. SIMULATIONS ACCURACY

The representation of the Wayang Windu geothermal field is very conceptual. The geometry and the property of the field are based on literature only since no site investigations were made and no data were available. Parameters such as rock materials distribution, mineral composition, transport processes (advection, diffusion, dispersion, adsorption, and decay), porosity-permeability relationship, thermal gradient and presence of structural units (faults, folds, and so forth.), would be increasing the accuracy of the field. However, since the scope of this research is to proof the TOUGHREACT code ability to inject the gel into high permeability zones, the accuracy of the field would be a concern for further studies and industrial needs.

As explain previously, the composition of the reservoir fluid does not represent the reality due to lack of samples information and accurate data in the literature. Therefore, the choice is made in this research to approach as much as possible the pH condition of the reservoir regardless accurate species concentration since it is a major factor of the gel emplacement. The reservoir fluid composition is thus the result of trial and error simulations to reach the pH desired. Similar manipulations were realized concerning the injected solutions. Even though the colloidal silica concentration ($SiO_2(aq)$) is accurate to respect the weight percentage desired, the other species of the solutions are manipulated to achieve the desired pH condition, either for the gel solution or the highly alkaline solution. Therefore, the composition of solution used in the industry would increase the accuracy of the simulation.

The amount of gel injected in the initial solution seems to be a bit high regarding the industrial purpose and might be the result of either a too large injection rate or a too high colloidal silica concentration in the injected solution. However, these simulations are built based on many guesses. For instance, the extent of the well to be sealed is 140 m in this case, but it might be smaller in reality. Also, the distance from the well that the gel grouts significantly is around 45 cm in this research, however, companies might want the gel to seal a smaller area around the well. Also, the injection rate and concentration are chosen to reduce the permeability around the well drastically, however, such a reduction might be not necessary for the well recovery.

The gel used in this study is based on the colloidal silica gel under investigation at the Lawrence Berkeley National Laboratory (Druhan et al. 2014). However, implementing into the TOUGHREACT database the properties of industrial gel might be more accurate.

An already highly refined grid is used to simulate the gel injection in this study. However, by increasing the number of grid cells would result in more accurate results.

Finally, the black spot of this research is the lack of model validation based on experimental data. As a cause, the use of these grouting techniques mainly within the oil and gas industry which do

not share their operation reports. Regarding academic researchers, the novelty of this study does not permit to find appropriate experiments in the literature. However, researchers, such as Druhan et al. (2014), used the TOUGHREACT code to model colloidal silica gel injection for another purpose than well sealing. This research might reinforce the validity of the model.

7.2. MODEL LIMITATIONS

Four factors affect the results of the simulations. The first one is related to the chemical reaction involved in the gelation process. A chemical reaction has to be defined to create the gel and this based on the injected components. However, even though the colloidal silica is about 5 wt% of the injected solution, not all species are converted to gel. Also, some water should also be introduced in the gel structure, but the TOUGHREACT code does not allow to implement water in the chemical reaction. The gel creation is simplified to a result of SiO_2(aq) precipitation in SiO_2(am). Therefore the gel concentration might be slightly biased and difficult to predict.

The gelation kinetics of colloidal silica is not fully understood and needs further investigation. The model creates a significant amount of gel instantly upon contact with the slightly acidic fluid of the reservoir. However, in reality, the gel would form after a certain while. The gelation time of the injected gel has to be understood to make the model more accurate.

The blocking mechanism in TOUGHREACT is considered regarding increasing volume fraction of the gel into the pore throats. This deviates from the reality since the RRF described in Chapter 2 is based on the mobility of the fluid and not the gel adsorption. In the model, the gel is formed and adsorbed by the medium, which reduces the permeability of the rock. In real conditions, the viscosity of the colloidal silica condition increases to a point where it is too viscous to displace and therefore grout the pores. This mechanism is not taken into considerations in this model.

TOUGHREACT allows injecting only water or predefined component using its well function. Therefore, solutions to which the composition can be manipulated are injected using cells turned into source/sink condition. However, TOUGHREACT allows injecting only one designed solution by source/sink cell. In the case of multiple solutions of different compositions to inject, this could bias the result as the hypothetical well would have a wrong geometry and the solutions would be injected at different location although close to one another.

CHAPTER 8. CONCLUSION

The main goal of this research was the development of a model able to simulate the emplacement of grouting gel into geothermal reservoirs and the possibility of estimating the most optimal injection regime of the gel. More precisely, this model was developed to simulate pre-treatment of clogged well recovery operation. Chemical treatment of the well can remove the clogging materials using dissolving acids. However, the chemicals injected tend to flow preferentially into the high permeability zones remaining around the well. The model simulates, therefore, the permeability reduction of the high permeability zones surrounding the well by injection of colloidal silica gel. The gel injection seals the well vicinity completely and allows proceeding with the recovery treatment.

Using the TOUGHREACT code developed by Thunderhead Engineering, it was possible to model the injection of colloidal silica solution which precipitates to form a gel upon contact with the reservoir fluid if pH conditions are met. Kinetic of colloidal silica gel is not well known and difficult to simulate. However, pH is considered as the major factor controlling the gelation of the colloidal silica solution. Therefore, it was used as a trigger in the model to simulate the gel precipitation. The gel injection was simulated reducing the pH solution to almost neutral conditions and precipitated upon contact with the slightly acidic reservoir fluid.

Sensitivity analysis regarding porosity-permeability relation, reservoir temperature, injection rate, and colloidal silica concentration was performed. Changing the permeability-porosity relation showed a slight effect on the permeability reduction because of the variation between the two functions. Starting at the same initial porosity, the difference between the two relations increases until hitting a maximum at a particular reduced porosity. From the maximum, the difference decreases until the porosity is completely reduced. However, the relative difference between the two relations keeps increasing with decreasing porosity.

Reducing the reservoir temperature resulted in a faster gel formation because of the temperature effect on the kinetic rates of the gel. Regarding Arrhenius equation, when the temperature is decreased, the dissolution rate decreases faster than the precipitation rate. Thus, the precipitation becomes more predominant compared to the dissolution rate. At a certain threshold temperature, the precipitation rate is become so dominant compared to the dissolution rate that the gel solution available is entirely precipitated. It results in the maximum gel precipitation possible and, therefore, the maximum permeability reduction possible regarding the amount of gel solution injected. However, the time to reach the complete sealing and the volume of gel injected are almost equal, and the variations regarding permeability reduction is not important.

One of the main interest of this model was to predict the most optimal injection regime of the gel. The results show that it is possible to observe the permeability reduction around the well, and its corresponding extent, following the gel propagation. Also, trial and error simulations regarding injection rate and colloidal silica concentration allow estimating the time needed to seal completely

the area surrounding the well. Since the simulation crashes when an unrealistic pressure is experienced, it is possible to consider the area around the well completely grouted when such pressure increase happens at the well location and makes the simulation end.

Moreover, the model allows to estimates the maximum extent from the well that can achieve a complete sealing. Depending on the injection rate and colloidal concentration chosen, permeability reduction time's curves come together at a particular location from the well and permeability is no further reduce beyond it, no matter the time of injection. However, the permeability reduction between the well and this particular location continues to increase with time until reaching a complete sealing. These two features are therefore strong indications about the most optimal injection regime as it gives the time needed to seal the direct vicinity of the well and the extent from the well that can achieve a complete shut-off.

The sensitivity analysis also showed that with the same injection regime, it is more advantageous to inject a highly concentrated colloidal silica solution than a less concentrated solution. It is because a smaller volume of gel is injected with the first solution to realize a similar grouting. Similarly, it was found that for a similar sealing with the same colloidal silica concentration, the use of a small injection rate during a long time is more advantageous than a high injection rate during a short time. Also, the analysis showed that for a same amount of gel injected, a better grouting is achieved with a lower injection rate and a higher colloidal silica concentration than with a higher injection rate and a lower colloidal silica concentration. Gel concentration is the main factor to control as it allows to achieve similar grouting as significant injection rate but with a significantly smaller amount of gel injected.

Another objective was to apply the model to the Wayang Windu geothermal field, Indonesia. This aim was realized in a very conceptual way as only few information about the field were available in the literature, and no experimental data from industry were readily accessible. As a result, the amount of gel injected in this study might be too high for industrial purpose. Therefore, a key outcome of this study is the recognition that TOUGHREACT can simulate colloidal silica grouting gel injection but that it must be developed in conjunction with an accurate understanding of the gel and the aquifer properties. These must be well characterized to achieve useful results and predictions. It is clear that the model can be applied to any situation knowing the field characteristics since two different hypothetical fields were modeled with various pressure and temperature conditions.

It was showed as a base scenario that with an injection rate of 13.37 kg-H_2O/s and a 5 wt% colloidal silica solution, a complete grouting of the area next to the well could be realized after approximately 3.6 hours of injection. This operation results in the injection of 8.66 m^3 of gel reducing the permeability to zero over a distance of roughly 5 cm from the well and decreasing the permeability significantly to the extent of about 45 cm. This result fits the industrial expectations, and the injection regime appears to be a good option.

An optimum injection regime can be predicted if the costs in terms of time of injection and volume of the gel are known. The optimum injection regime can be achieved by playing with the gel concentration and the injection rate. If the time of injection plays a significant role regarding costs, it can be reduced both by increasing the gel concentration and the injection rate. As explain above, similar results regarding permeability reduction and time of injection can be achieved by increasing the gel concentration or the injection rate. However, the amount of gel injected with the highly concentrated solution is significantly smaller than with the high injection rate resulting in lower costs.

Also, this research investigates the effect of pH on the precipitation and removal of the colloidal silica gel. It was showed that the removal of the gel was possible with the injection of a highly alkaline solution that increases the pH of the area around the well and dissolves back to liquid phase the gel that was previously formed. The removal of the gel is performed through a different conceptual simulation because it was done before the conception of hypothetical field based on the Wayang Windu field. Through this simulation, the area around the well is grouted with an injection of 12.53 m^3 of gel and is removed with the injection of 243.32 m^3 of an alkaline solution.

CHAPTER 9. RECOMMENDATIONS FOR FURTHER WORK

Recommendations for further work would be to validate the model using experimental data. Particularly regarding the amount of gel injected to be able to use the model for industrial purposes.

The gelation kinetic regarding chemical reactions can be studied and predicted at reservoir scale, most specifically to predict the gelation time accurately.

In the case of the Wayang Windu geothermal field representation, further investigation of the site have to be done to increase the accuracy of the simulations and to try matching the current situation.

Also, one continuous simulation could be performed so that blocking from and gel and removal can be simulated with the same reservoir conditions.

Finally, the behavior of the gel can be investigated regarding other parameters that those already investigated in this research.

REFERENCES

Ahmed, T. & Meehan, D.N., 2012. *Advanced Reservoir Management and Engineering*.

Anon, LUDOX® Sigma-Aldrich.

Arrhenius, S.A., 1889. Über die Dissociationswärme und den Einflusß der Temperatur auf den Dissociationsgrad der Elektrolyte. *Z. Phys. Chem.*, 4, pp.96–116.

Ashat, A., 2011. RESERVOIR MODELING OF THE NORTHERN VAPOR-DOMINATED TWO-PHASE ZONE OF THE WAYANG WINDU GEOTHERMAL FIELD, JAVA, INDONESIA. *PROCEEDINGS*.

Asrizal, M. et al., 2006. UNCERTAINTY QUANTIFICATION BY USING STOCHASTIC APPROACH IN PORE VOLUME CALCULATION, WAYANG WINDU GEOTHERMAL FIELD, W. JAVA, INDONESIA.

Bandyopadhay, I. et al., 2006. In situ stress analysis in deviated wells using inversion method: a case study from volcanic pyroclastics of WayangWindu Field, Java Indonesia.

Bear, J., 1972. *Dynamics of Fluids in Porous Media*.

Bogie, I. & Mackenzie, K.M., 1998. The application of a volcanic facies model to an andesitic stratovolcano hosted geothermal system at WayangWindu, Java Indonesia.

Bogie, I., Kusumah, Y.I. & Wisnandary, M.C., 2008. Overview of the Wayang Windu geothermal field, West Java, Indonesia. *Geothermics*, 37(3), pp.347–365.

Burns, L.D. et al., 2008. New Generation Silicate Gel System for Casing Repairs and Water Shutoff. In *SPE Symposium on Improved Oil Recovery*. Society of Petroleum Engineers.

Corey, A.T., 1954. The Interrelation Between Gas and Oil Relative Permeabilites. *Producers Monthly*, 19(1), pp.38–41.

Druhan, J.L. et al., 2014. A reactive transport model for geochemical mitigation of CO2 leaking into a confined aquifer. *Energy Procedia*, 63, pp.4620–4629.

Ezekwe Nnaemeka, 2010. Petroleum Reservoir Engineering Practice: Porosity of Reservoir Rocks.

Fitts, C.R. (Charles R., 2012. *Groundwater science*,

FracFocus Chemical Disclosure Registry, 2016. Fluid Flow in the Subsurface (Darcy's Law).

Gallagher, P.M., Conlee, C.T. & Rollins, K.M., 2007. Full-Scale Field Testing of Colloidal Silica Grouting for Mitigation of Liquefaction Ris. *Journal of Geotechnical and Geoenvironmental Engineering*, 133, pp.186–196.

Gallagher, P.M. & Finsterle, S., 2004. Physical and Numerical Model of Colloidal Silica Injection for Passive Site Stabilization. *Vadose Zone Journal*, 3(3), pp.917–925.

Gallagher, P.M. & Lin, Y., 2009. Colloidal Silica Transport through Liquefiable Porous Media. *Journal of Geotechnical and Geoenvironmental Engineering*, 135(11), pp.1702–1712.

Gallagher, P.M. & Mitchell, J.K., 2002. Influence of colloidal silica grout on liquefaction potential and cyclic undrained behavior of loose sand.

van Genuchten, M.T., 1980. A Closed-form Equation for Predicting the Hydraulic Conductivity of Unsaturated Soils1. *Soil Science Society of America Journal*, 44(5), p.892.

Green, D.W. & Willhite, G.P., 1998. *Enhanced Oil Recovery*

Hadi, J. et al., 2005. Overview of Darajat Reservoir Characterization: A Volcanic Hosted Reservoir. , pp.24–29.

Haitjema, H.M., 1995. Analytic Element Modeling of Groundwater Flow.

Helleren, J., 2011. Numerical Simulation of Chemical Flow-Zone Isolation. *Adsorption Journal Of The International Adsorption Society*, (June).

Howsam, 1990. *Water Wells - Monitoring, Maintenance, Rehabilitation* Silsoe College, Cranfield Institute of Technology, & UK, eds., University Press, Cambridge.

Hubbert, M.K., 1940. The theory of ground-water motion. *Transactions, American Geophysical Union*, 21(2), p.648.

Hund, W.J., Loomis, A.G. & Lamber Samuel Ernest, 1936. Method of treating wells with acids.

Iler, R.K., 1979. *The chemistry of silica : solubility, polymerization, colloid and surface properties, and biochemistry*, Wiley.

Jurinak, J.J. & Summers, L.E., 1991. Oilfield Applications of Colloidal Silica Gel. *SPE Production Engineering*, 6(4), pp.406–412.

Jurinak, J.J., Summers, L.E. & Bennett, K.E., 1989. Oilfield Application of Colloidal Silica Gel. *SPE International Syposium on Oil field chemistry*.

Krumrine, P.H. & Boyce, S.D., 1985. Profile Modification and Water Control With Silica Gel-Based Systems. In *SPE Oilfield and Geothermal Chemistry Symposium*. Society of Petroleum Engineers.

Laidler, K.J., reaction rate | chemistry | Britannica.com.

Lakatos, J. et al., 1999. Application of silicate-based well treatment techniques at the Hungarian oil fields. *SPE annual technical conference*.

Lasaga, A.C. et al., 1994. Chemical weathering rate laws and global geochemical cycles. *Geochimica et Cosmochimica Acta*, 58(10), pp.2361–2386.

Layman, E.B. & Soemarinda, S., 2003. THE PATUHA VAPOR-DOMINATED RESOURCE WEST JAVA, INDONESIA.

Masterton, W.L. & Hurley, C.N., 2004. *Chemistry - Principles and Reactions* Thomson Le.,

Mishra, S. et al., 2014. Effect of Polymer Adsorption on Permeability Reduction in Enhanced Oil Recovery. *Journal of Petroleum Engineering*, 2014, pp.1–9.

MIT Physics Department, 2003. Polymer gels.

Moore, J.N. et al., 2002. PETROLOGIC EVIDENCE FOR BOILING TO DRYNESS IN THE KARAHA-TELAGA BODAS GEOTHERMAL SYSTEM, INDONESIA.

Moridis, G. et al., 1996. A Field Test of a Waste Containment Technology Using a New Generation of Injectable Barrier Liquids.

Moridis, G.J., Finsterle, S. & Heiser, J., 1999. Evaluation of alternative designs for an injectable subsurface barrier at the Brookhaven National Laboratory Site, Long Island, New York. *Water Resources Research*, 35(10), pp.2937–2953.

Nabzar, L., Chauveteau, G. & Roque, C., 1996. A New Model for Formation Damage by Particle

Retention. In *SPE Formation Damage Control Symposium*. Society of Petroleum Engineers.

Nasr-El-Din, H.A. & Taylor, K.C., 2005. Evaluation of sodium silicate/urea gels used for water shut-off treatments. *Journal of Petroleum Science and Engineering*, 48(3–4), pp.141–160.

Noll, M.R. et al., 1993. Pilot field application of colloidal silica gel technology for in situ hot spot stabilization and horizontal grouting. *7th National Outdoor Action Conf.*, pp.207–219.

Noll, M.R., Bartlett, C. & Dochat, T.M., 1992. In situ permability reduction and chemical fixation using colloidal silica. *In:proceeding of the 6th national outdoor action conference on aquifer restoration*.

North-Abbott, M.A. et al., 2001. Colloidal silica barrier deployment at Brookhaven national laboratory.

P. Persoff et al., 1995. Injectable Barriers for Waste Isolation.

Palandri, J.L. & Kharaka, Y.K., 2004. A compilation of rate parameters of water-mineral interaction kinetics for application to geochemical modeling. *U.S. Geological Survey*.

Pruess, K., Oldenburg, C. & Moridis, G., 1999. TOUGH2 User guide. *Exchange Organizational Behavior Teaching Journal*, (November).

Purnanto, M.H. & Purwakusumah, A., 2015. Fifteen Years (Mid-Life Time) of Wayang Windu Geothermal Power Station Unit-1: An Operational Review.

Reed, M.H., 1982. Calculation of multicomponent chemical equilibria and reaction processes in systems involving minerals, gases and an aqueous phase. *Geochimica et Cosmochimica Acta*, 46(4), pp.513–528.

Selle, O., 2005. An Experimental Study of Viscous Surfactant Flooding for Enhanced Oil Recovery.

Seright, R.S. & Liang, J., 1995. A Comparison of Different Types of Blocking Agents. In *SPE European Formation Damage Conference*. Society of Petroleum Engineers.

Society of Petroleum Engineers, 2015. Types of gels used for conformance improvement.

Spycher, N. et al., 2009. Application of TOUGHREACT V2.0 to environmental systems, In Proceedings of Tough symposium 2009 Lawrence Berkeley National Laboratory.

Steefel, C.I. & Lasaga, A.C., 1994. A coupled model for transport of multiple chemical species and kinetic precipitation/dissolution reactions with application to reactive flow in single phase hydrothermal systems. *American Journal of Science*, 294(5), pp.529–592.

Suminar, A., Molling, P. & Rohrs, D., 2003. Geochemical contributions to a conceptual model of Wayang Windu field Indonesia.

Susanto, A. & Kimura, Y., 2008. Energy Security : Tohoku University.

Thunderhead Engineering, 2007. PetraSim: User Manual.

Utami, P., 2000. CHARACTERISTICS OF THE KAMOJANG GEOTHERMAL RESERVOIR (WEST JAVA) AS REVEALED BY ITS HYDROTHERMAL ALTERATION MINERALOGY.

Vinot, B., Schechter, R.S. & Lake, L.W., 1989. Formation of water-soluble silicate gels by the hydrolysis of a diester of dicarboxylic acid solubilized as microemulsions. *SPE Reservoir Engineering (Society of Petroleum Engineers)*, 4(3), pp.391–39714236.

Wibowo, H., 2006. Spatial data analysis and integration for regional-scale geothermal prospectivity mapping,West Java, Indonesia.

Xu, T., 2008. Incorporation of aqueous reaction kinetics and biodegradation into TOUGHREACT: Application of a multi-region model to hydrobiogeoChemical transport of denitrification and sulfate

reduction. *Lawrence Berkeley National Laboratory*.

Xu, T. et al., 2006. TOUGHREACT - A simulation program for non-isothermal multiphase reactive geochemical transport in variably saturated geologic media: Applications to geothermal injectivity and CO2 geological sequestration. *Computers and Geosciences*, 32(2), pp.145–165.

Xu, T. et al., 2004. TOUGHREACT User ' s Guide : A Simulation Program for Non- isothermal Multiphase Reactive Geochemical Transport in Variably Saturated Geologic Media. *Lawrence Berkley National Laboratory*.

Xu, T. et al., 2009. TOUGHREACT Version 2.0, In Proceedings of TOUGH Symposium 2009 Lawrence Berkeley National Laboratory.

Xu, T. et al., 2011. Toughreact version 2.0: A simulator for subsurface reactive transport under non-isothermal multiphase flow conditions. *Computers and Geosciences*, 37(6), pp.763–774.

Xu, T., Pruess, K. & Brimhall, G., 1999. An improved equilibrium-kinetics speciation algorithm for redox reactions in variably saturated subsurface flow systems. *Computers & Geosciences*, 25(6), pp.655–666.

Xu, T., Spycher, N. & Sonnenthal, E., 2012. TOUGHREACT User's Guide: A Simulation Program for Non-isothermal Multiphase Reactive Transport in Variably Saturated Geologic Media, version 2.0. *Lawrence Berkeley …*, (October), pp.1–5.

Yeh, G.-T. & Tripathi, V.S., 1991. A Model for Simulating Transport of Reactive Multispecies Components: Model Development and Demonstration. *Water Resources Research*, 27(12), pp.3075–3094.

Zheng, L. et al., 2009. On mobilization of lead and arsenic in groundwater in response to CO2 leakage from deep geological storage. *Chemical Geology*, 268(3), pp.281–297.

APPENDIX

APPENDIX 1. WAYANG WINDU GEOTHERMAL FIELD

A1.1. INTRODUCTION

The Wayang Windu geothermal field (Figure 31) is located in the province of West Java, Indonesia, near the town of Pangelengan at approximately 150 km southeast of Java (capital city of Indonesia) and about 35 km south of Bandung (capital city of West Java) (Asrizal et al. 2006; Bogie et al. 2008). The field is part of cluster of geothermal fields surrounding Bandung that also includes Darajat (Hadi et al. 2005), Kamojang (Utami 2000), Karaha-Telaga Bodas (Moore et al. 2002), Papandayan (Wibowo 2006), Patuha (Layman & Soemarinda 2003), Tanpomas (Wibowo 2006) and Tangkuban Perahu (Wibowo 2006). The elevation of the field lies between 1500 and 2100 m above sea level (asl) (Purnanto & Purwakusumah 2015).

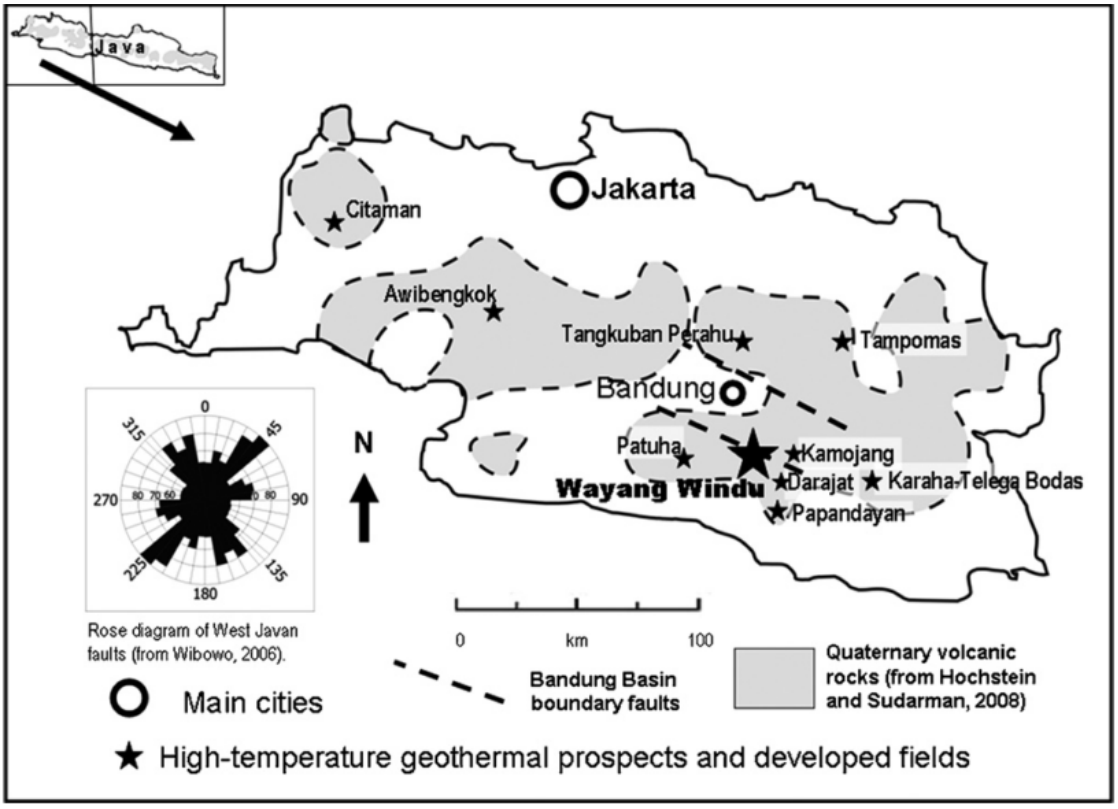

Figure 31: The distribution of Quaternary volcanic rocks and high-temperature geothermal field in West Java, Indonesia (Bogie et al. 2008)

The field extent is estimated to be approximately 4 km wide in the north following an E-W direction and to expand 14 km to the south beneath a series of aligned, small volcanic centers, where it

decreases to approximately 2 km across. As a result, the Wayang Windu field is approximated to have an overall potential resource area of 40 km² (Bogie et al. 2008).

A1.2. GEOLOGY

The Wayang Windu field is located in Pleistocene rocks ranging in age from about 1.0 to 0.147 million years. At that time, two main volcanoes were active in the region, the Malabar Volcanic Complex and the Wayang Windu lava domes, respectively. The volcanoes produced relatively young lavas in part of the field strata, with the last product aged of about 147,000 years ago. These rocks were overlain by younger sediments and epiclastic volcanic product into the Wayang Windu valley less than 50,000 years ago (Susanto & Kimura 2008).

The stratigraphy of the field as been reported by Bogie, I. & Mackenzie (1998) who applied volcanic facies models to subdivide the different volcanic facies at depth. These strata define a series of overlapping andesitic piles. Microdiorite, diorite porphyry dikes, and dolerite are found, but very limited coring and blind drilling prevented the clear recognition of major intrusive in the field. The volcanic units are predominated by andesitic lavas, pyroclastic, and epiclastic deposits. Ash deposits of regional extent happen throughout these volcanic piles. Fourteenth different beds are found at Wayang Windu with a thickness ranging from 5 to 30 m. These beds can be linked to wells while many thinner ones with isolated occurrence occur randomly. Figure 32 shows a cross section of the field extending from the North to the South.

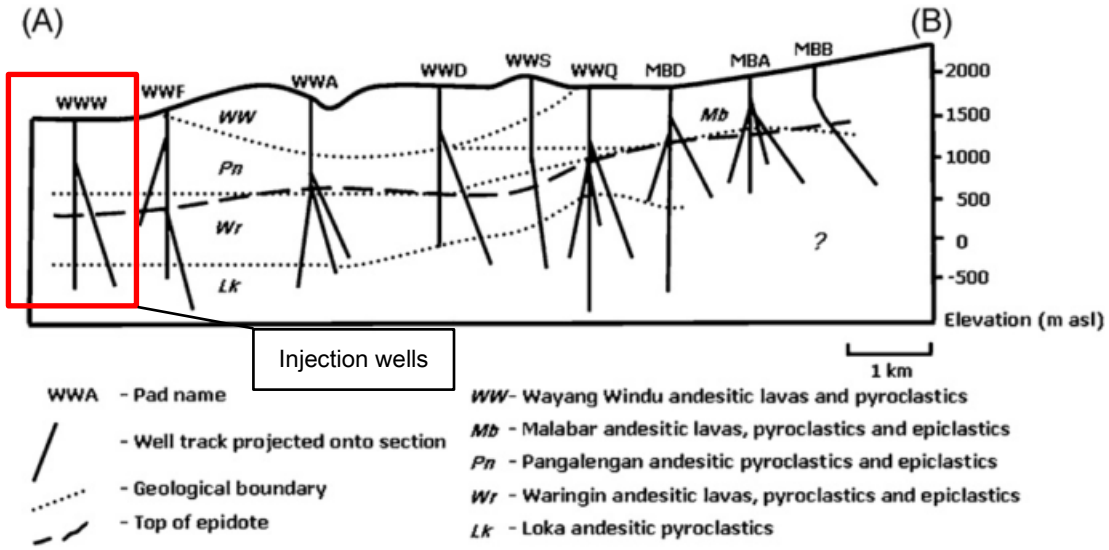

Figure 32: Cross section of the Wayang Windu geothermal field showing well tracks, geological units (extended north and south from that of (Bogie, I. & Mackenzie 1998) *) and the top of epidote* (Bogie et al. 2008).

Structurally the Wayang Windu field follows to regional patterns in the south, with faulting showing steep dips (>80°) and strikes of 30-40° and 330-340°. In the north, however, deformation results from movements along a boundary fault. Also, the wells localized the presence of structural permeability with the most permeable geologic structure following the regional trend of 40°. Because these structures tend to be similar to a regional fault, it is likely that they are strike-slip

faults. In their research, however, Bandyopadhay et al. (2006) discover that the calculated stress field did not match with the regional orientation, but had the least principal stress striking at 310°, following an overall normal faulting regime. Therefore, the 40° striking faults are likely to be regional strike-slip faults reactivated as more permeable normal faults due to a switch from the regional compressive regime to a local extensional regime. Moreover, the extension may be even stronger further to the north, at the boundary and within the Bandung Basin (Bogie et al. 2008).

A1.3. RESERVOIR CHARACTERISTICS

The Wayang Windu geothermal field has a deep, hot, neutral pH, liquid reservoir that is overlain by a perched vapour-dominated two-phase reservoir (Figure 33). Pressures and temperatures versus elevation within the deep liquid reservoir are similar throughout the field. In the north, the top of the reservoir is at 400 m asl, and it goes down towards the south where the top of the liquid reaches approximately the sea level elevation. The reservoir has almost the same vertical pressure distribution throughout, leading it to be considered as a contiguous body. Also, because it is near pressure equilibrium, there is little fluid flow in the reservoir (Suminar et al. 2003).

Two-phase vapour-dominated reservoirs overlie the deep liquid reservoir. The largest located in the north appears to be coalesced over two fluid upwelling centers, while the two in the south are separated, resulting in three vapour-dominated reservoirs over four fluid upwelling centers. Unlike the deep liquid reservoir, the characteristics of the vapour-dominated reservoir differ progressively towards the south: the reservoir are found deeper in the field, their thicknesses decrease and their pressure, temperature, and gas content increase (Bogie et al. 2008).

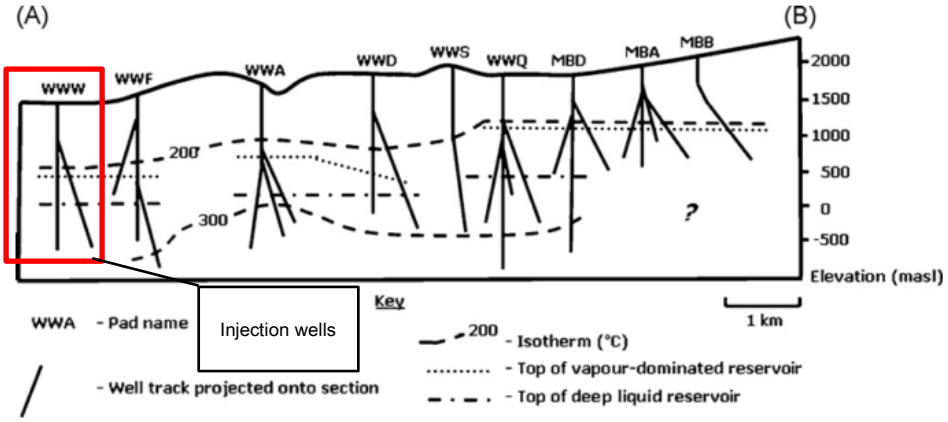

Figure 33: Cross section of the Wayang Windu geothermal field showing well tracks, isotherms and the known location of the top of the vapour-dominated and deep liquid reservoirs (Bogie et al. 2008).

A1.4. HYDROTHERMAL ALTERATION

Hydrothermal alteration in the Wayang Windu field is mainly developed in the pyroclastic deposits with more structurally limited alterations zones in the lava flows. At the top of the field, the presence of Kaolinite, alunite, natroalunite and rare native sulfur is noticeable. Increasing depth, interlayered illite-smectite rather than the only smectite is observed, until the point where the transition to a propylitic assemblage happens with its top marked by the occurrence of corrensite and epidote. Further down, illite becomes the main sheet silicate. At greater depth, secondary amphibole, orthoclase, and magnetite making up a high-temperature potassic assemblage are found. Finally,

in the deep liquid reservoir, wairakite, prehnite, and epidote are common alterations and vein minerals.

Apart from a gradual transition, with illite-smectite and corrensite detected shallow in the vapour-dominated reservoirs, and prehnite in the lower parts of the deep liquid reservoir, there is no clear hydrothermal alteration of the liquid and vapour-dominated reservoirs (Bogie et al. 2008).

A1.5. FLUIDS CHEMISTRY

The fluid composition of the Wayang Windu geothermal field is neutral throughout the reservoir. The precise composition of the fluids can vary widely depending on where the sample are taken. No updated data could be accessed for this research. However, two different fluid composition from the literature are found (Table 33 and 34).

Table 33: Chemical composition of a geothermal well Wayang Windu field in Indonesia (concentration in mg/kg) (Mahon et al. 2000).

Location	Temp [°C]	Sample Date	Elevation [m]	pH (25°C)	Li	Na	K	Mg	Ca	Cl	B	CO2	SO4	SiO2
Well 13	100	1996	1700	6.3	33	11250	3060	0.6	885	22160	692	<10	75	355

Table 34: Chemical analyses of hot spring waters at the G. Wayang Windu (concentration in ppm) (Sudarman et al. 1986).

Sample Number	Temp [°C]	pH (25°C)	Na	K	Ca	Mg	HCO3	Cl	SO4	SiO2
1.	49	6.45	61.3	32	33.6	22.4	306	2	85	42
2.	50	6.79	80	28	35.2	27.2	418	5	45	145
3.	36	6.69	90.7	9.7	50	46.8	560	1	50	52
4.	61	6.07	66.7	16.7	56.8	37.6	325	20	145	75
5.	46	6.12	50.3	11.3	70.8	30.6	220	6	214	52
6.	48	6.41	18.6	8.7	22.4	10.6	115	1	50	60
7.	92	1	10.9	6.8	16	8.6	----	1	2400	85